High Throughput DFT Calculations on Single Atom Catalysts for Solar Fuel Generation

Narasimhan Viswananthan

Materials Science & Engineering

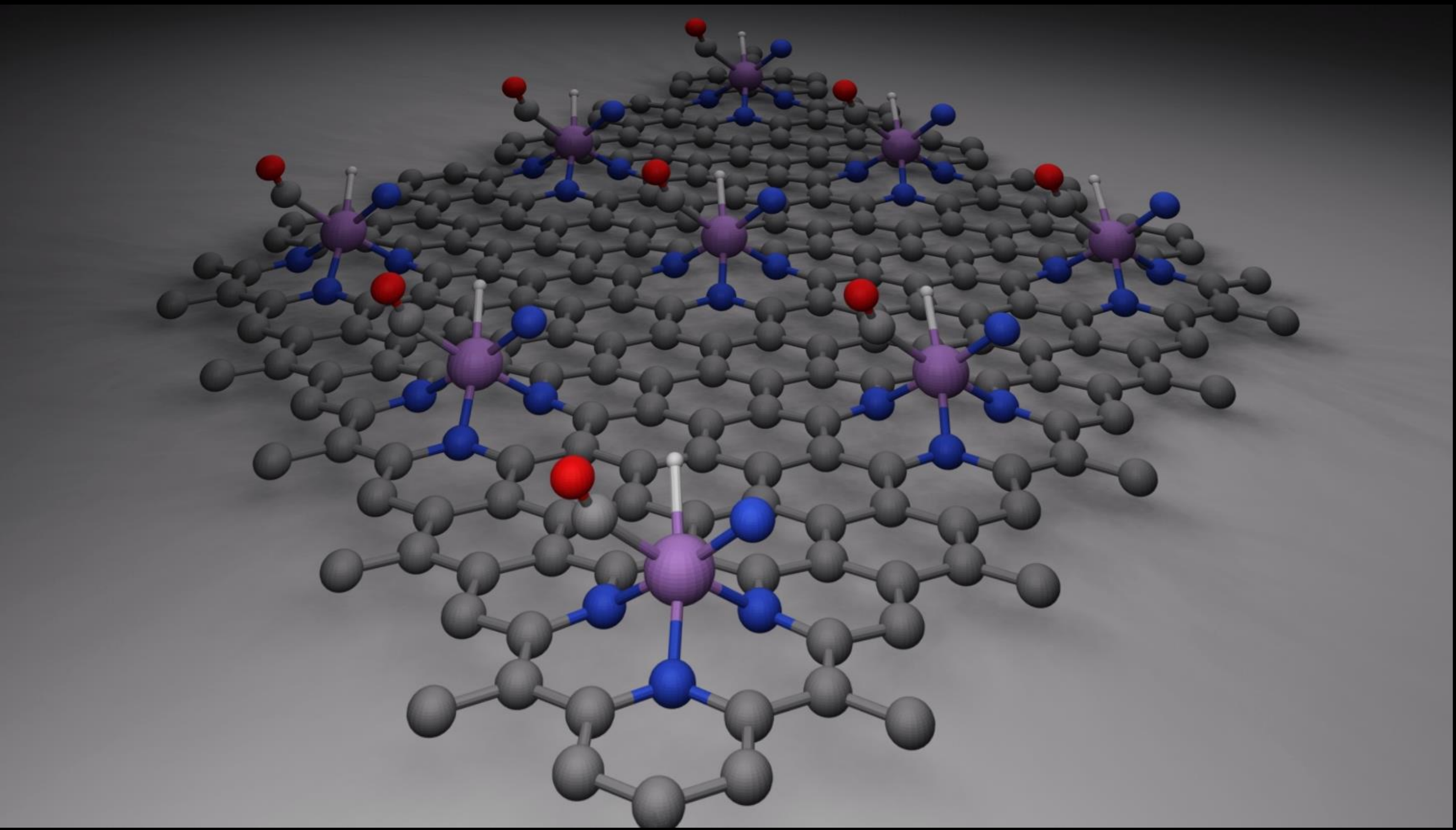

High Throughput DFT Calculations on Single Atom Catalysts for Solar Fuel Generation

By

Narasimhan Viswanathan

in partial fulfilment of the requirements for the degree of

Master of Science

in Materials Science and Engineering at the Delft University of Technology,

to be defended publicly on **September 25, 2020**

Student Number	4741404

Daily Supervisors

Dr. Süleyman Er,	Dutch Institute of Fundamental Energy Research
Dr. İlker Tezsevin,	Dutch Institute of Fundamental Energy Research

Thesis committee

Dr. Marcel Sluiter,	Delft University of Technology
Dr. Amarante Böttger,	Delft University of Technology
Dr. Poulumi Dey,	Delft University of Technology
Dr. Süleyman Er,	Dutch Institute of Fundamental Energy Research

"Neither money pays, nor name, nor fame, nor learning; it is the character that can cleave through the adamantine walls of difference"

Swami Vivekananda

ABSTRACT

Fossil fuels have been the primary source of rising energy requirements for humankind. However, the extensive use of fossil fuels has led to an increase in Earth's surface temperature. To tackle rising energy demands and the increase in Earth's surface temperature, various organizations like Inter-governmental Panel for Climate Change and the European Environmental Agency have suggested the use of renewable energy as an alternative energy supply. E.g., the use of hydrogen as an alternative fuel in transportation will reduce greenhouse gas emissions. Besides, converting CO_2 and N_2 to fuels and industrial feedstock like CO or NH_3 can curb the Earth's increasing surface temperature. As a result of this, in this thesis, the catalysts for the synthesis of hydrogen from water-splitting (hydrogen evolution reaction- HER), conversion of CO_2 to CO via carbon dioxide reduction reaction (CO_2RR), and reduction of N_2 from air to NH_3 (Nitrogen reduction reaction-N_2RR) are studied.

The conventional catalysts used for these reactions are Pt for HER, Cu for CO_2RR Cu, and Ru for N_2RR. Although these catalysts are active and exhibit a high yield of products, they have some disadvantages, such as the long-term availability and cost of Pt and Ru. On the other hand, Cu suffers from the low selectivity for the conversion from CO2 to CO. To overcome these disadvantages; scientists have developed a new kind of catalyst with a higher specific activity, known as the Single-Atom Catalysts (SAC). The SACs use fewer precious elements than the conventional bulk catalysts without compromising the activity. The use of binding energy (E_B) as a descriptor for the reactions mentioned has been proven in the literature. Therefore, E_B is used in this thesis to predict novel SACs through high-throughput DFT calculations using 3-N doped graphene as the substrate. The descriptor for HER is the E_B of H atom, for CO_2RR is E_B of CO, and that of N_2RR is E_B of N on the respective catalyst surfaces. These calculated binding energies are compared against the descriptor E_B on the conventional catalysts to obtain the novel SACs. With E_B as the descriptor, the candidate catalysts for HER are B, Cr, Mn, Fe, Co, Ni, Ge, Ru, In, Sb, La, and Pb. The candidate catalysts for N_2RR are Ru, Mo, and Cr. The candidate catalysts for CO_2RR are Mg, Al, Ca, Zn and Se,. In addition to this, the charge dissipation of the adsorbent species on the SAC and the effect of atomic size on the E_B is studied. It was seen that the computational predictions go hand in hand with the predictions of existing experiments for HER and CO_2RR.

ACKNOWLEDGEMENT

There are many people to thank for the successful completion of this project. Firstly, I would like to thank Dr. Süleyman Er for kindly agreeing to my request to do a master thesis work in the Autonomous Energy Materials Discovery [AMD] group at DIFFER. His inputs and suggestions throughout the thesis have been extremely valuable. All the constructive criticisms have contributed to developing me as a good researcher and a good human being. I also would like to thank Dr. Marcel Sluiter for his suggestions through the thesis and my master's degree. He has always taken a keen interest in developing my skills and took the time to make sure that I acquired them. His counselling sessions, whenever I was stressed, was something I needed. I am incredibly thankful to both my supervisors for their support and goodwill during this thesis. I want to extend my thanks to Dr. Amarante Böttger and Dr. Poulumi Dey for kindly consenting to be a part of my defense committee.

I cannot thank enough my daily supervisor İlker Tezsevin. He has been a constant support and a pillar of strength throughout my thesis project and internship. This thesis would not have been possible without his help and contribution. He has been a great teacher to me from the start of my internship project at DIFFER. His determination and motivation to work have always made an impact on me. I am sure that this learning experience I had from him will be an asset to me. On a lighter note, I will never forget these two things: first, our discussions after coming out of meetings with Suleyman! And his expression whenever I say I have a new idea!

A huge thanks to the AMD group: Murat Sorkun, Elif Sorkun, Qi Zhang, Xuan Zhou, and Dr. Abishek Khetan at DIFFER. Their inputs and invaluable suggestions on my presentations have been a massive help during my thesis preparations and the poster presentations. A special thanks to Murat for helping me out with my codes. Also, thank you for all the snacks which you people bought for the office. They kept me running during my late working hours at DIFFER.

I want to thank Nitin Prasad for all his insightful suggestions and discussion during my thesis. Thank you for helping me find answers to the questions I had regarding catalysis. I would also like to thank Dr. Rifat Kamarudheen for all the heated discussions and debates on science, academia, and everything around! I would also like to thank Kiran George and Dr. Vivek Sinha for giving me insights about planning my thesis work. I would also like to thank Devyani Sharma for the much-needed coffee breaks and conversation between my work. Late-night discussions and motivational talk from Samuel Mani has played a massive role in me, keeping up my spirits through this thesis. Thank you so much for that! I want to thank my friends Saran, Preetha, Kammath, Reuben, Apurva, Shrinidhi, Thejus, Arun, Hitha, Mamta, Sid, Geo, Jesil and all my friends back home for helping me during this time.

Last but not least, my family has been supportive and encouraging of my decisions during this time. I thank Amma, Appa, Vivek, Yamini, Rohit, Prabhat, and Ammama for their love and support. I am indebted to them for all that they have done for me. I wish my granddad was here to see me complete this master's. He was dearly missed during this time.

Narasimhan Viswanathan
Eindhoven, September 2020

Table of Contents

1. Introduction 1

1.1 Motivation 2

1.1.1 Single-Atom Catalysis (Catalysts) 3

1.1.2 3N-Graphene in the perspective of catalysis 5

1.2 Prediction of novel catalysts 7

1.3 Research Aim 8

2 Scientific background 11

2.1 Hydrogen Evolution Reaction (HER) 11

2.2 CO_2 reduction reaction (CO_2RR) 12

2.3 N_2 reduction reaction (N_2RR) 13

2.4 Density Functional Theory (DFT) 14

2.4.1 Born-Oppenheimer approximation 14

2.4.2 Hartree-Fock Method 14

2.4.3 Density Functional Theory 15

2.4.4 Hohenberg-Kohn Theorem 15

2.4.5 Kohn-Sham Theory 16

2.4.6 Local density approach (LDA) 17

2.4.7 Generalized gradient Approximation (GGA) 17

2.4.8 Pseudopotential (PP) 17

2.4.9 Vienna Ab initio Simulation Package (VASP) 18

2.5 Binding Energy 18

2.6 Bader charges and Quantum Theory of Atoms in Molecules 18

3 Computational Methods and Automation Strategy 21

3.1 Roadmap of calculations 21

3.2 Input orientations and positions of the adsorbents on the various catalyst surfaces 22

3.2.1 Input orientations and positions of adsorbents on single metal atoms 22

3.2.2 Orientation of adsorbents on 3NG 23

3.3 Methodology 25

3.3.1 Methodology for Vacuum correction for non-neutral calculations 27

3.4 Calculation of H, N, and CO energies 28

3.5 Automation scripts and file handling 28

3.5.1 Pre-run files for energy calculations 30

3.5.2 Post-run files and accuracy check for energy calculations 32

4 Results and Discussions 35
4.1 Calculation on Slab catalysts 35
4.2 Binding Energy of adsorbents on Single Metal Atoms 35
4.3 Binding Energy of Single-Atom Cations 37
4.4 Optimization of Graphene and 3NG 39
4.5 KPOINT and ENCUT optimization 39
4.6 Metal adsorption on 3NG: energetics and stability of the SAC 41
4.6.1 Energetics of Metal adsorption on 3-N-Graphene 41
4.7 Adsorption of H atom on 3N-Graphene-Metal- Binding Energy and Geometrics 44
4.7.1 H adsorption on 3N-Graphene-Metal 44
4.7.2 Candidate Single-Atom Catalysts for Hydrogen Evolution Reaction 44
4.8 Adsorption of N atom on 3N-Graphene-Metal -Binding Energy and Geometrics 47
4.8.1 Binding Energy and Geometrics of N on 3N-Graphene-Metal 47
4.8.2 Candidate SACs for N_2RR 47
4.9 Adsorption of CO on 3N-Graphene-Metal - Binding Energy and Geometrics 50
4.10 Bader charge calculations and relation of the Binding Energy and the atomic radii 53
4.11 Validation of results with available experiments from the literature 54
4.11.1 Comparing the binding of metals on 3NGM in experiments and this work 54
4.11.2 Comparison of Hydrogen Evolution Reaction results with experiments 55
4.11.3 Comparison of Carbon dioxide reduction predictions with experiments 56
5 Conclusion and Outlook 59
5.1 Conclusion 59
5.2 Outlook 59
6 Bibliography 61
Appendix 66
A. Molecular energies of H, N and CO 68
B. Binding Energy of CO, H and N on different substrates 69
C. VASP calculation with developed code 71

List of Figures

Figure 1-1: Renewable fuels: Process of converting CO_2 into fuels and N_2 into fuel/fertilizer (adapted witch changes from DIFFER website [10]). 2

Figure 1-2: Representation of Single-Atom Catalyst: The image shows a metal atom anchored on a 3N-doped Graphene sheet, with Hydrogen being adsorbed on the metal atom. 4

Figure 1-3: Activity comparison of bulk, nanoparticles, and single atoms 4

Figure 1-4 Two different nitrogen doping on graphene: 3N-Graphene and 4N-graphene doping on the graphene sheet with a metal atom adsorbed in the vacancy. 6

Figure 1-5 Volcano Plot for HER: Plot of current density v/s the binding energy of H on the catalyst. The top of the volcano plot is where the catalytic activity is the best available catalyst, and the corresponding E_B is what is the desirable descriptor for the reaction [15]. 7

Figure 1-6: Periodic table showing all the metals studied for the calculations on 3NG. 8

Figure 2-1: HER mechanism: Schematic representation of HER mechanism on the Pt(111) surface. 12

Figure 2-2: RWGS mechanism on catalyst surface. (a) Shows the formate reaction mechanism on the Cu (111) surface. (b) The volcano plot for CO_2RR with Au on the top of the curve. 13

Figure 2-3: Volcano plot and reaction mechanism of N_2RR. (a) Shows the Reaction mechanism of N_2RR on the catalyst surface. The adsorbed N* and H*react to form NH_3. (b)The volcano plot for N_2RR on v/s the rate of the reaction. The volcano plot shows that Ru is the best available catalyst for N_2RR [17]. 14

Figure 3-1:File arrangement used in hard disk: This figure depicts how files are arranged for energy and geometry optimization. 22

Figure 3-2: Input orientation of adsorbents on the SMAs: (a) Orientation of H/N on the SMAs. (b) Orientation of CO on the SMA with CO on SMA. (c) CO parallel to the SMA (d) CO on top of the SMA with oxygen closer to the SMA substrate. 23

Figure 3-3: Orientations of adsorbent H atom on catalyst surface. (a) Shows the H/N atom adsorbed on top of the single metal atom (b) Shows the H/N atom adsorbed at an angle of 45^0 to the catalyst surface and in the direction of the hollow site of graphene (c) Shows the H/N atom adsorbed at an angle of 45^0 to the catalyst surface and in the direcction of N atom. 24

Figure 3-4: Orientations of CO on the 3NGM (a) CO on top of metal atom (b) CO in the direction of hollow site in 3NG and (c) CO in the direction of nitrogen atom doped on the graphene sheet. (d) is the extra orientation only for CO- Oxygen is at a 45^0 angle to the carbon atom. 25

Figure 3-5: Flow chart of automated SM, SMC and 3NG calculations 29

Figure 3-6: Figure showing the angle of the adsorbent species 3NGM in the direction of the nitrogen atom. The adsorbent species is dissecting the corner angle of the equilateral triangle. This means that the adsorbent species is at 45° to the z-axis and 30° each to the x-axis and y-axis 32

Figure 4-1: Heatmap of EBHon the SMAs. 36

Figure 4-2: The heatmap of atom EBNon various SMAs. 37

Figure 4-3: Heatmap of EBCO on various SMAs. 37

Figure 4-4: Heatmap EBH of on SMC 38

Figure 4-5Heatmap of EBN of N on SMC 38

Figure 4-6: Heatmap of EBCO of CO on SMC 39

Figure 4-7: Graphite cell downloaded from the Materialsproject website[50] 39

Figure 4-8: Graph of energy of 3NG with different KPOINT sets v/s the time required for the calculation: For KPOINTS after 8x8x1, the energy does not change much, but the calculation becomes expensive. 40

Figure 4-9: Graph of the energy of 3NG substrate with different ENCUT input values v/s the time for the calculation required for the calculation. 41

Figure 4-10: E_B comparison of metal on 3NG with respect to SM and metal cohesive energy 42

Figure 4-11: Geometries of Be, Al and Hg on 3NG: (a) Final geometry of Be atom on the 3NG graphene sheet. (b) Geometry of Al on 3NG. (c) Final geometry of Hg on 3NG. 43

Figure 4-12: Output geometries of E_B of H atom on 3NGM for different SACs considered. 44

Figure 4-13: E_B of hydrogen atom on 3NGM. The candidate catalysts are the ones in between the target lines (orange lines) 46

Figure 4-14: Final Geometries of N atom on 3NGM 47

Figure 4-15: E_B of N atom on 3NGM. The candidate catalysts are Ru, Mo, Cr. The candidate catalysts can be seen between the red lines. The green line is the benchmark catalyst Ru (0001) 49

Figure 4-16: Final geometries of all the CO-3NGM systems. 50

Figure 4-17: E_B of CO on 3NGM . The candidate SACs are shown between the two dashed red lines. The green line is the E_B of CO on the Cu(111) slab surface. This is the benchmark to predict the SACs. 52

Figure 4-18 Relation of E_B of Metal on 3NGM and Bader dissipation of Hydrogen atom on the 3NG sheet 53

Figure 4-19: Plot of Bader charges on Metal for 3NGM-H system and atomic radii 54

Figure 4-20: SEM image of dispersed Co atoms on 3NG. The SEM image shows the Co atoms dispersed on 3NG. the white dots shoes the Co atoms and the darker area is the substrate. Note the areas where the white dots are clustered together. This indicates the areas where the nano-clusters are formed [26]....55

Figure 4-21: Performance comparison of Co-3NG and other catalysts. (a) Compares the current density and the potential between Pt(111), Co on graphene, Co on 3NG, and nitrogen-doped graphene. Co-3NG is still not as good as the conventional Pt catalyst, but still comparable to the other catalysts. (b) Compares the turnover frequency of various catalysts. (c) SEM image of the Co on 3NG. Well dispersed Co atoms (white specks) on 3NG. This also proves that the Co atoms are stable on the 3NG substrate [58]. 56

Figure 4-22: Periodic table with candidate SACs for HER, CO_2RR and N_2RR....57

List of tables

Table 1: The characteristic properties of SACs, homogenous and heterogeneous catalysts (adapted with changes from [14]).... 5

Table 2: The total number of calculations done in this thesis....29

Table 3: Comparison of lattice parameters from experiments and this work 35

List of Abbreviations

HER	Hydrogen Evolution Reaction
N_2RR	Nitrogen Reduction Reaction
CO_2RR	Carbon Dioxide Reduction Reaction
IPCC	International Panel on Climate Change
SAC	Single Atom Catalyst(s)
SMA	Single Metal Atom(s)
SMC	Single Metal Cation(s)
3NG	3 Nitrogen (doped) Graphene
3NGM	Metal immobilized on 3NG
4NG	4 Nitrogen (doped) Graphene
LDA	Local Density Approximation
GGA	Generalized gradient Approximation
PBE	Perdew–Burke-Ernzerhof
RPBE	Revised Perdew–Burke-Ernzerhof
PP	Pseudo Potential
HK	Hohenberg-Kohn
KS	Kohn Sham
E_B	Binding Energy
TOF	Turn Over Frequency

1

INTRODUCTION

In this modern era of technology, humankind makes use of numerous gadgets in day to day life. As all these devices are integrated into our lives, the daily energy requirement increases. Current energy use is at an all-time high, and a significant part of this energy comes from fossil fuels [1]. Fossil fuels are an attractive option because of their high calorific value and their ease of handling. But the combustion of fossil fuels leads to the formation of CO_2 and other greenhouse gases. Greenhouse gases alter the incoming solar radiation and outgoing thermal radiation, hence changing the surface temperature of the Earth [2]. Decreasing air quality in cities, recurring floods and landslides worldwide, frequent fires in the Amazon region, and bush fires in Australia are all indications of climate change. [3][4][5][6][7]. To counter the global warming and rising surface temperature crisis, organizations like Intergovernmental Panel on Climate Change (IPCC) and European Environment Agency have rolled out reports to help the policymakers with scientific assessments, future implications, risks, and methods to adapt to sustainable development. The suggestions from the reports are summarized into the following points [8][9] and Figure 1-1 [10]:

1. The shift from conventional fuels to renewable (solar) fuels - helps in the reduction of fossil fuel usage in the generation of electricity and other needs like transportation. The electrolysis of water produces renewable hydrogen. This is a prospective renewable fuel because the calorific value of hydrogen is comparable to that of fossil fuels [11]. The combustion of H_2 only leads to the formation of H_2O, a non-pollutant. Additionally, the synthesis of H_2 through electrolysis is less polluting compared to that of the current industrial techniques of manufacturing hydrogen[11].
   Furthermore, as shown in Figure 1-1, the reaction of H_2 produced from the electrolysis of water on reaction with N_2 from air forms NH_3. NH_3 is not only a valuable fertilizer[12] but can also be decomposed to form H_2 fuel [12] or used as a hydrogen storage material [13].
2. Conversion of CO_2 to fuels and industrial feedstocks- CO_2 on reaction with H_2 can forms CO. This can be used as an industrial feedstock to produce gasoline or higher-end carbon chains (shown in Figure 1-1). If implemented, such conversion technologies can lead to a significant reduction of emissions and the reduction of global warming.

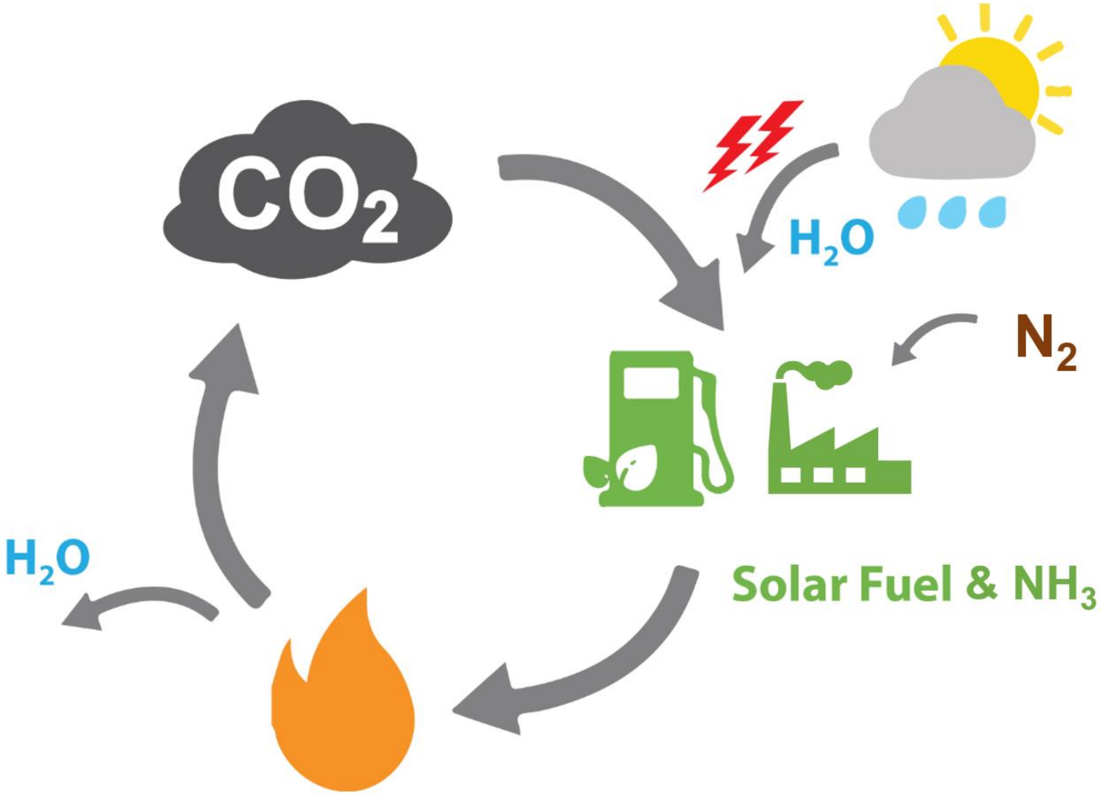

Figure 1-1: Renewable fuels: Process of converting CO_2 into fuels and N_2 into fuel/fertilizer (adapted witch changes from DIFFER website [10]).

These suggestions can be chemically depicted using the following reactions:

- H_2 evolution reaction (HER) produces renewable hydrogen.
- CO_2 reduction reaction (CO_2RR) converts the pollutant CO_2 to CO, which is to be converted to higher-end chains like gasoline or plastics.
- N_2 reduction reaction (N_2RR) converts the nitrogen to ammonia, which can be later used as a fuel or as a fertilizer feedstock.

Though these reactions provide solutions to global warming and its impacts, the molecules considered here (H_2O, CO_2, and N_2) are thermodynamically stable. Therefore, for these reactions to happen, the reactants must overcome a high activation energy barrier. To lower the activation barrier, and thus to proceed the reaction at a higher rate, we use materials known as catalysts. The catalysts can be either homogeneous or heterogeneous catalysts. As the name suggests, in homogeneous catalysis, the catalyst and the adsorbents will be in the same phase, while in heterogeneously catalyzed reactions, the catalyst and the adsorbents will be in different phases; e.g., the catalyst might be solid, and the adsorbent might be a liquid or gas. Single-atom catalyst(s) (SACs) are new kind of catalysts which inherit properties from both the homogenous and heterogeneous catalysts [14]. In a SAC, the catalytically active metal clusters are downsized to single isolated atoms, anchored on a substrate. In this thesis, the SACs are studied as a viable replacement for traditional catalysts.

1.1 Motivation

The best available catalysts for HER is Pt (111) [15], CO_2RR is Cu (111)[16], and N_2RR is Ru (0001)[17], all of them being heterogeneous catalysts. Homogeneous catalysts can also be used for catalyzing these reactions. Still, since the reaction occurs in a liquid medium, the separation of the products from the solution becomes expensive and, at times, an inefficient process. Hence for the above reactions, the heterogeneous catalysts are preferred. However, the heterogeneous catalysts have a few disadvantages, which are:

- **Mediocre selectivity**: The catalyst's ability to drive the reaction towards a specific product is known as the selectivity of the catalyst. Selectivity is one of the most important properties to determine the catalytic activity. Generally, for heterogeneous catalysts, the catalytic selectivity is not high. E.g., when Cu is used as the catalyst for CO_2RR, a mixture of products like ethane, ethanol, acetic acid, and CO is obtained. This calls for an additional product separation process, which is undesirable [18]. This calls for a novel catalyst with higher selectivity. Literature shows that the SACs have a better selectivity compared to the conventional heterogeneous catalysts.
- **High material cost**- As mentioned, for HER and N_2RR, Pt and Ru is the best available catalysts. However, these catalysts are expensive [19]. The SACs use considerably lesser amounts of catalysts compared to the heterogeneous catalysts. In this regard, the catalysts become cheap, and the processes become (more) economically viable [20].
- **Limited abundance in nature**-For HER, the catalyst used is Pt. The quantity of Pt in nature is limited. It is estimated that by 2050, there will not be enough Pt available for all required applications [21]. This calls for the reduction in the quantity of Pt metal catalyst used in the reactions. An ideal scenario will be if a novel catalyst replaces the existing Pt for HER. It is hypothesized that SACs can achieve this while maintaining the yield of the reactions [20][22][23].
- **Low metal atom efficiency**-Here the atomic efficiency refers to the ratio of product produced to the amount of metal (catalyst) atoms used. Compared to the heterogeneous catalysts, the SACs have a higher atomic efficiency [24]. For a specific amount of product, improving the metal atom efficiency automatically reduces the number of metals used for catalysis, hence decreasing the metal cost and solving the problem of availability of the metal to an extent.
- **Lack of uniform active sites** – In the heterogeneous catalysts, the active sites are usually random. This contributes towards the lower selectivity of the catalyst. In SACs, the active sites are uniform in nature, and therefore the SACs exhibit better performance than the conventional heterogeneous catalysts.

An ideal catalyst for any reaction would possess the advantages of both heterogeneous and homogeneous catalysts[14]. Also, all the reasons mentioned above call for a novel and cheaper catalyst. SACs are suggested as the novel kind of catalysts that possess the advantages of both heterogeneous and homogeneous catalysts. Hence, in this thesis, we focus on predicting novel SACs.

1.1.1 Single-Atom Catalysis (Catalysts)

In a SAC, the catalytically active bulk structures are downsized to single isolated atoms and anchored on a substrate. The catalytic system used in this thesis is shown in Figure 1-2.

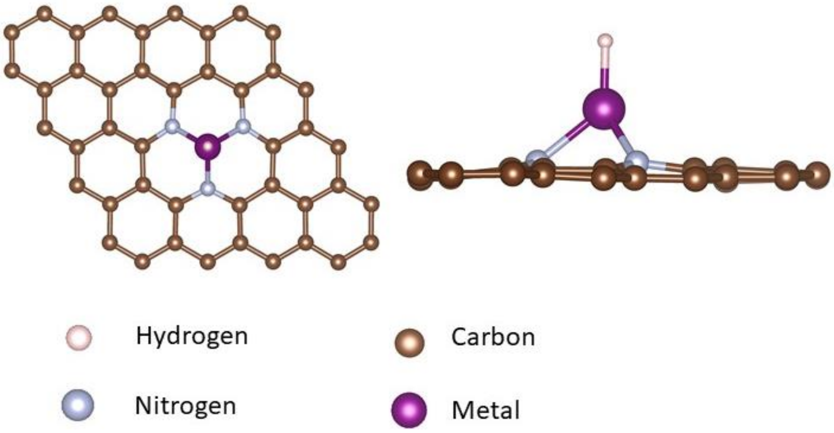

Figure 1-2: Representation of Single-Atom Catalyst: The image shows a metal atom anchored on a 3N-doped Graphene sheet, with Hydrogen being adsorbed on the metal atom.

In SAC, the active site is only a Single Metal Atom (SMA) where the catalytic reaction takes place. In **Figure 1-3,** as the metal size decreases, the specific activity of the catalyst increases [24]. This solves the problem of using more massive amounts of noble metals for reactions, and therefore reducing the cost of the catalysts.

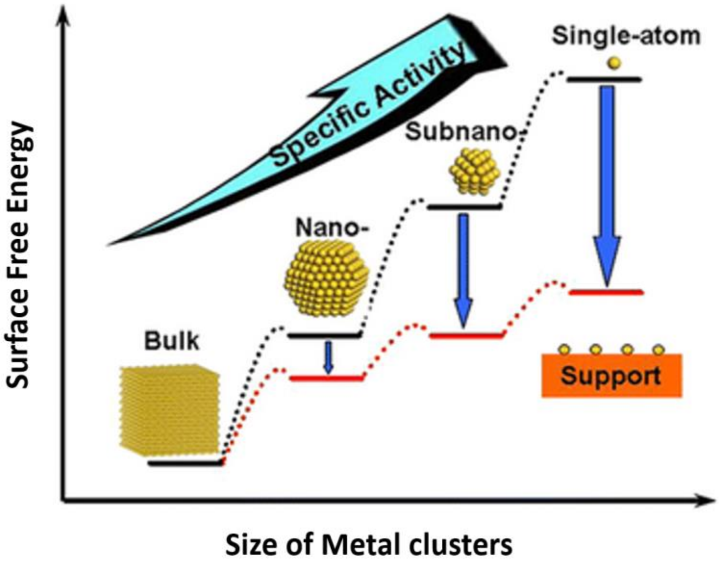

Figure 1-3: Activity comparison of bulk, nanoparticles, and single atoms

In addition to the advantages of SACs mentioned, few more properties of SACs in contrast to the conventional catalysts are discussed below [14], [24]:

1. **Catalyst recovery:** In the conventional homogeneous catalyst, the catalyst will be in the solution phase, and the recovery of the products from the solution phase will be an inefficient process. In the heterogeneous catalysts and the SACs, since the catalyst is in the gaseous phase, the product recovery happens during the reaction itself [14].
2. **Stability of the catalyst:** As the SMAs are anchored to the substrate in a SAC, at higher temperatures and harsh reaction conditions, the SMAs become mobile and tend to form agglomerates on the substrate surface. This a disadvantage of the SAC[25]. Currently, this issue is addressed by lowering the metal loading on the catalyst substrate. The choice of the substrate also plays a vital role in the stability of SACs.

3. **Active Sites/Larger available surface area for catalysis:** As shown in Figure 1-3, as the size of the catalyst decreases, the surface area of the catalyst increases[14]. Due to this, the adsorbent has a higher probability of finding an active site. Hence, a higher surface area catalyst is preferred. SACs provide higher catalyst surface area (per gram of catalyst) for the reaction than the conventional heterogeneous catalysts, and hence a higher activity during the reaction. This is a desirable quality for a catalyst [24].
4. **SACs, a bridge between homogenous and heterogeneous catalysts:** By tuning properties like catalyst recovery, selectivity, and atomic efficiency, the catalytic property of SACs can be significantly enhanced. This tunable property of SACs makes them an attractive option. Therefore, SAC can be called as a bridge between homogenous and heterogeneous catalysts. More comparisons between SACs and homogeneous and heterogeneous catalysts are tabulated in
5. Table 1.

Table 1: The characteristic properties of SACs, homogenous and heterogeneous catalysts (adapted with changes from [14])

Property	Homogeneous catalysts	SACs	Heterogeneous catalysts
Catalyst recovery	Difficult and expensive	Easy and cheap	Easy and cheap
Thermal stability	Poor	Poor	Good
Selectivity	Excellent/good	Excellent/good/ Poor	Good/poor
Active Site	Uniform	Relatively uniform	Non-uniform
Atomic efficiency	High	High	Relatively low

At higher temperatures and harsh reaction conditions, the SMAs become mobile and tend to agglomerate, forming bigger structures like nanoparticles [26]. Therefore, the selection of the support material plays a vital role in the activity of the catalysts. In Figure 1-3, the contribution of the substrate towards the catalytic activity has been represented by the red line. According to Figure 1-3**,** the substrate effects increase as the geometries change from the bulk scenario to the SAC scenario. According to Sabatier's principle [17], the adsorbent needs to bind not too strong or not too weak on the active site.

Hence, the substrate should be chosen in such a way that the SMA remains bound to the substrate. To make sure that the SMA remains bound to the substrate, the electronegativity difference of the atom binding the SMA and the SMA should be larger. Rivera et al. [25] shows that N doped graphene as a substrate for the SAC is a desirable option (as discussed in chapter 1.1.2). Due to its proven applicability, nitrogen-doped graphene has been chosen as the substrate for the high throughput scanning of SACs in this thesis [25].

1.1.2 3N-Graphene in the perspective of catalysis

2D sheets are generally considered as suitable support materials for catalytic reactions[25]. In addition to this, it is hypothesized that the electronic properties of the substrate might influence the catalytic property of the SAC. Hence, a highly active substrate is necessary. Therefore, in this thesis, a 2D substrate is chosen over the other forms of substrates, such as bulk metal catalysts or binary alloys.

In this thesis, a 2-D sheet of 3 N doped graphene is used. 2-D sheets are found to be catalysts and supports for SACs [27][25]. Rivera et al. compares the performance of graphene as a substrate for SACs with other available substrates. Graphene is seen to yield better effects as a substrate due to its structure and bonding[25]. Nevertheless, it is seen that some metals do not sit anchored on the graphene sheet as they tend to agglomerate on the surface[25]; hence a defect is created on the graphene sheet, and the carbon atoms around the vacancy are replaced with a more electronegative element such as nitrogen. This partially solves the problem of metals agglomerating on the surface[25]. Hence, we use a single vacancy graphene with three nitrogen doping.

Figure 1-4 shows various types of doping on the graphene sheet. The 3N doping on graphene is called the pyridinic graphene. Here, some of the graphene rings have nitrogen atom(s) in place of carbon atom(s). Based on the position of the nitrogen atom, two alternative structures were prepared as shown in Figure 1-4. Figure 1-4(a) shows single vacancy graphene doped with three nitrogen atoms (3NG), and Figure 1-4(b) shows double vacancy graphene doped with four nitrogen atoms (4NG).

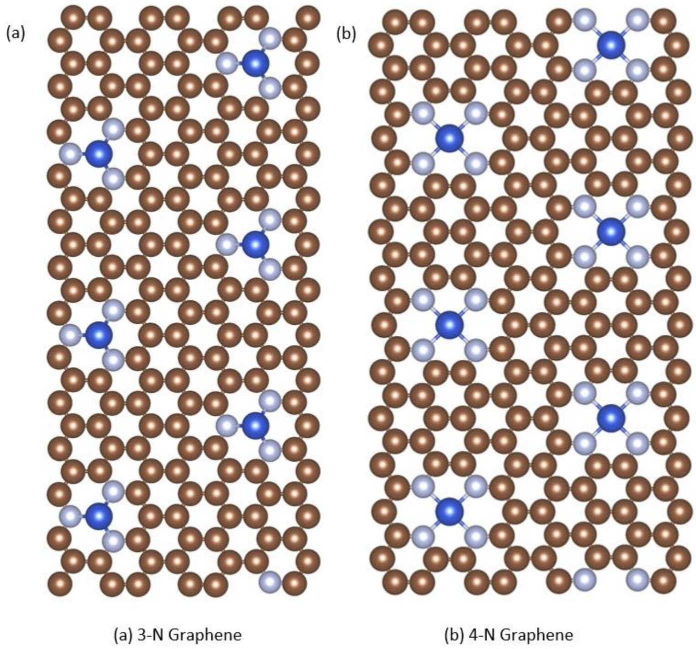

(a) 3-N Graphene (b) 4-N Graphene

Figure 1-4: Two different types of nitrogen doping on graphene. 3N-Graphene and 4N-graphene doping on the graphene sheet with a metal atom adsorbed in the vacancy.

The following are some crucial conclusions from Rivera et al.:

- Thermodynamically, pyridinic N is more stable than the rest. This is because the *p-orbitals* of pyrrolic N contributes to the bonding towards the metal atoms.
- Though this is counter-intuitive, the 3NG exposes a higher surface area of the metal atom than the 4NG. This is because of the vacancy size in 3NG is smaller than that of 4NG. Since there is a bigger vacancy area and more number of nitrogen atoms in 4NG, it is hypothesized that the charge on the metal atom will be more positive. Hence, due to stronger metal-nitrogen interaction, the metal-adsorbent interaction will be weaker than that of the 3NG case.

As mentioned in the previous section, the selection of the substrate plays a vital role in the catalytic activity of the SACs. Depending on the support material used, the single metal atoms may agglomerate on the catalyst surface to form sub-nano particles or nanoparticles [22]. The following can be implemented to avoid agglomeration of SMAs:

- Lowering the metal atom loading: To avoid the agglomeration, the metal loading on the substrate can be reduced. This way, it can be ensured that metal-metal interaction on the substrate is limited hence lowering the probability of the metals to form an agglomerate on the surface [26]
- Enhancing metal support interactions: To increase the interaction of the metal with the substrate. This is ensured by creating vacancies on the substrate and hence increasing the interaction with the substrate [25]

The selection of 3NG as the substrate material helps to resolve these problems. In graphene, the carbon atoms are arranged in a honeycomb shape, where the **σ** bonds form the six-membered carbon ring and the **π** electrons will be delocalized, and hence are free to move over the graphene sheet[28]. These delocalized **π** electrons enhance metal-support interactions. The nitrogen doping facilitates the stronger adsorption of the metal atoms hence reducing the tendency of the single metal atom(s) (SMAs) to agglomerate on the surface [25][28][29][30].

1.2 Prediction of novel catalysts

As explained in the literature, the conventional catalyst for HER is Pt (111), for N_2RR is Ru (0001), and for CO_2RR is Cu (111) surfaces [16]. From the perspective of the thesis, it is important to note that there is a necessity to explain why these catalysts are currently the best options and how their properties can be used in this thesis.

To predict a suitable catalyst for a reaction, the complete reaction mechanism must be studied. But this is a time-consuming process. To avoid this, catalysts are predicted using '*descriptors'* of the reaction such as . the binding energy (E_B) of the adsorbent on the catalytic surface, the change in the electronic properties like the density of states (DOS), the charge dissipation of the adsorbent on the catalytic surface, the chemical softness of the catalyst, etc.. For the HER, Norskov et al. have described the binding energy of H as an important parameter in selecting a catalyst[15]. **Figure 1-5** shows the plot of E_B -current density plot for HER. The top of the volcano plot is the point where the best catalysts are present[15]. This is the desirable E_B we look for in the novel catalysts.

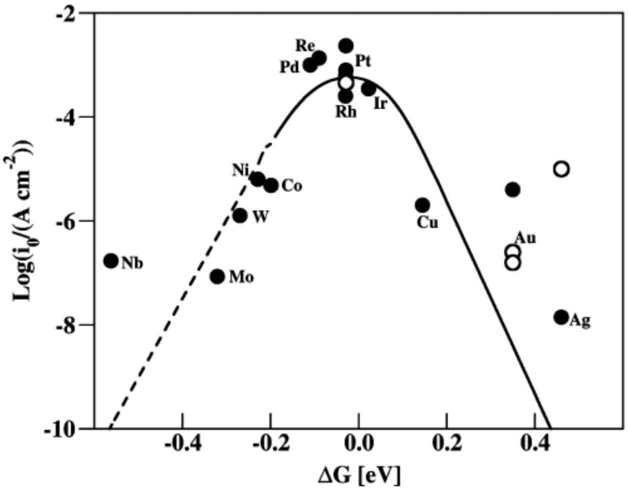

Figure 1-5 Volcano Plot for HER: Plot of current density v/s the binding energy of H on the catalyst. The top of the volcano plot is where the catalytic activity is the best available catalyst, and the corresponding E_B is what is the desirable descriptor for the reaction [15].

Analogous volcano plot has also been determined for CO_2RR and N_2RR, and the benchmark catalysts and the descriptors steps are decided. Even though E_B has conventionally been used as a descriptor to predict catalysts for reactions like HER, N_2RR,, and CO_2RR[16], it has not been used to study the SAC. In this thesis, we will use binding energy as a descriptor to predict novel SACs. (In this thesis, henceforth the E_B of H/N/CO on the catalyst surface will be mentioned as E_B of descriptor species)

1.3 Research Aim

The research aims of the thesis are outlined below:

- The main aim of the thesis is to predict SACs for H_2RR, N_2RR and the CO_2RR. The SACs studied in the thesis are all the metals and semi-metals (shown in Figure 1-6) immobilized on the 3NG substrate.
- To compare the characteristics of SMAs before and after doping it on the 3NG substrate. This will show the effect of graphene on the catalytic activity of the SMA.
- To understand the effect of surface charging and observe the specific trend of charging v/s binding energies of adsorbents, if any.
- To study the size effects of the metal atom on the binding strength of the adsorbent.

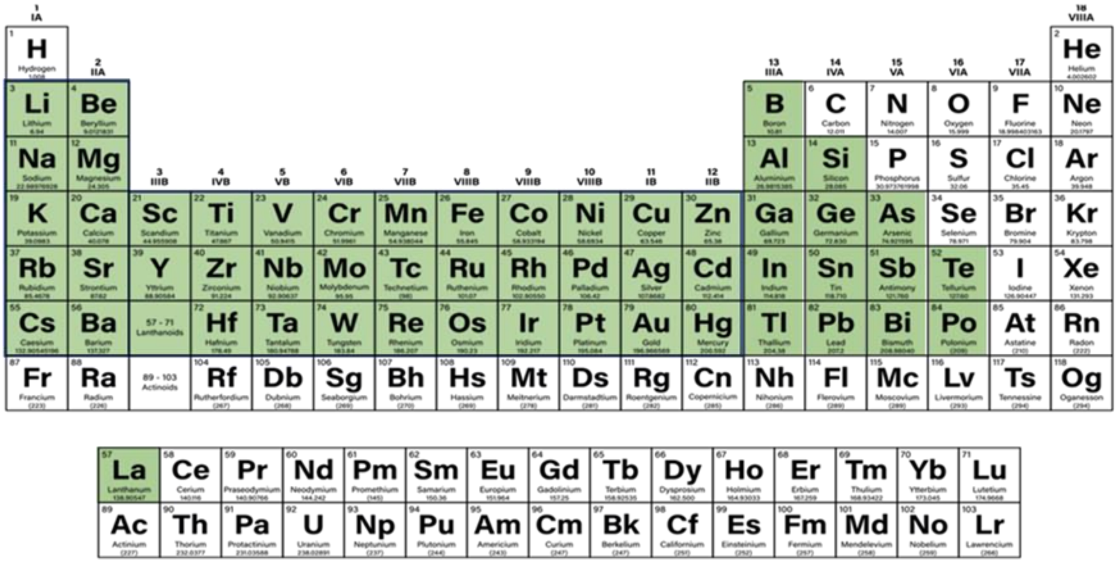

Figure 1-6: Periodic table showing all the metals studied for the calculations on 3NG.

To fulfil these research aims, the following actions were taken:

a) To predict a novel SAC for the reactions, E_B of the descriptor on the metal-doped 3NG (3NGM) is calculated using DFT calculations in VASP. The substrate considered is 3NG and the catalysts are all the metals and the semi-metals in the periodic table (as shown in the Figure 1-6). The obtained E_B is compared against the E_B of the descriptors on conventional catalysts (meatal surface slabs). The novel SACs are predicted using this value as a benchmark [15] [16][17].

b) The Bader charge calculations are also done to investigate how the charge transfers from the adsorbent to 3NGM. These calculations can also be used to find the relation of the E_{B} to the charge transfer. A trend Is expected to be seen from this study beterrn the E_{B} and the charge transfer.

c) To study the size effects of the metal atom, the atomic radii of the *d-transition* elements are plotted against the Bader charge of the hydrogen atom and the E_B of the metal atom on 3NG.

2

Scientific Background

In this section, the reaction mechanism of HER, CO_2RR, and N_2RR are discussed in detail. The definition of terms like E_B is discussed, and the equations used to calculate the same are also shown. In addition to this, the density functional theory and the mechanism of H_2RR, CO_2RR, and N_2RR are explained briefly

2.1 Hydrogen Evolution Reaction (HER)

Hydrogen as a fuel poses attractive *green* advantages like *zero-emission* of CO_2 and other toxic pollutants [31]. Hence, this can be considered as renewable energy if the H_2 is produced from solar fuels or other renewable sources of energy. Hydrogen fuel is currently used in fuel cell cars as a possible replacement for the traditional gasoline/diesel in the vehicles. Now, hydrogen is manufactured from fossil fuels [32]. This process is expensive, and it is also to be noted that this industrial process releases CO_2 into the atmosphere [32]. The overall reaction for HER is shown below [33]:

$$2H_2O \rightarrow 2H_2 + O_2 \tag{1}$$

One of the mechanisms of HER is shown in Figure 2-1. This mechanism is shown in the following steps:

$$2H_2O \rightarrow 2H_2O^* \tag{2}$$

$$H_2O^* \rightarrow OH^- + H^* \tag{3}$$

$$H^* + H_2O \rightarrow OH^- + H_2 \tag{4}$$

$$2H^* \rightarrow H_2 \tag{5}$$

For all the reactions, '*' indicates that the species are adsorbed on the catalyst surface

In the first step of the mechanism, the water molecule gets adsorbed on the catalyst surface. This H_2O molecule will be split into OH* and H* (Equation (2)) and react with another adsorbed water molecule to form H_2^* and O_2^* (Equation (3)). In the following step, H_2^* and O_2^*will be desorbed from the surface (Equation (4)). As mentioned, the binding energy is generally considered as a good *descriptor* for the heterogeneous catalysis reactions[15]. The E_B of H on the metal surface at the top of the volcano plot is the target value. Hence Pt (111) facet is considered as the benchmark catalyst for HER in this work[16]. To estimate the performance of SACs for HER, the calculated H binding energies of H atom on SACs will be compared against the H binding interactions on the Pt(111) surface.

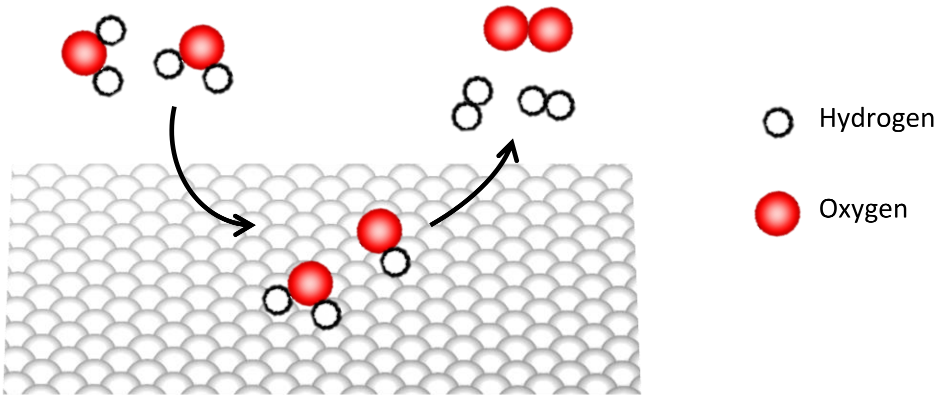

Figure 2-1HER mechanism: Schematic representation of HER mechanism on the Pt(111) surface.

2.2 CO_2 reduction reaction (CO_2RR)

CO_2RR is used to produce fuels and a higher-end carbon chain. This can be achieved by a reaction such as reverse water gas shift reaction (RWGS)[34]. The CO_2 released into the atmosphere from various sources is one of the raw materials for this reaction. This leads to better air quality and, hopefully, a reduction in the surface temperature of the Earth. With RWGS reaction, we get CO, which can be used as a building block for high-value chemicals, such as through Fischer-Tropsch synthesis. Equation (7) shows the RWGS reaction [35]:

$$CO_2 + H_2 \rightarrow CO + H_2 \qquad (6)$$

The formate reaction mechanism (also shown in Figure 2-2 (a)) for the reaction is as follows:

$$H_2 \rightarrow 2H^* \qquad (7)$$

$$CO_2 + 2H^* \rightarrow HCOO^* + H^* \qquad (8)$$

$$HCOO^* + H^* \rightarrow CO^* + OH^* + H^* \qquad (9)$$

$$CO^* + OH^* + H^* \rightarrow CO + H_2O \qquad (10)$$

In the first step of the formate mechanism, H_2 will be adsorbed on the catalyst surface as $2H^*$ (Equation (7)). Following this, the CO_2 will be adsorbed on the surface as CO_2^* (Equation (8)). The adsorbed CO_2 will react with adsorbed H^* to form $HCOO^*$ (note that in this mechanism, the hydrogen atom will form a bond with a carbon atom and not an oxygen atom) (Equation (9)). This $HCOO^*$ will further decompose to CO^* and OH^*. The CO^* will be desorbed from the surface, and the OH^* and H^* will react to form H_2O and desorb from the surface (Equation (10)). There are other mechanisms through which this reaction proceeds, namely carboxyl and redox mechanism[35]. Even though in Figure 2-2(b)[36] gold catalyst is at the top of the curve, literature[16] shows that accepts that Cu is the ideal (electro)catalyst for CO_2RR because of the total higher yield of the reaction. However, the selectivity of Cu(111) catalyst is not as high as Au(111) catalyst. With this in mind, the E_B of CO on SACs is compared against the E_B of CO on the Cu(111) to predict the novel SAC catalyst.

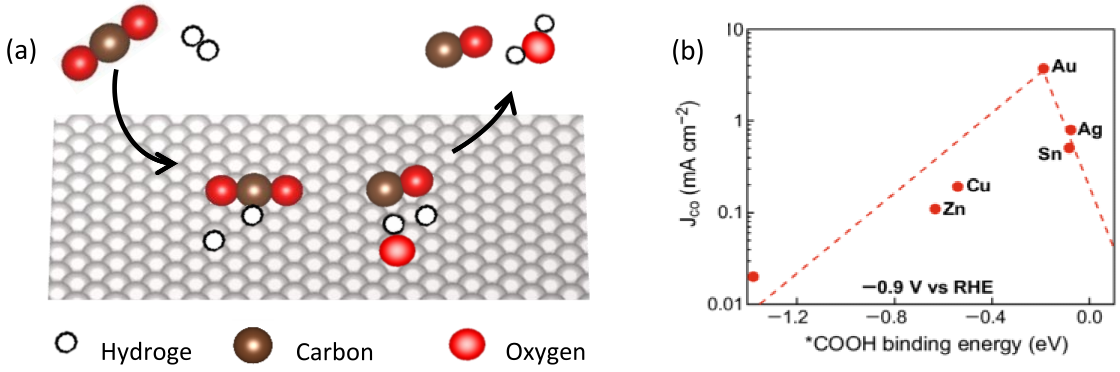

Figure 2-2 RWGS mechanism on catalyst surface: (a) Shows the formate reaction mechanism on the Cu (111) surface. (b) The volcano plot for CO_2RR with Au on the top of the curve.

2.3 N_2 reduction reaction (N_2RR)

As mentioned in the Introduction, ammonia can be used as an industrial feedstock or an alternative for hydrogen storage. In the reaction mechanism of N_2RR, as shown in Equations (13)-(16), and in Figure 2-3 (a), the N_2 molecule at higher temperatures is adsorbed on the catalyst surface as N atom (Equation (12)). Following this, the H_2 molecule is adsorbed as H atom (Equation (13)). The adsorbed N atom reacts with an adsorbed hydrogen atom to form NH_3 (Equation (14)) and reacts with adsorbed H to give NH_3^*. This ammonia molecule will be desorbed from the surface as the product (Equation (16)).

The Nitrogen reduction reaction is shown by:

$$N_2 + 3H_2 \rightarrow 2NH_3 \tag{11}$$

The reaction mechanism is as follows:

$$N_2 \rightarrow 2N^* \tag{12}$$

$$H_2 \rightarrow 2H^* \tag{13}$$

$$N^* + 3H^* \rightarrow NH_3^* \tag{14}$$

$$NH_3^* \rightarrow NH_3 \tag{15}$$

The ‘*’ denotes that the species is adsorbed on the catalyst surface.

Figure 2-3 (b) shows the volcano plot of the rate of the reaction v/s the E_B of N on the catalyst surface. The volcano plot shows that Ru is the best available catalyst for N_2RR [17]. In this case, the selectivity and the conversion of Ru(0001) catalyst is higher than that of the other catalysts. For this reason, the E_B of N on the SACs are compared against the E_B of N on the Ru(0001) to predict the novel catalyst

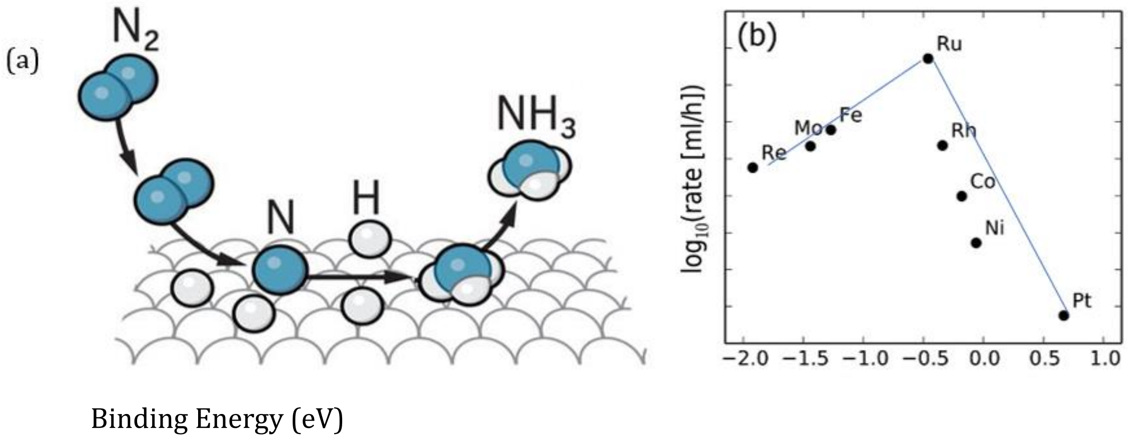

Figure 2-3: Volcano plot and reaction mechanism of N_2RR: (a) Shows the Reaction mechanism of N_2RR on the catalyst surface. The adsorbed N* and H*react to form NH_3. (b)The volcano plot for N_2RR on v/s the rate of the reaction. The volcano plot shows that Ru is the best available catalyst for N_2RR [17].

2.4 Density Functional Theory (DFT)

To find the ground state energy, the Schrödinger equation must be solved. The time-independent Schrödinger equation is given by:

$$H\Psi = E\Psi \tag{16}$$

Where H is the Hamiltonian operator, Ψ is the wavefunction and E is the energy. Generally, this can only be solved for elementary (hydrogen like) H atom system or the electron in a well system. To solve the equation Max Born and Robert Oppenheimer suggested an approximation where the atomic nuclei and the electrons are considered separately. In this section, the use of DFT in catalysis and its basics are briefly explained.

2.4.1 Born-Oppenheimer approximation

Max Born and Robert Oppenheimer, in 1927, postulated that the motion of the atomic nuclei and electrons can be treated separately. This reduced the computational complexity of the problems. Compared to the electrons, the nucleus is heavy; hence whenever a nucleus moves, the electrons associated with it also move instantaneously and occupy the electronic ground state of that corresponding nuclear configuration. This decoupling of nuclear and electronic dynamics is called the Born-Oppenheimer approximation, and can be expressed as [37]:

$$E_{atom} = E_{nucleus} + E_{electron} \tag{17}$$

2.4.2 Hartree-Fock Method

As mentioned, the Schrödinger equation is easy to solve for single-electron systems. However, in reality, materials are made up of hundreds of atoms that contain thousands of electrons. Dealing with this 'many-body problem' or 'n-electron system' is not so easy due to the size of the system. To solve this problem, Douglas Hartree, in 1928, came up with a method that considered each body is independent and only interacted with each other in an averaged way [37]. This simplifies the n-electron system to a situation where the electrons become a set of non-interacting one electrons. Hence, the total energy is the sum of independent energies, and can be written as:

$$E = E_1 + E_2 + E_3 + \cdots + E_n \tag{18}$$

Using the one-electron Hartree method Hartree and Fock in 1930 enhanced the technique with a focus on wave functions, and the total energy equation can be written as:

$$E = E_{kin} + E_{ext} + E_H + E_x \tag{19}$$

Where E_{kin} is the kinetic energy, E_{ext} is the external potential (energy which accounts for the attractive nuclei-electron interaction), E_H is the Hartree energy, and E_x is the exchange energy. One major disadvantage of this method is that it is only valid for small systems and that its practical applications are still limited [37].

2.4.3 Density Functional Theory

To solve the shortcomings of the HF method, Walter Kohn and Lu J Sham came up with DFT, which is explained in the following sections[38].

2.4.3.1 Electron Density

The first Hohenberg-Kohn theorem demonstrates that the electron density determines the electronic ground state properties. The electron density of the noninteracting electrons is the square of the wavefunction at that point. We focus on the non-interacting system because in DFT, the electrons do not interact with each other. This physical term is the basis of the next Hohenberg Kohn theorem and Kohn-Sham theory in DFT. The mathematical expression of electron density is [37]:

$$\rho(r) = \sum |\Phi_i(r)|^2 \tag{20}$$

Note that in the above equation, we used the *Kohn-Sham* (KS) orbitals Φ_i instead of wavefunction $\Psi_i \int \rho(r)dr = n$ (21)

Where n is the total number of electrons.

2.4.4 Hohenberg-Kohn Theorem

The first Hohenberg-Kohn (HK) theorem states that the external potential (is the measure of the interaction between electrons and nuclei) is a unique functional of the electron density. Hohenberg and Kohn [39] assumed an arbitrary number of electrons in a box, which are moving under the influence of an external potential *v(r)* and the mutual Coulomb repulsion. The Hamiltonian has the form:

$$H = T + V + U \tag{22}$$

Where T is the kinetic energy, V is the external potential, and U represents the electron-electron interactions. Hohenberg and Kohn also showed that the external potential and the ground state wavefunction is a unique functional of n(r).

The second Hohenberg Kohn theorem identifies a way to find out a way to calculate the ground state energy through the variational principle. It states that at a given *v(r)* if we minimize the system energy with varying the system electron density, we reach the bottom of the energy well. This energy functional can be written as [39]:

$$E \equiv \int v(r)n(r)dr + F[n(r)] \tag{23}$$

Where, $F[n(r)]$ is the universal functional,

$$F[n(r)] \equiv (\Psi, (T + U)\Psi) \tag{24}$$

The ground state energy and the ground state density is determined by the minimization of the energy functional in equation (23). The difficulty here is that F[n(r)] is still unknown. F[n(r)] mostly is represented by the following equation

$$F[n(r)] = \frac{1}{2}\iint \frac{n(r)n(r')}{|r-r'|} dr dr' + G[n(r)] \tag{25}$$

Where G[n(r)] is the universal functional of density[39].

2.4.5 Kohn-Sham Theory

G[n(r)] can be re-written as:

$$G[n] \equiv T_s[n] + E_{xc}[n] \tag{26}$$

Where T_s is the kinetic energy, and E_{xc} is the exchange-correlation energy of an interacting system with density n(r). For an arbitrarily varying n(r), the E_{xc} term is not easy to define, but for a slowly varying n(r), it can be shown that,

$$E_{xc}[n] = \int n(r)\epsilon_{xc}(n(r))dr \tag{27}$$

Where, $\epsilon_{x0}(n)$ is the exchange and correlation energy per electron of a uniform gas of density n. Kohn and Sham assumed that the above equation constitutes an adequate representation of exchange and correlation effects in the system under consideration and ϵ_{xc} is known from the theories of the homogeneous electron gas.

From the stationary property of external potential, the energy equation is calculated subject to the following condition:

$$\int \delta n(r)dr = 0 \tag{28}$$

Then,

$$\int \delta n(r)\left\{\phi(r) + \frac{\delta T_s[n]}{\delta n(r)} + \mu_{xc}(n(r))\right\} dr = 0 \tag{29}$$

Where,

$$\phi(r) = v(r) + \int \frac{n(r')}{|r-r'|} dr' \phi(r) = v(r) + \int \frac{n(r')}{|r-r'|} dr' \tag{30}$$

And the chemical potential (μ) contribution to exchange and correlation term can be written as:

$$\mu_{xc} = \frac{d(n\epsilon_{xc}(n))}{dn} \tag{31}$$

For a given μ and ϕ , the single particle Schrödinger equation is solved:

$$\{\frac{1}{2}\nabla^2 + [\phi(r) + \mu_{xc}(n(r))]\psi_i(r) = \epsilon_i\psi_i(r) \tag{32}$$

And setting,

$$n(r) = \sum_{i=1}^{N} |\psi_i(r)|^2 \tag{33}$$

Where n is the number of electrons.

Kohn et al. describes the following procedure for calculating the energy: Equation(29)-(34) are to be solved self consistently, and initially, n(r) is assumed and $\psi(r)$ and μ_{xc} is calculated using equations (25) and (26), respectively. After finding a new n(r) from equations(32) and (33), the energy equation can be written as:

$$E = \sum_1^N \epsilon_i - \frac{1}{2}\iint \frac{n(r)n(r')}{|r-r'|} dr dr' + \int n(r)\big[\epsilon_{xc}\big(n(r)\big) - \mu_{xc}\big(n(r)\big)\big]dr \tag{34}$$

This procedure of computing the energy is continued until there is no significant change in energy.

In the following sections, few approximations used to find the functional are described.

2.4.6 Local density approach (LDA)

The LDA assumes that the complex system can be transformed into smaller systems with uniform electron densities. Hence, the E_{xc} term in equation (35) can be expanded as:

$$E_{xc} = E_x + E_c \tag{35}$$

Two cases of G[n] are discussed by Kohn and Sham in [38]. In the first case, they considered the slowly varying electron density case, in which the n(r) can be related to E_{xc} as described in the equation (27). This gives a correct density to the order of ∇^2, inclusive, and an exact answer is obtained for the slowly varying case.

But the LDA fails for highly dense systems. When we apply the LDA to highly dense systems, we observe that near the surface of the molecules, where the KS orbitals overlap, the assumption in equation (30) is not valid and leads to an erroneous result. It is noteworthy that LDA is useful for bulk metal systems, but not for surface calculations. To include the spin effects in LDA calculations, another approximation, Local Spin Density Approximation (LSDA), was also implemented, where the spin + and spin – cases were considered in equation (27) [40].

2.4.7 Generalized gradient Approximation (GGA)

Real systems are not homogenous systems and have a varying density landscape. The GGA captures the electron density and its variation at a given point. GGA overcomes the disadvantage of LDA, such as the over-estimation of binding energies, which gives an increase in the lattice constant and a decrease in the cohesive energies.

Popularly used GGA functionals are PW91 (Perdew Wang 91)[41] and the PBE (Perdew, Burke, and Ernzerhof) [42][43][44]. PW91 has been popularly applied in various calculations. However, the PW91 has some disadvantages; it shows spurious wiggles in exchange-correlation functional both at high and low electron densities [40].

PBE functional presents a simplified and improved GGA version. This functional has proven to be computationally efficient for surface calculations and is one of the most frequently used functional now. Another version of PBE, RPBE, is useful for hydrogen bonding or adsorption calculations. This is regarded as one of the best functionals to calculate the E_B of adsorbents on catalyst surfaces. In addition to this, RPBE performs very well for the strongly adsorbed systems when the interaction of CO, H, and N interactions with transition metal surfaces [45]. Since this thesis also uses the same adsorbent systems, RPBE was chosen as the functional for the DFT calculations in this thesis. [45].

2.4.8 Pseudopotential (PP)

The PP approach mimics the characteristics of the actual potential while reducing the computational time for the calculation[40]. This is done by freezing the core electrons by choosing a suitable cut-off radius while calculating the forces and the energy for the valence electrons. This is done because the information from core electrons is limited, while a vast amount of computing time is spent to obtain these results. It was observed that the PP or the effective potential is a reliable tool for calculations, especially on large systems. This approach is used in this thesis.

2.4.9 Vienna Ab initio Simulation Package (VASP)

DFT calculations in this thesis were carried out using the Vienna *Ab initio* Simulation Package (VASP) [46], [47]. VASP is a computer program for atomic scale materials modeling, e.g., first-principles electronic structure calculations and quantum-mechanical molecular dynamics. The input files for VASP are:

- POSCAR-The POSCAR files contain information on the position of the atoms in the system under consideration
- POTCAR- This file contains the PP and exchange-correlation functional data
- INCAR is the file that contains information regarding the force for convergence, magnetic moment, smearing, dipole corrections, etc. and controls the run with the given flags,
- KPOINTS are the sampling points in the Brillouin zone, the region closest to the origin (0,0,0).

Ground-state atomic positions, bond distances, total energies, and magnetic moments are all obtained from VASP calculation generated output files. In the current work, these output files have been accessed with in-house developed scripts.

2.5 Binding Energy

The binding energy (E_B) is the energy change upon the adsorption of adsorbent on the catalyst surface. The binding energy or, in this case, relative energy is calculated by the general equation:

$$E_\mathrm{B} = E_\mathrm{final} - E_\mathrm{initial} \tag{36}$$

Similar equations will also be used for the charged species calculations. This will be explained in the following section. The energies for the systems will be calculated in this manner, and the final corrected energy will be subtracted from the energy of graphene as in the equations shown above.

2.6 Bader charges and Quantum Theory of Atoms in Molecules

The quantum theory of atoms in molecules explains how the atoms and make up molecules. Richard Bader once said, “There are no bonds, only bonding!” [48]. This statement changes our view on how the atoms are bonded with each other to form molecules. To define the energetics and interaction in many-body problem using DFT can be a challenging task. One way to do this is to decompose the properties of molecules into contributions from individual atoms. Bader suggested that the molecule be divided into (Bader)volumes. These Bader volumes are separated from each other using surfaces called the zero-flux surfaces. The theory of atoms in molecules defines atoms as a region in space, which is bound by surfaces through which there is zero flux gradient of electron density. From a molecule point of view, these zero-flux surfaces lie in the bonding region between atoms. The advantage of the Bader partitioning is that it can be observed through experiments or can also be calculated [48], [49].

Bader's theory of atoms in molecules can be used for charge analysis, charge distribution, the global hardness of the atoms, which is used to quantify the cost of removing charges from particles or the ionization potential, and the bond strength. The Henkelman group developed a code that can efficiently partition the charge density in materials into Bader volumes [48]. Generally, in molecular systems, the charge density reaches a minimum between the atoms. According to Bader[49], the charge inside the Bader volume is a good approximation of the charge of the atom, and generally, there is only one peak for the charge density inside such a volume. There are exceptions for this, though; in cases were *f-centers* are present, there can be multiple charge peaks inside the Bader volume.

The grid-based method finds the steepest ascent paths to the grid point until the charge density maximum is reached. It is the grid-based approach that gives the algorithm its efficiency. The algorithm finds out the charge density of the core and the valence charge separately. The core charge density is written to AECCAR0, and the valence charge is written to AECCAR2 file, respectively. The two charge densities are summed to the CHGCAR_sum. To obtain the correct value for charges, a fine fft mesh is used. This is achieved by changing the NG (X, Y, Z) F flags in INCAR [48].

3

Computational Methods & Automation Strategy

In this chapter, the roadmap of the calculations, methodology, and automation scripts are explained.

3.1 Roadmap of calculations

In this thesis work, calculations are made in four different ways:

- **Interaction of adsorbents with Single Metals:** In these calculations, the energy and geometry of the adsorbents, H, N and CO on the SMAs were studied. These calculations are expected to give the effect of the 3NG substrate on the SMA catalytic activity. The SMAs were placed in a 15x15x15Å box, and the adsorbent interactions were studied in different geometries, as will be explained in the following sections. The lowest energy among these orientations are recorded, and the bond distances are recorded. These bond distances are used as initial geometries for further studies of single metal cations (SMC) with adsorbents and SACs with adsorbents.
- **Interaction of adsorbents with Single Metal Cation:** When the metal atom is anchored on 3NG sheet, it is expected to become a positively charged centre. To learn These calculations, compare the E_B of the adsorbents on the SMCs and 3NG. This study is done to see if the SMC mimics the adsorbent surface interaction on the SAC. This way, the effect of substrate on the SAC activity can be studied in greater depth.
- **Optimization of Graphene:** The 3NG for the following calculations are made from the graphene bulk downloaded from the Materialsproject website [50]. The constructed surface is optimized as explained in the methodology and results section.
- **Optimization of metal on 3NG:** The optimization of metal on 3NG is done by varying the ISIF values. Two methods are adapted to calculate the $E_{B.}$ In the first method, E_B is calculated using the SMA energy as the reference energy of metal atom. In the second method, the interaction between the metals is also taken into consideration. The SMAs on the 3NG sheet might agglomerate on the surface of the graphene sheet[26]. To check this, the E_B of the metals is found out with respect to the metal-metal interaction energy instead of the SMA energy explained earlier. The metal-metal interaction energy is obtained from the cohesive energy of the metal bulk.
- **Interactions of adsorbents with metal doped 3NG**: This study predicts the novel SAC for the above-mentioned reactions. To mimic the SAC as an electrocatalyst, studies are done on the catalyst surface with an extra electron also. It is to be noted that these calculations are done on the SMAs which do not agglomerate on the surface of the catalyst.

- **Interactions with the surface slabs of conventional metal catalysts:** As mentioned in Motivation and Scientific background, the novel SACs are predicted by comparing the E_B of the SACs to that of descriptors on conventional bulk catalysts. For this comparison, the E_B of the descriptor species is calculated on the bulk catalyst, namely E_B of H on Pt(111) slab for HER, E_B of N on Ru(0001) slab for N_2RR, E_B of CO on Cu(111) slab for CO_2RR.

As mentioned in the Research Aim, the E_B of adsorbents is calculated for all the metals and semi-metals in the periodic table. This results in a total of approximately 3000calculations. To do such a huge number of calculations, the files and the folders must be arranged carefully to prevent human errors. For this purpose, the folders were arranged as shown in Figure 3-1. It is to be noted that this file arrangement is only depicted for the SM, SMC and 3NG- adsorbent calculations. This file system used for Bader charged calculation and slab catalysts are similar to the one showed in Figure 3-1.

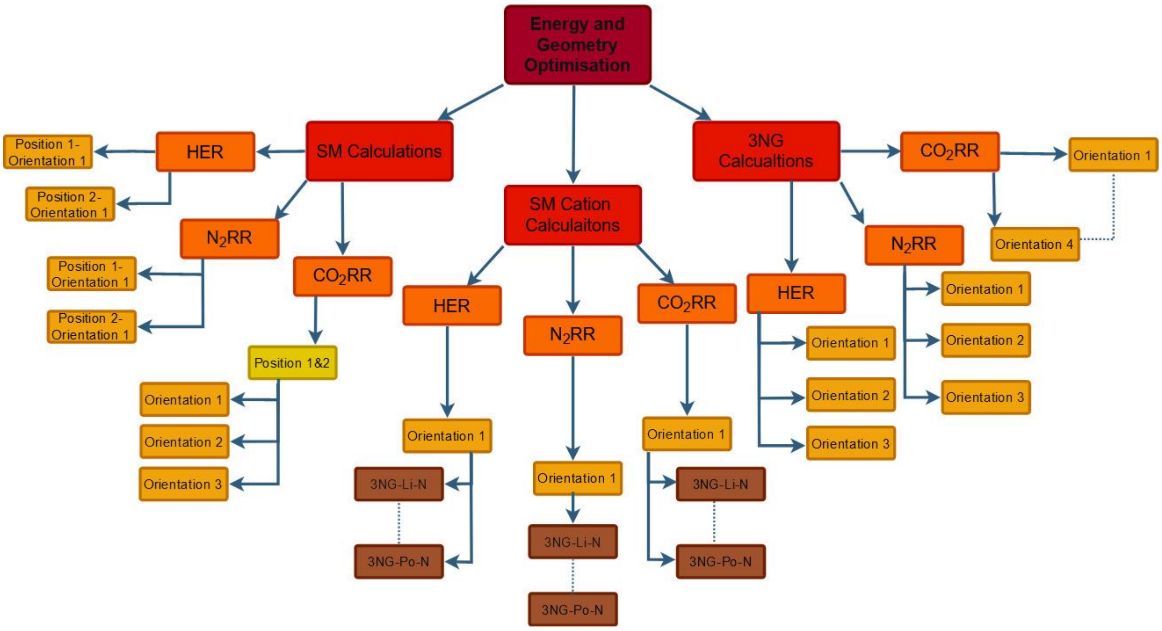
Energy and Geometry Optimisation
SM Calculations
SM Cation Calculaitons
3NG Calcualtions
HER
N2RR
CO2RR
Position 1-Orientation 1
Position 2-Orientation 1
Position 1&2
Orientation 1
Orientation 2
Orientation 3
Orientation 4
3NG-Li-N
3NG-Po-N

Figure 3-1File arrangement used in hard disk: This figure depicts how files are arranged for energy and geometry optimization.

3.2 Input orientations and positions of the adsorbents on the various catalyst surfaces

To find the lowest possible binding energy on the catalyst surface, different orientations and positions of the adsorbent must be tried. This will make sure that the results obtained are not local minims and makes sure that the final geometry is accurate. These orientations are explained in the following sections.

3.2.1 Input orientations and positions of adsorbents on single metal atoms

In this section, the orientation of adsorbents on SMAs are discussed. For the single atom adsorbents like H and N, there are no different orientations since the single atoms are symmetrical. For the CO molecule, three different orientations were tried and shown in the Figure 3-2.

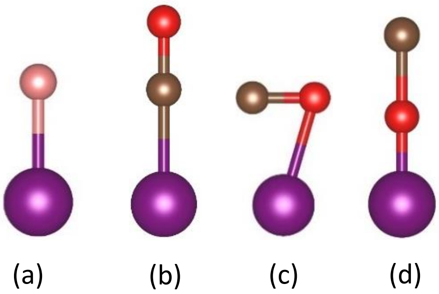

Figure 3-2: Input orientation of adsorbents on the SMAs: (a) Orientation of H/N on the SMAs. (b) Orientation of CO on the SMA with CO on SMA. (c) CO parallel to the SMA (d) CO on top of the SMA with oxygen closer to the SMA substrate.

The calculations are done on SMAs with two input distances i.e. adsorbents are 2Å and 1.5 Å from the SMA (before optimization). This is done to avoid the local minima in energy, which leads to an erroneous result. For the mono-atomic adsorbents on the SMAs, only one orientation is tried because both the adsorbent and the substrate are (assumed to be) spherical. For CO, three different orientations are tried, and the optimization that yields the lowest energy of them is saved to the final results. Most importantly, the output bond-distance of these calculations are used as input for the subsequent calculations namely- 3NG calculations and SMC calculations e.g. if the Cu-H output bond-distance is 1.8A, then the input H atom on 3NG-Cu is placed at 1.8A from the Cu atom. I have found that this yields accurate results faster.

3.2.2 Orientation of adsorbents on 3NG

Various orientations of the adsorbents must be considered to arrive at the accurate energy value during the calculations. For this the adsorbents were placed at different orientations on the catalyst surface. The orientations of the H/N adsorbent on the surface is shown in the Figure 3-3.

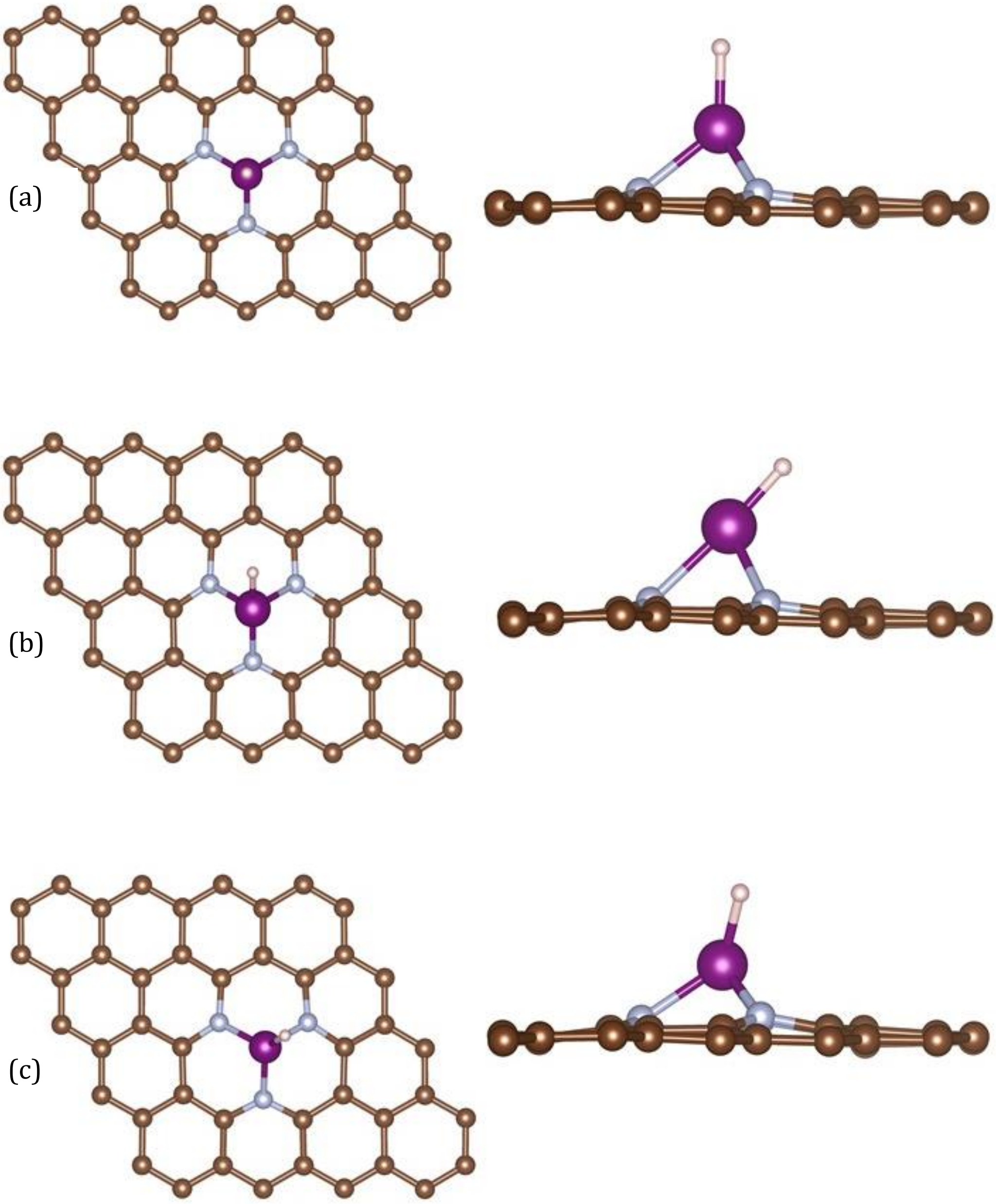

Figure 3-3 Orientations of adsorbent H atom on catalyst surface: (a) Shows the H/N atom adsorbed on top of the single metal atom (b) Shows the H/N atom adsorbed at an angle of 45^0 to the catalyst surface and in the direction of the hollow site of graphene (c) Shows the H/N atom adsorbed at an angle of 45^0 to the catalyst surface and in the direcction of N atom.

Since CO is a diatomic molecule, in addition to the three combinations depicted above, an additional geometry with the C atom on top of the metal, but the oxygen atom is at an angle to the catalyst surface. All the geometries of CO on the surface is shown below in figure 3-4.

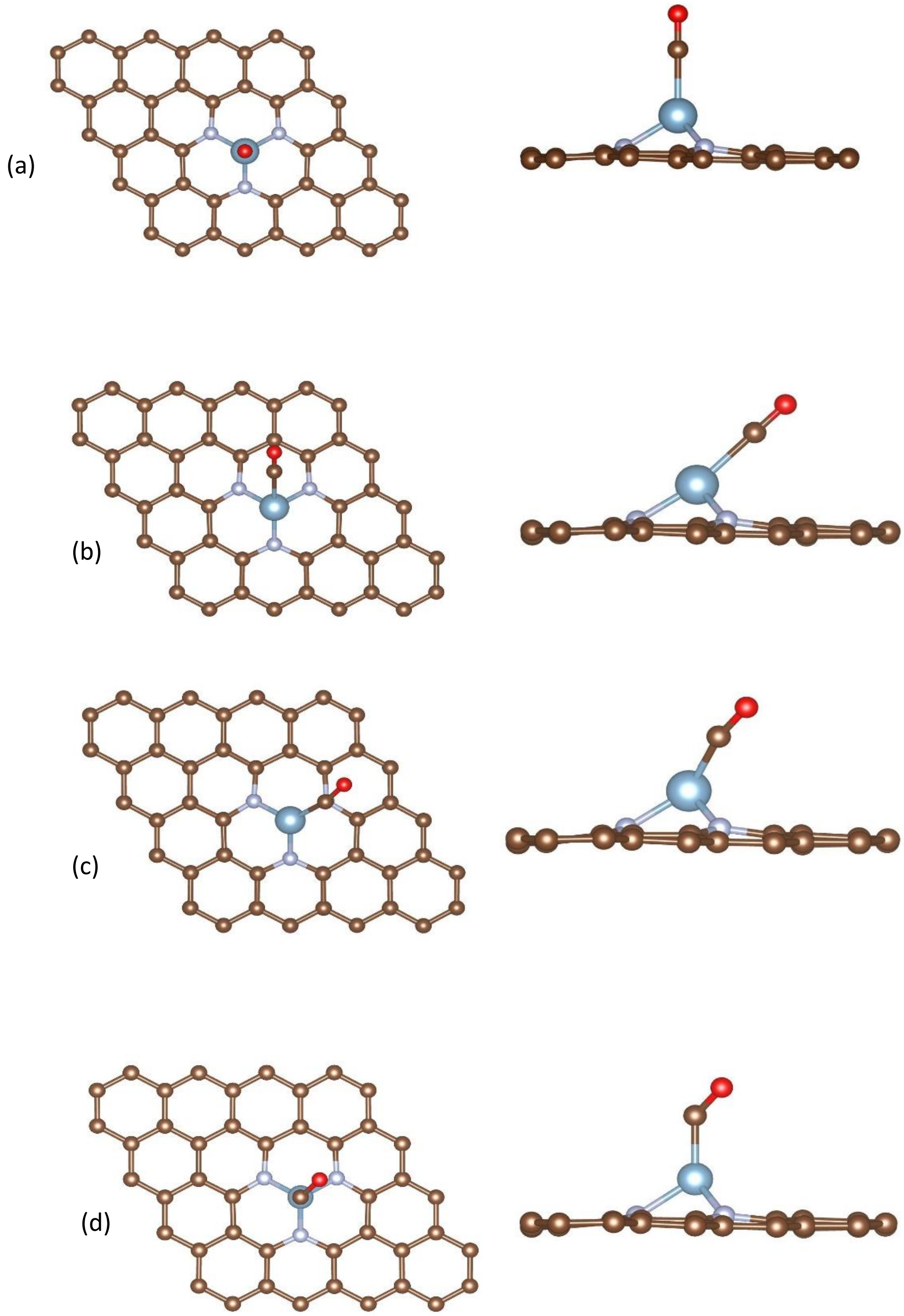

Figure 3-4Orientations of CO on the 3NGM: (a) CO on top of metal atom (b) CO in the direction of hollow site in 3NG and (c) CO in the direction of nitrogen atom doped on the graphene sheet. (d) is the extra orientation only for CO- Oxygen is at a 45^0 angle to the carbon atom.

3.3 Methodology

Vienna Ab initio Simulation Package was used to perform all the DFT calculations in this thesis. The Projector Augmented Wave (PAW) pseudopotentials for electron-ion interactions along with Revised Perdew-Burke-Ernzerhof (RPBE) exchange and correlation approximations were used for all the calculations. The 4x4x1 graphene supercell with a 15x15x15Å vacuum space was used to avoid the periodicity in the *z-direction*. A kinetic energy plane-wave basis set of 400 eV was used for all the calculations, and the convergence criteria for structural optimizations were that the force acting on each atom was smaller than 0.02ev/Å. The Brillouin zone of the system under consideration was sampled using an 8x8x1 k-point sampling. The cut-off energy and k-point sampling used are optimized for the 3NG sheet. This will be discussed in depth in the Results and Discussions. All the calculations were spin-polarized. Nevertheless, metals such as Cs and In did not converge on the addition of spin polarization. Hence, spin polarization was not considered for these cases. The binding energy of metal on 3NG with respect to SMA energy is given by:

$$E_{\mathrm{B}}^{\mathrm{3NG-M}} = E_{\mathrm{3NG-M}} - E_{\mathrm{3NG}} - E_{\mathrm{SM}} \tag{37}$$

Where E_B^{3NG-M} is the E_B of the metal on 3NG, E_{3NG-M} is the energy of metal adsorbed 3NG (obtained from VASP calculations), $\mathrm{E_{3NG}}$ is the Energy of 3NG and, E_SM is the energy of the SMA in the gas phase.

The E_B of the metal on 3NG with respect to cohesive energy of the metal is given by:

$$E_{\mathrm{B}}^{\mathrm{M}} = E_{\mathrm{3NG-M}} - E_{\mathrm{3NG}} - E_{\mathrm{cohesiveSM}} \tag{38}$$

Where the $E_\mathrm{cohesiveSM}$ is the cohesive energy per metal atom

The cohesive energy is calculated by optimizing the metal bulk and dividing the obtained energy by the number of atoms in the bulk structure. This is given by the equation:

$$E_{\mathrm{cohessive\ M}} = \frac{E_{\mathrm{Mbulk}}}{number\ of\ metal\ atoms\ in\ bulk} \tag{39}$$

Where E_Mbulk is the energy of the metal bulk lattice.

The binding energy of the H atom on the metal adsorbed 3NG (3NGM) is given by

$$E_{\mathrm{B}}^{\mathrm{3NG-M-H}} = E_{\mathrm{3NG-M-H}} - E_{\mathrm{B}}^{\mathrm{M}} - 0.5 * E_{\mathrm{H2}} \tag{40}$$

Where$E_{\mathrm{B}}^{\mathrm{3NG-M-H}}$ is the $\mathrm{E_B}$ of the H atom on 3NGM, $E_{\mathrm{3NG-M-H}}$ is the energy of Hydrogen on 3NGM and, E_{H2} is the energy of the $\mathrm{H_2}$ molecule in the gas phase.

The binding energy of N atom on 3NGM is given by

$$E_{\mathrm{B}}^{\mathrm{3NG-M-N}} = E_{\mathrm{3NG-M-N}} - E_{\mathrm{B}}^{\mathrm{M}} - 0.5 * E_{\mathrm{N2}} \tag{41}$$

Where$E_{\mathrm{B}}^{\mathrm{3NG-M-N}}$ is the E_B of the N atom on 3NGM, $E_{\mathrm{3NG-M-N}}$ is the energy of N on 3NGM and, E_{N2} is the energy of the $\mathrm{N_2}$ molecule in the gas phase.

The binding energy of CO molecule on 3NGM is given by

$$E_{\mathrm{B}}^{\mathrm{3NG-M-CO}} = E_{\mathrm{3NG-M-CO}} - E_{\mathrm{B}}^{\mathrm{M}} - E_{CO} \tag{42}$$

Where$E_{\mathrm{B}}^{\mathrm{3NG-M-CO}}$ is the E_B of the CO molecule on 3NGM, $E_{\mathrm{3NG-M-CO}}$ is the energy of N CO on 3NGM (obtained from VASP calculations) and, E_{CO} is the energy of the CO molecule in the gas phase.

For single metal calculations, the binding energy of H on SM is given by

$$E_{\mathrm{B}}^{\mathrm{SMH}} = E_{\mathrm{SM-H}} - E_{\mathrm{SM}} - 0.5 * E_{\mathrm{H2}} \quad (43)$$

Where, E_B^{SMH} is the E_{B} of the H atom on SMAs, E_{HSM} is the energy of H on SMA.

The binding energy of N atom on SMs is given by

$$E_B^{SMN} = E_{NSM} - E_{SM} - 0.5 * E_{N2} \quad (44)$$

Where, E_B^{SMN} is the E_{B} of the N atom on SMA, E_{NSM} is the energy of N on SMA.

The binding energy of CO molecule on SMs is given by:

$$E_B^{SMCO} = E_{COSM} - E_{SM} - E_{CO} \quad (45)$$

Where, E_B^{SMCO} is the E_{B} of the CO molecule on SMAs, E_{COSM} is the energy of CO on SMA.

The E_{B} for the charged scenario will be explained in the following section.

The code from the Henkelman group [48] was used to make Bader charge calculations. While using the code, a fine Fast Fourier Transform grid was also used to evaluate the correct Bader volumes. NGXF=NGYF=NGZF=400 was used for all the calculations. All the other parameter was kept unchanged for these set of calculations.

3.3.1 Methodology for Vacuum correction for non-neutral calculations

When the metals are immobilized on the graphene sheet, they act as positive-charged centers. To calculate this effect of metals as positive-charged centers on the graphene sheet, the E_{B} of H, N, and CO on the positively charged single metal (SM) is calculated. To account for the total number of electrons that are different from that of the neutral surface, VASP adds a homogeneous background charge and proceeds with the calculation. However, this by itself is not sufficient to yield an accurate result because, when the system is not neutral, there will be an additional Coulomb interaction, which leads to erroneous results. To correct this error, the ideal way is to calculate the energy for a cell with an infinite vacuum, which cannot be done in VASP. Hence the next way is to calculate the energies for the system with different vacuum values, e.g., 15 Å, 30 Å, 45 Å 60 Å, etc. and to extrapolate these energies to infinite vacuum [51]. Tezsevin et al. proved that the application of periodicity corrections has a significant impact on the results, and it is necessary to only correct the periodicity errors for an additional vacuum length other than 15 Å. In addition to this, Bal et al. has shown that the for charged surfaces (for 2-D surfaces), the adsorption energy is proportional to the inverse of vacuum spacing (L^{-1}) between slabs [52]. Hence, a plot with adsorption energy v/s the L^{-1} is made, and the energy at infinite vacuum value is found out from the plot. The following equation is used to find out the corrected energy,[51]:

$$E_{corrected} = E_2 - m * \frac{1}{L_2} \quad (46)$$

Where m is the slope of the curve E_{B} v/s $\frac{1}{L}$.

$$m = \frac{E_2 - E_1}{\frac{1}{L_2} - \frac{1}{L_1}} \qquad (47)$$

Where E_1 and E_2 are energies corresponding to L_1 and L_2 (15 Å and 30 Å length), respectively.

For the case of charged species calculations on single metal cation (cation-adsorbent interaction), the NELECT tag was added to INCAR, and a suitable NELECT was defined based on the following equation:

$$NELECT = \left(\sum_{1}^{N} n_N \times (number\ of\ electrons\ in\ POTCAR) \right) - 1 \qquad (48)$$

Where *N* is the number of the total number of atoms in the simulation cell, and n is the number of atoms included for species N in the POSCAR file.

For the single metal cation (SMC)-adsorbent interactions, the geometry and energy optimization was done on vacuum sizes of 15x15x15 Å and 30x30x30 Å to account for the Columbic interaction.

The submission scripts, sample input files for all these calculations are given in the Appendix.

The code from the Henkelman group [48] was used to make Bader charge calculations. While using the code, a fine Fast Fourier Transform grid was also used to evaluate the correct Bader volumes. NGXF=NGYF=NGZF=400 was used for all the calculations. All the other parameter was kept unchanged for these set of calculations.

3.4 Calculation of H, N, and CO energies

To calculate the gas phase energies of the H, N, and CO species, the H_2, N_2, and CO molecules are placed in a 15x15x15 A vacuum box, and the energies are calculated. The gas-phase energies of H and N, E_H and E_N are calculated as follows:

$E_H=0.5*E_{H2}$

$E_N=0.5*E_{N2}$.

The remaining parameters, like ENCUT and KPOINTS, remain same for these calculations.

3.5 Automation scripts and file handling

In this section, the necessity of automation codes and few codes with examples will be explained. As mentioned earlier, the E_B of adsorbent on the catalyst surface is calculated for carried out for all the metals and semimetals in the periodic table (immobilized on 3NG substrate). Making all the input files manually for the whole calculation set is a tedious task. To give an idea of the scale of the calculations carried out, the number of calculations is shown below.

The number of calculations on the catalytic substrate, N

$$N= N_p*N_o*N_R*N_M \quad (49)$$

Where N_p is the various number of positions tried,

N_o is the total number of orientations of various adsorbents

N_R is the number of times the optimization had to be carried out; Metal on 3NG was optimized five times before the final value was reached

N_M is the number of metals = 52 for all the calculations

Table 2 shows the values of the above-mentioned variables for different calculations in the thesis.

Table 2: The total number of calculations done in this thesis

Substrate	N_p	N_o	N_R	N_M	Total Calculations (using equation 50)
SMA	2	5	1	52	520
SMC	1	3	2	52	312
3NG–metal optimization	1	1	5	52	260
3NGM-adsorbant	1	10	1	52	520
Bader Calculations	1	10	1	52	530
The calculation to find out cohesive Energy	1	1	5	52	260
Total number of calculations					2392
Total number of files					9568

To avoid any errors and to reduce the workload in the process of preparing the input, the calculation submission and result dataset analysis were automated. For all the calculations done on SM, SMC, and 3NG substrates, a multi-step approach was used to carry out the calculations, as shown in Figure 3-5. This flow diagram is followed for the calculations. The first set of calculations done in any substrate is the energy calculation (i.e., finding the adsorption energy of adsorbent on the substrate); after this, the d-orbital of the optimized energy and geometry is found out using the DOS calculations. Following this, the Bader calculations are done to find the charge dissipation of adsorbent on the substrate. The automation scripts are explained using the codes used for HER as an example.

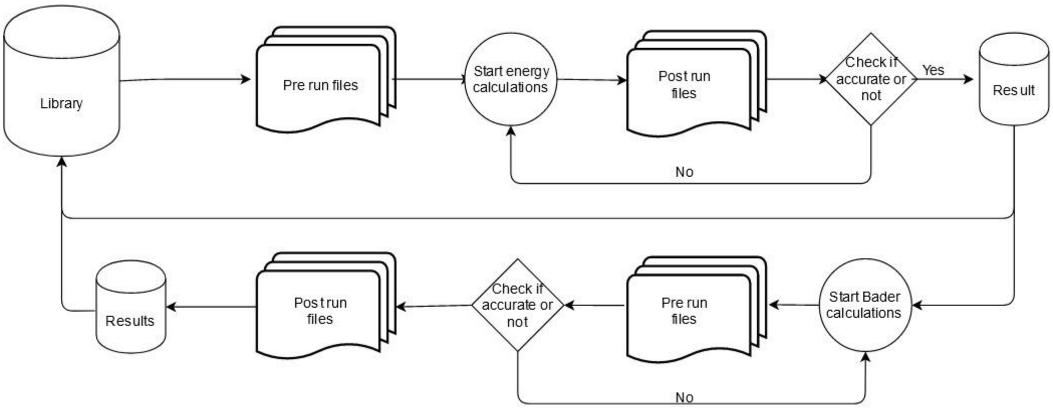
Library
Pre run files
Start energy calculations
Post run files
Check if accurate or not
Yes
Result
No
Start Bader calculations
Pre run files
Check if accurate or not
No
Post run files
Results

Figure 3-5 Flow chart of automated SM, SMC and 3NG calculations

3.5.1 Pre-run files for energy calculations

In this section, the scripts developed for making the pre-run files are discussed in detail. This contains preparing the POSCAR, POTCAR INCAR, and KPOINTS and submitting these files to the computing cluster to run the calculations.

3.5.1.1 Script for Hydrogen on top orientation - HER

The pre-run files are the directories with files before the calculations start. These are the "*orientation 1*" or various other orientation directories, as shown in Script 1. The script makes the metal directories (the 3NG-Li-N and other) and the respective POSCAR, POTCAR, INCAR, and KPOINTS. To make the metal directories, a list is created in the Library with all the metals on which the calculations are done. Every HER/N_2RR/CO_2RR folder contains "*runscript"* file, which makes the required files and submits the calculations. The *runscript* written in *bash* for the HER calculations (for the top orientation) is shown below:

```
#! /bin/bash
# Code to automatically submit H on metal calculations
# the graphene layer is optimised in the previous step
# Author Narasimhan Viswanathan
while IFS=, read -r Metal bonddist; # reads the metal list (The ‘Metal”
reads the name of the metal immobilized on 3NG and bonddist reads the
bond-distance of the adsorbent to the single metal atom)
do
mkdir 3NG_top _H_${Metal}     #makes the directory-orientation-top
cd 3NG_top_H_${Metal}
cp ~/bin/POSCAR_3NG_H .       # makes POSCAR files
source POSCAR_3NG_H
cp ~/bin/pot_H .              # makes POTCAR files
source pot_H
cp ~/DIFFER/thesis/Library/INCAR ./INCAR # copies INCAR
cp ~/DIFFER/thesis/Library/KPOINTS . # copies KPOINTS
# begin submit script
cat >submitvasp<<!
#! /bin/bash
#PBS -l nodes=1:ppn=12:mse
##PBS -q guest
#PBS -m ae
#PBS -m abe
#PBS -M N.Viswanathan@differ.nl
#PBS -N ${Metal}_3NG_H
module load vasp
cd \$PBS_O_WORKDIR
echo \$PBS_O_WORKDIR
echo "vasp isgoing to run " >> log.txt
mpirun vasp
echo "\$line", \$(grep y= OUTCAR | tail -c 19)>>../energies_top_H.csv
# After the calculation are done, the energy is copied to a csv file
done
!
# end submit script
qsub submitvasp #submits the calculation to the sever
cd .. #return to the parent directory
done < ~/DIFFER/thesis/Library/metals_BD.csv #List of metals and the
corresponding bond distances file in Library
```

Script 1: Script to automatically submit H on metal calculations after creating the POSCAR and POTCAR according to the list of the metals.

The CONTCAR file contains information regarding the cell shape, size, and the position of atoms. This file is written by VASP software in direct co-ordinates. This CONTCAR file of 3NG-M optimization is to be converted to cartesian coordinates and copied from the 'contcars' directory. Once this is done, the metal coordinates are recorded as mx, my, and mz, respectively. To find out the position of adsorbent H on the metal atom, the mz value is added to the Metal-Adsorbent bond-distance and written to the new POSCAR file. The POSCAR_3NG_H script is as in script 2:

```
#! /bin/bash
# Code to generate the POSCAR file for a specific metal for the Top
orientation

cp ~/DIFFER/thesis/Library/3NG_metal/contcars/CONTCAR_$Metal ./POSCAR
#Copies the optimized CONTCAR of metal immobilised on graphene as POSCAR
to the current directory
sed -i '6s/.*/C N '"${Metal}"' H/' POSCAR
sed -i '7s/.*/28 3 1 1 /' POSCAR
mz=$(cat POSCAR | sed -n '40p'| tail -c 19)
z=$(cat POSCAR | sed -n '5p'| tail -c 20)
mx=$(cat POSCAR | sed -n '40p'| cut -d' ' -f3)
my=$(cat POSCAR | sed -n '40p'| cut -d' ' -f5)
hz=$( echo "scale=11; $mz+$bonddist/$z" |bc)
sed -i '40 a '"${mx}"' '"${my}"' '"${hz}"' ' POSCAR #Writes the calculated
co-ordinates to POSCAR
```

Script 2: Script to make the POSCAR file for the H atom on top of the metal anchored on 3NG

It Is noteworthy that the POTCAR file is concatenated in the same order of elements as in POSCAR file (in script 2). KPOINTS and INCAR are the same for all the calculations. hence they are copied from the Library directory. The POSCAR_3NG_H script is as follows:

cat ~/Library/POTCAR_C ~/Library/POTCAR_N ~/Library/POTCAR_H ~/Library/POTCAR_${metal} >>POTCAR

3.5.1.2 Pre-run script logic for Orientations 2 and 3

For orientation two and orientation 3, the adsorbent atom/molecule must be at 45°, in two different directions (as shown in Figure 3-5). To generate the POSCARS automatically, the atoms should be considered as points, the atomic positions as the cartesian points, and the bonds as vectors. The magnitude of such a vector will be the bond length between the adsorbent species (i.e., C–M, H–M, or N–M). The adsorbent is at an angle of 45° to the *z-axis*. This means that the *z co-ordinate* of both the orientations (2&3) will be

$$BD_z = BD * \sin(45^o) \tag{50}$$

For orientation 2 the adsorbent is in the direction of the diametrically opposite carbon atom. From Figure 3-3, the x-coordinate of the metal and the adsorbent is the same. This means that the BD contribution from the vector in y-direction or the *y coordinate* is the same as that of BD_z, which makes it:

$$BD_y = BD * \sin(45^o) \tag{51}$$

For orientation 3, the adsorbent atom is the direction to the nitrogen atom of 3N-G. It is to be noted that the triangle formed by the three nitrogen atoms is equilateral. When the adsorbent is adsorbed in the direction of nitrogen atom, the vector is bisecting the corner of the equilateral triangle as shown in

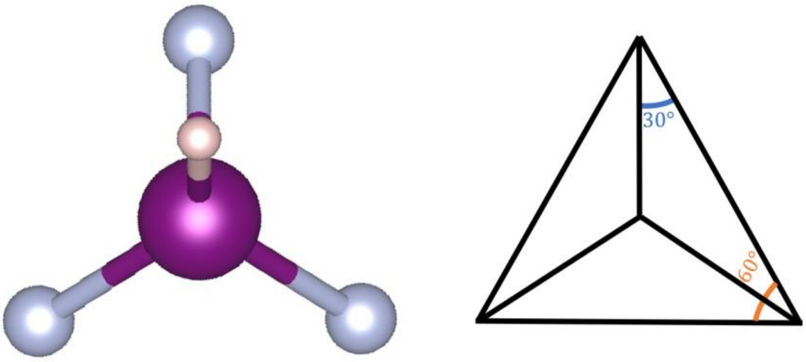

Figure 3-6 Figure showing the angle of the adsorbent species 3NGM in the direction of the nitrogen atom. The adsorbent species is dissecting the corner angle of the equilateral triangle. This means that the adsorbent species is at 45° to the z-axis and 30° each to the x-axis and y-axis

Since the z coordinate of the adsorbent species is as shown in equation (50), this will make the x-coordinate of the adsorbent species as:

$$BD_x^N = BD * \sin(45^o) * \cos(30^o) \tag{52}$$

Furthermore, the y co-ordinate as:

$$BD_y^N = BD * \sin(45^o) * sin\ (30^o) \tag{53}$$

The script for generating the POSCAR is updated with the above equations, following which the *runscritpt* is updated accordingly. This is shown in Appendix

3.5.2 Post-run files and accuracy check for energy calculations

After the calculations are finished, the files will be present in the working directory. The energy values are searched using a script and written to the "energy.csv" file. This is done after it is made sure that the calculations have reached the required accuracy. To check the accuracy of the completed calculation, the keywords *'required accuracy'* is searched for in the OUTCAR. The following script is used for this:

```
#! /bin/bash
#Code to check if the calculations have reached the required accuracy or
not. If the calculation has reached the required accuracy, then
the name of the directory is printed to a file 'list'; if not, it is
printed to the 'tobererun' file.
rm accuracy
rm list
rm tobererun
path=pwd
for d in 3NG_*
do
        cd $d
        echo "$d" $(grep -r accuracy OUTCAR) >> ../accuracy
        if grep -q accuracy OUTCAR ; then
                echo "$d" >> ../list
        else
                echo "$d" >> ../tobererun
        fi
        cd ../

done
```

Script 3: Script to check the accuracy of a calculation

Since Script 3 is a utility script, the script must be changed according to the folder name. Script 3 can also be included in the calculation submission script to check for accuracy- this way, the output files will only be available once the calculation has reached the required accuracy. To avoid losing the files, a separate script for accuracy check was used throughout the thesis. Once the accuracy check is done, the output files (the CONTCAR, CONTCAR.xyz, and the energy.csv files) are copied to the Library. The energies are searched for a specific orientation using script 4. To extract the energy values from the OUTCAR, we search the last line of the search results for *'y='* in OUTCAR.

```
#! /bin/bash
# Code to search for the energies from the converged calculations
rm energies_grp.csv
cat ~/DIFFER/thesis/Library/metals_groep | while read line
do
        cd 3NG_${line}
        echo "$line", $(grep y= OUTCAR | tail -1 | tail -c 19) >>
../energies_grp.csv
        cd ..
done
```

Script 4: Script to extract energy values from the output file

The geometries of the converged calculations should also be checked along with the energies. The geometries provide insight into the trend of adsorption at the same time revealing if the adsorbent atoms remain stuck to the catalyst surface. The geometries were analyzed in Maestro, which is part of the Schrödinger software suite[53]. With Schrodinger, it is easy to visualize all the geometries of a particular orientation in a tile format. The input formats must be converted from VASP to .xyz files. The following script is used to convert the CONTCAR to CONTCAR.xyz:

```
#! /bin/bash
# Code to convert the direct coordinates to cartesian coordinates
# Input- POSCAR file in direct coordinates
# Output- POSCAR file in cartesian coordinates
rm POSCAR_tmp
head -n 8 POSCAR_direct > POSCAR
ct=9
while [ ${ct} -le 40 ]
do
        line=${ct}p
        jnk=${ct}
        xd=$(cat POSCAR_direct | sed -n $line | awk '{print $1}')
        yd=$(cat POSCAR_direct | sed -n $line | awk '{print $2}')
        zd=$(cat POSCAR_direct | sed -n $line | awk '{print $3}')
        a1uc=$( cat POSCAR_direct | sed -n 3p | cut -d' ' -f6)
        b1uc=$(cat POSCAR_direct | sed -n 4p | cut -d' ' -f5)
        b2uc=$( cat POSCAR_direct | sed -n 4p | cut -d' ' -f9)
        c3uc=$( cat POSCAR_direct | sed -n 5p | cut -d' ' -f13)
        xc=$( echo "scale=10; ${xd}*${a1uc}+${yd}*${b1uc}" | bc -l)
        yc=$( echo "scale=10; ${yd}*${b2uc}" | bc -l)
        zc=$( echo "scale=10; ${zd}*${c3uc}" | bc -l)
        #sed -i '$jnk a '"${xc}"' '"${yc}"' '"${zc}"' ' POSCAR
        echo $xc $yc $zc >> POSCAR_tmp
        let "ct++"
done
head -n 32 POSCAR_tmp >> POSCAR
```

Script 5: Script to convert POSCAR co-ordinates for VASP to POSCAR in xyz (cartesian) coordinates

In the above scripts, the POSCAR_direct or the CONTCAR is copied as POSCAR/CONTCAR, and a temporary file POSCAR_tmp is made. After this, the x, y, and z direct co-ordinates from the files are stored as xd, yd, and zd (‘d’ stands for direct). The cartesian coordinates are the product of (xd, yd, and zd) and the unit cell parameters (a1uc, b1uc, b2uc, and c3uc).

After this, to prepare the graphs, the lowest energy of all the orientations is extracted, and the graphs are prepared. For this, an automated script is made, where the graphs are made. All the graphs shown in this thesis are made with these scripts.

4

Results & Discussions

As mentioned previously, various kinds of calculations were carried on different kinds of substrates in this thesis work, namely, energy calculations, energy calculations with Coulombic interactions, and Bader charge calculations. In this section, the results obtained from these calculations will be shown, and the novel SACs predicted from these calculations will be validated using the available experimental data.

4.1 Calculation on Slab catalysts

To predict the novel SACs, the obtained E_Bs are compared against the $E_{Bslab,}$ as mentioned previously. To carry out calculations on the slab, the first step is to optimize the bulk metals. From Table 3, the experimental lattice parameters and the lattice parameters in this work agree with each other. It should also be noted that for the sake of comparison, the bulk catalyst calculations were also carried out with the same parameters as that of SACs.

Table 3: Comparison of lattice parameters from experiments and this work

Metal	Space group & #	Bulk Lattice Parameter (Å)	
		Experimental	**This work**
Ru	*P63/mmc* – 194	4.28 [54]	4.30
Pt	*Fm-3m* – 225	3.92 [55]	4.00
Cu	*Fm-3m* – 225	3.61 [56]	3.68

The E_B of H atom on the Pt (111) surface is calculated as -0.29 eV, E_B of N atom on the Ru(0001) surface is calculated as -1.00eV, and the E_B of CO on the Cu(111) slab is estimated as -0.45 eV. These calculated E_Bs are the benchmark values against which the E_B of adsorbents on SACs are compared to predict the novel SACs.

4.2 Binding Energy of adsorbents on Single Metal Atoms

In this section, the E_B of adsorbents on SMA is explained. As explained in the earlier sections, the calculations are done initially on the SMA substrates.

To avoid the saddle points in the calculations, the H atom is adsorbed at 2A and 1.5A from the surface of the SMA. These results yielded almost similar energies for both the cases. For the metals with different energies for the above-mentioned inputs, the lowest energy is taken as the final value. The final energies of adsorption for all the different adsorptions are shown in Figures 4-1 – 4-3.

For hydrogen adsorption on SMA, *s-block* elements have positive binding energy. This does not mean that they are not interacting with the hydrogen atom, but that the interaction is very weak. For the case of Cs and Ba, ea It can be clearly seen that *d-transition* metals and B atom bind the H atom the strongest compared to the other metals. It can also be seen that the *s-block* metals have positive E_B. The E_B are positive because of the weak interaction between the adsorbent and metal atom. The E_Bs are calculated using the following equation

$$E_B^{SMA-H} = E_{Hads} - E_{SM} - 0.5 * E_{H2}$$

Where E_{Hads} is the energy of H atom adsorption energy on the SMA.

E_{SM} is the energy of the single metal atom and E_{H2} is the energy of H_2 molecule.

The adsorption of N and CO also show a same trend for *d-transition* metals.

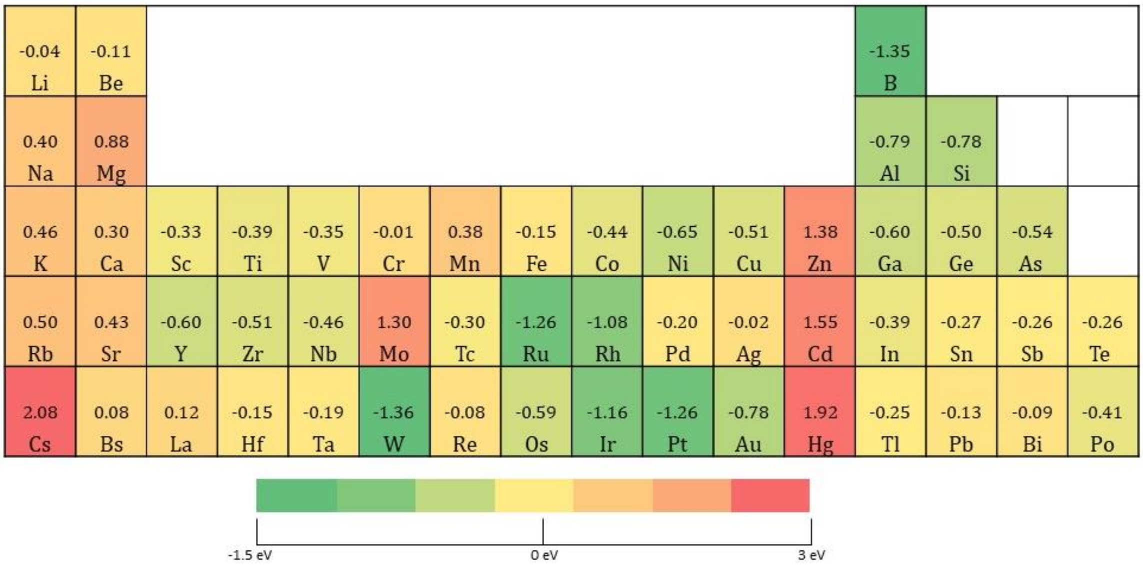

-0.04 Li	-0.11 Be											-1.35 B			
0.40 Na	0.88 Mg											-0.79 Al	-0.78 Si		
0.46 K	0.30 Ca	-0.33 Sc	-0.39 Ti	-0.35 V	-0.01 Cr	0.38 Mn	-0.15 Fe	-0.44 Co	-0.65 Ni	-0.51 Cu	1.38 Zn	-0.60 Ga	-0.50 Ge	-0.54 As	
0.50 Rb	0.43 Sr	-0.60 Y	-0.51 Zr	-0.46 Nb	1.30 Mo	-0.30 Tc	-1.26 Ru	-1.08 Rh	-0.20 Pd	-0.02 Ag	1.55 Cd	-0.39 In	-0.27 Sn	-0.26 Sb	-0.26 Te
2.08 Cs	0.08 Bs	0.12 La	-0.15 Hf	-0.19 Ta	-1.36 W	-0.08 Re	-0.59 Os	-1.16 Ir	-1.26 Pt	-0.78 Au	1.92 Hg	-0.25 Tl	-0.13 Pb	-0.09 Bi	-0.41 Po

Figure 4-1: Heatmap of E_B^H on the SMAs.

Figure 4-2 Shows the heatmap of E_B of N atom on the SMAs. The results are similar to that of H adsorption on SMAs. The *s-block* metals interact weakly with the SMAs, the *d*-block elements interact the strongest compared to all the other elements in the periodic table. However, it is notworthy that N atom interacts stronger with the *d-block* atoms towards the left of the periodic table, while H interacts weakly with these atoms.

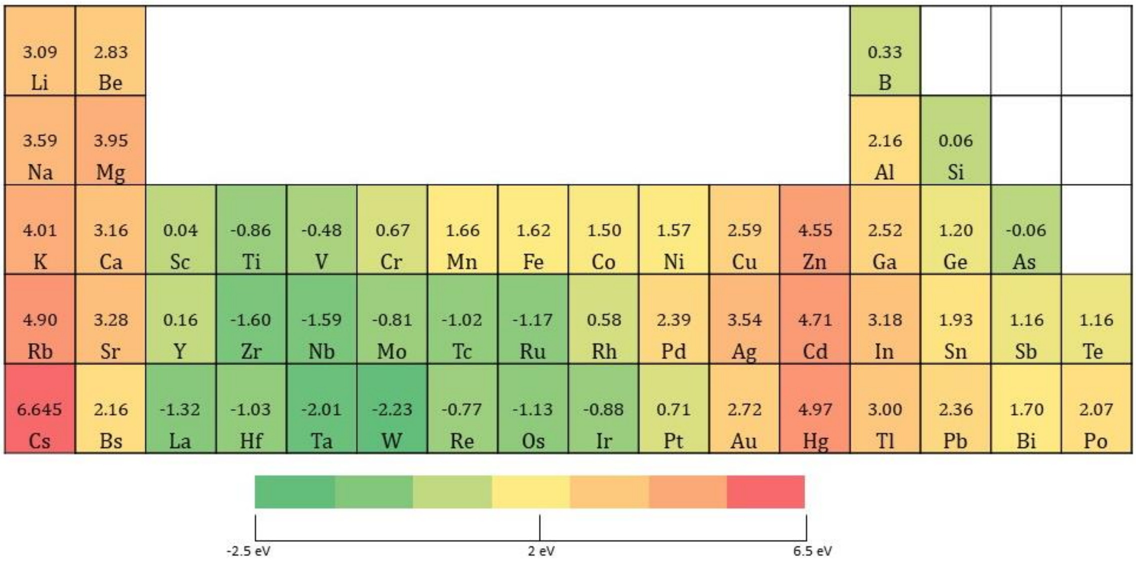

3.09 Li	2.83 Be											0.33 B			
3.59 Na	3.95 Mg											2.16 Al	0.06 Si		
4.01 K	3.16 Ca	0.04 Sc	-0.86 Ti	-0.48 V	0.67 Cr	1.66 Mn	1.62 Fe	1.50 Co	1.57 Ni	2.59 Cu	4.55 Zn	2.52 Ga	1.20 Ge	-0.06 As	
4.90 Rb	3.28 Sr	0.16 Y	-1.60 Zr	-1.59 Nb	-0.81 Mo	-1.02 Tc	-1.17 Ru	0.58 Rh	2.39 Pd	3.54 Ag	4.71 Cd	3.18 In	1.93 Sn	1.16 Sb	1.16 Te
6.645 Cs	2.16 Bs	-1.32 La	-1.03 Hf	-2.01 Ta	-2.23 W	-0.77 Re	-1.13 Os	-0.88 Ir	0.71 Pt	2.72 Au	4.97 Hg	3.00 Tl	2.36 Pb	1.70 Bi	2.07 Po

-2.5 eV
2 eV
6.5 eV

Figure 4-2: The heatmap of atom $E_{\mathrm{B}}^{\mathrm{N}}$ on various SMAs.

Figure 4-3 shows the E_{B}^{CO} on the SMAs. The trend is very similar to that of hydrogen adsorption on SMAs.

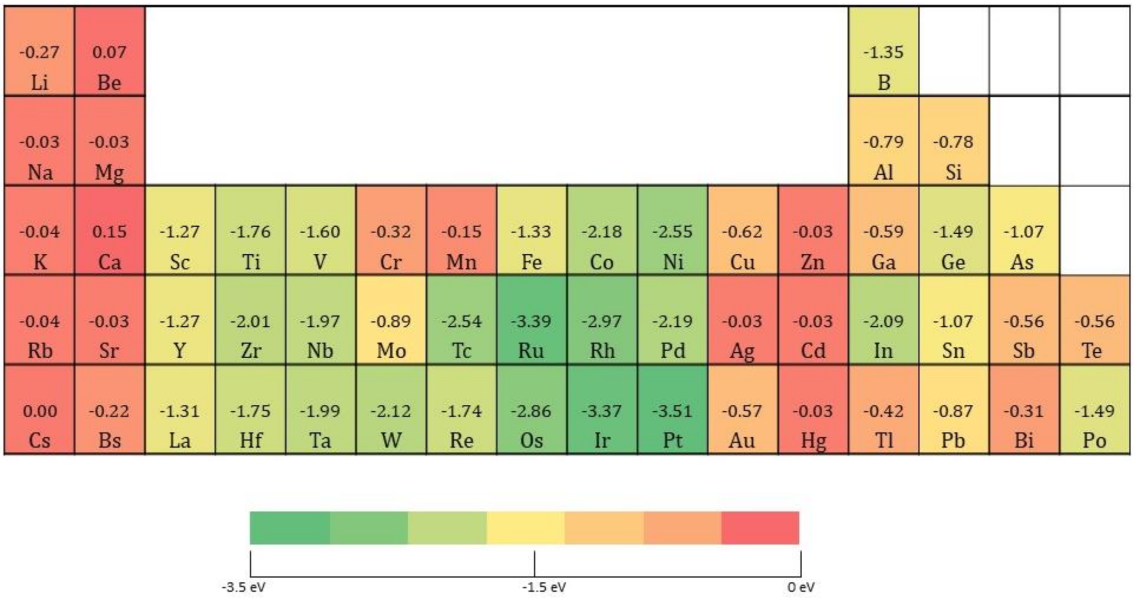

-0.27 Li	0.07 Be											-1.35 B			
-0.03 Na	-0.03 Mg											-0.79 Al	-0.78 Si		
-0.04 K	0.15 Ca	-1.27 Sc	-1.76 Ti	-1.60 V	-0.32 Cr	-0.15 Mn	-1.33 Fe	-2.18 Co	-2.55 Ni	-0.62 Cu	-0.03 Zn	-0.59 Ga	-1.49 Ge	-1.07 As	
-0.04 Rb	-0.03 Sr	-1.27 Y	-2.01 Zr	-1.97 Nb	-0.89 Mo	-2.54 Tc	-3.39 Ru	-2.97 Rh	-2.19 Pd	-0.03 Ag	-0.03 Cd	-2.09 In	-1.07 Sn	-0.56 Sb	-0.56 Te
0.00 Cs	-0.22 Bs	-1.31 La	-1.75 Hf	-1.99 Ta	-2.12 W	-1.74 Re	-2.86 Os	-3.37 Ir	-3.51 Pt	-0.57 Au	-0.03 Hg	-0.42 Tl	-0.87 Pb	-0.31 Bi	-1.49 Po

-3.5 eV
-1.5 eV
0 eV

Figure 4-3: Heatmap of $E_{\mathrm{B}}^{\mathrm{CO}}$ on various SMAs.

4.3 Binding Energy of Single-Atom Cations

Figure 4-4 shows the heatmap of $E_{\mathrm{B}}^{\mathrm{H}}$ on SMCs. Comparing Figure 4-1 and Figure 4-4, it is clear that the binding strength of H on SMCs reduces. The alkali metal cations do not interact with H atom as they have lost their valence electron. However, the alkaline earth metals interact stronger than the previous case. In the case of *d-block* cations, there is not much of a change seen except for the Sc group and Zn group. This behavior is expected to be due to the change in the number of valence electrons. For these groups, as Zn becomes Zn^+, the interaction with incoming species becomes easier. In the case of *p-block* cations, the boron group shows much lesser interaction with hydrogen, while for the others, there is not much change. For the boron group, when they become a cation, they are expected to resemble the properties of alkali metal SMA.

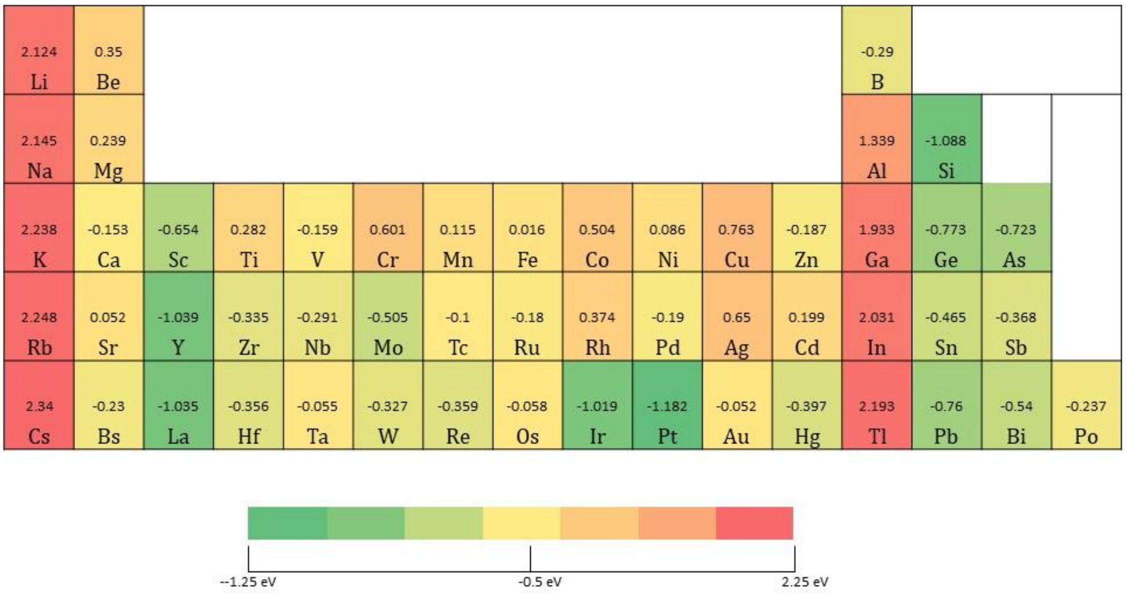

2.124 Li	0.35 Be											-0.29 B			
2.145 Na	0.239 Mg											1.339 Al	-1.088 Si		
2.238 K	-0.153 Ca	-0.654 Sc	0.282 Ti	-0.159 V	0.601 Cr	0.115 Mn	0.016 Fe	0.504 Co	0.086 Ni	0.763 Cu	-0.187 Zn	1.933 Ga	-0.773 Ge	-0.723 As	
2.248 Rb	0.052 Sr	-1.039 Y	-0.335 Zr	-0.291 Nb	-0.505 Mo	-0.1 Tc	-0.18 Ru	0.374 Rh	-0.19 Pd	0.65 Ag	0.199 Cd	2.031 In	-0.465 Sn	-0.368 Sb	
2.34 Cs	-0.23 Bs	-1.035 La	-0.356 Hf	-0.055 Ta	-0.327 W	-0.359 Re	-0.058 Os	-1.019 Ir	-1.182 Pt	-0.052 Au	-0.397 Hg	2.193 Tl	-0.76 Pb	-0.54 Bi	-0.237 Po

Figure 4-4: Heatmap $E_{\mathrm{B}}^{\mathrm{H}}$ of on SMC

Figure 4-5 shows the $E_{\mathrm{B}}^{\mathrm{N}}$ on the SMCs. the binding strength of alkali metals becomes weaker, while the bonding strength of alkaline earth metals becomes stronger, as seen for hydrogen. In the *d-block* metals the general trend is that the interaction becomes weaker except for the Zn group, as seen in the case of H-SMC interactions. In the *p-block* cations, the same trend was seen as the case of hydrogen.

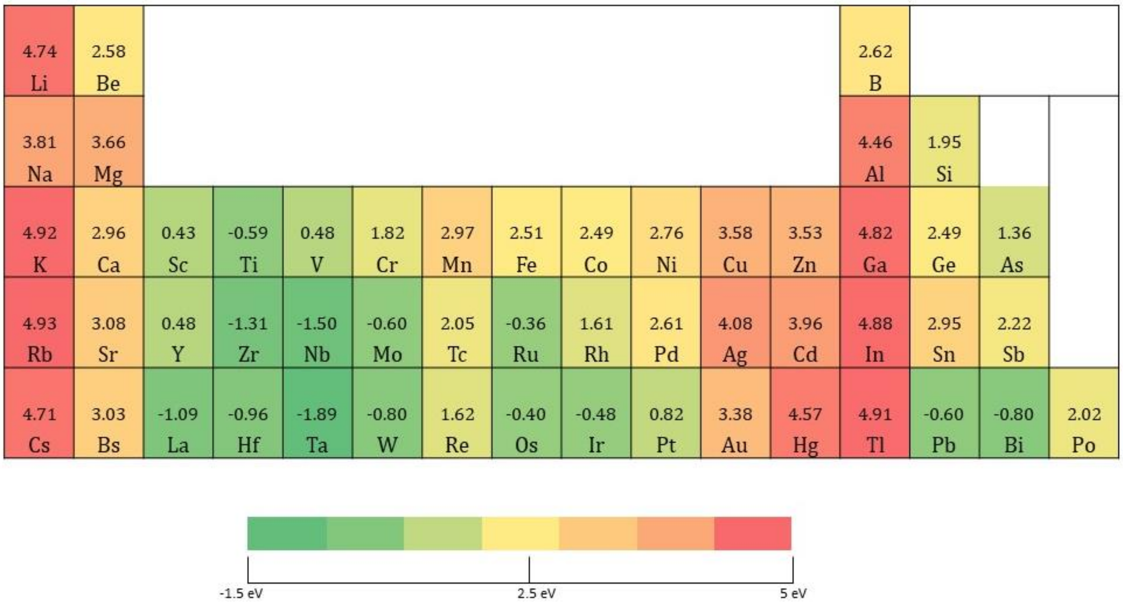

4.74 Li	2.58 Be											2.62 B			
3.81 Na	3.66 Mg											4.46 Al	1.95 Si		
4.92 K	2.96 Ca	0.43 Sc	-0.59 Ti	0.48 V	1.82 Cr	2.97 Mn	2.51 Fe	2.49 Co	2.76 Ni	3.58 Cu	3.53 Zn	4.82 Ga	2.49 Ge	1.36 As	
4.93 Rb	3.08 Sr	0.48 Y	-1.31 Zr	-1.50 Nb	-0.60 Mo	2.05 Tc	-0.36 Ru	1.61 Rh	2.61 Pd	4.08 Ag	3.96 Cd	4.88 In	2.95 Sn	2.22 Sb	
4.71 Cs	3.03 Bs	-1.09 La	-0.96 Hf	-1.89 Ta	-0.80 W	1.62 Re	-0.40 Os	-0.48 Ir	0.82 Pt	3.38 Au	4.57 Hg	4.91 Tl	-0.60 Pb	-0.80 Bi	2.02 Po

Figure 4-5Heatmap of $E_{\mathrm{B}}^{\mathrm{N}}$ of N on SMC

Figure 4-6 shows the heatmap of $E_{\mathrm{B}}^{\mathrm{CO}}$ on SMCs. In this case, the explained for SMC-H is valid except for alkali metals. The energy indicates that the SMCs are interacting with the CO.

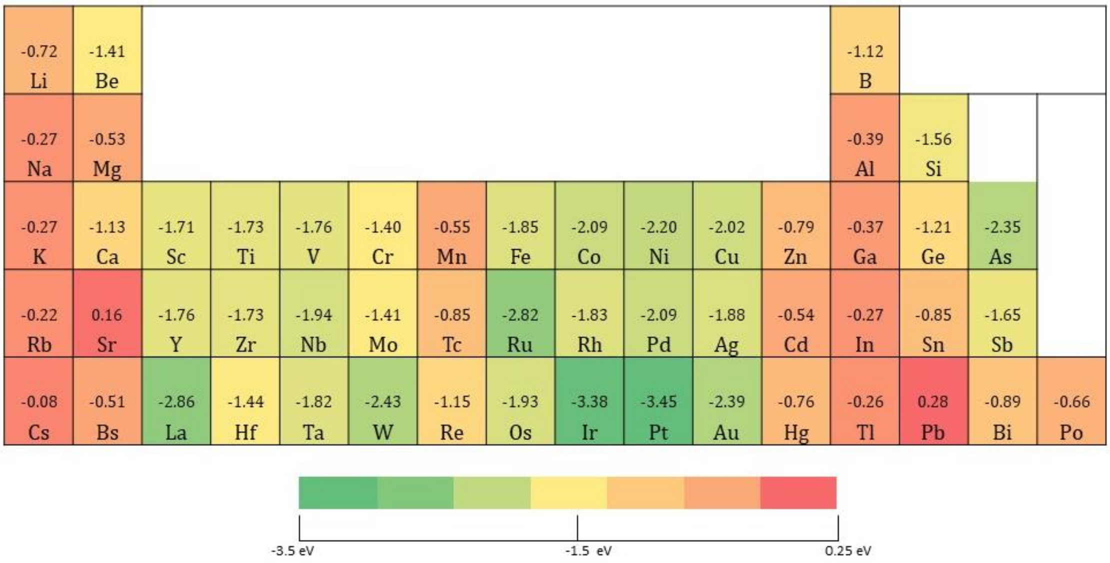

-0.72 Li	-1.41 Be											-1.12 B			
-0.27 Na	-0.53 Mg											-0.39 Al	-1.56 Si		
-0.27 K	-1.13 Ca	-1.71 Sc	-1.73 Ti	-1.76 V	-1.40 Cr	-0.55 Mn	-1.85 Fe	-2.09 Co	-2.20 Ni	-2.02 Cu	-0.79 Zn	-0.37 Ga	-1.21 Ge	-2.35 As	
-0.22 Rb	0.16 Sr	-1.76 Y	-1.73 Zr	-1.94 Nb	-1.41 Mo	-0.85 Tc	-2.82 Ru	-1.83 Rh	-2.09 Pd	-1.88 Ag	-0.54 Cd	-0.27 In	-0.85 Sn	-1.65 Sb	
-0.08 Cs	-0.51 Bs	-2.86 La	-1.44 Hf	-1.82 Ta	-2.43 W	-1.15 Re	-1.93 Os	-3.38 Ir	-3.45 Pt	-2.39 Au	-0.76 Hg	-0.26 Tl	0.28 Pb	-0.89 Bi	-0.66 Po

Figure 4-6: Heatmap of $E_{\mathrm{B}}^{\mathrm{CO}}$ of CO on SMC

4.4 Optimization of Graphene and 3NG

After the SMC and SM calculations are done, the optimization of graphene is done. For this, the C-mp48 graphite cell is downloaded from the Materialsproject website [50]. The graphite structure is shown in Figure 4-4. Following this, one layer is cleaved from this cell to make the graphene cell of apt size.

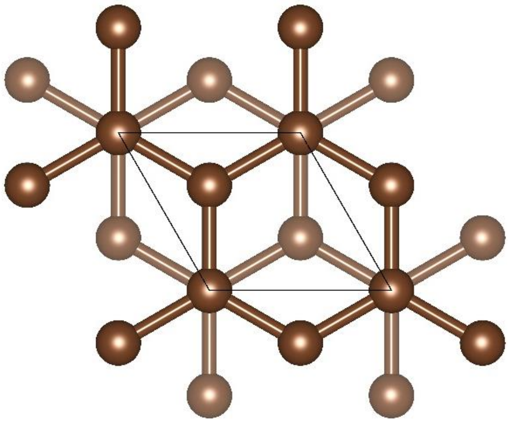

Figure 4-7: Graphite cell downloaded from the Materialsproject website[50] .

4.5 KPOINT and ENCUT optimization

After the 3NG was optimized, to select suitable KPOINTS and ENCUT, various KPOINTS and ENCUT values were tested on the 3NG. The energy obtained for calculation with different KPOINT is obtained and plotted against the corresponding CPU-time for calculation. These are compared against each other to find out the optimum value. The same process is done for choosing the ENCUT values also. Figure 4-7 and Figure 4-8 show the energy values obtained using different KPOINTS and ENCUT plotted against time for each calculation. Figure 4-7 shows that, the time for calculation increases as the KPOINTS increase. The energy rise for each step in KPOINTS does not have a linear relationship with the time for the calculation. The energy for KPOINTS 8x8x1 and 20x20x1 are -267.235 and -267.220 eV respectively. The energy difference is only 0.005%, while the calculation time for 20x20x1 KPOINTS is 72% higher than that of 8x8x1 case. This makes the calculation too expensive for a minor accuracy increase.

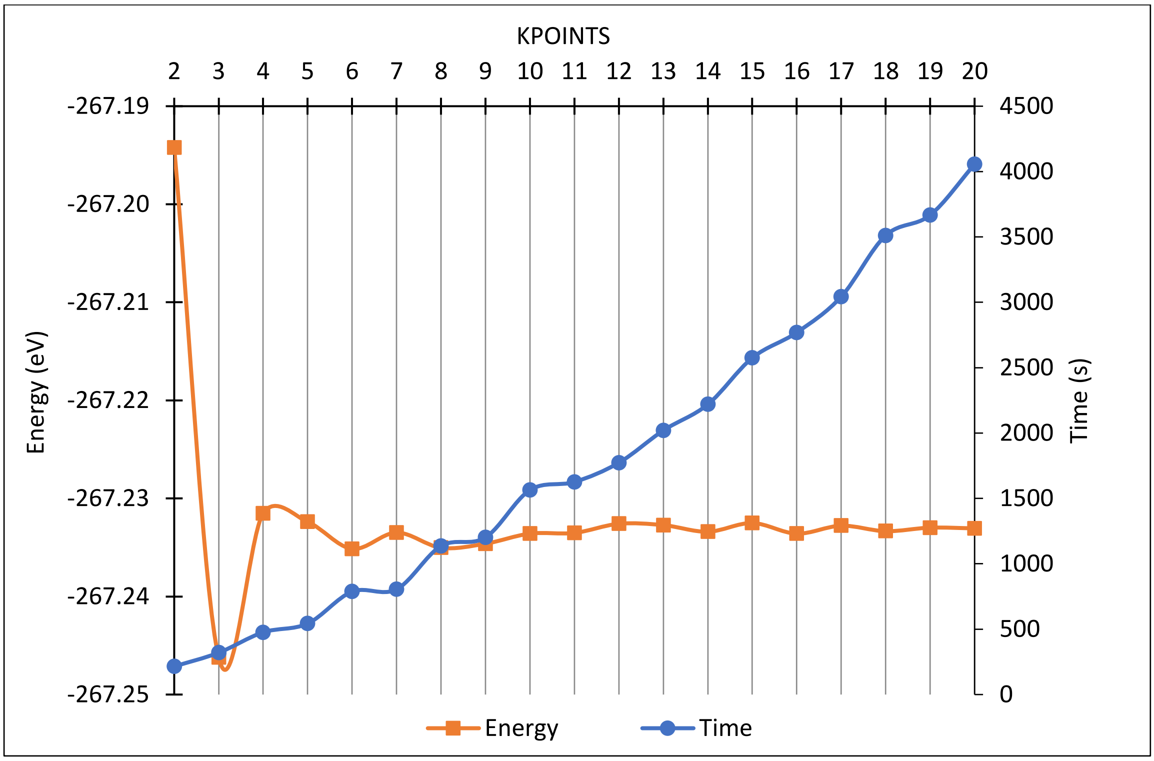

Figure 4-8: Graph of energy of 3NG with different KPOINT sets v/s the time required for the calculation: For KPOINTS after 8x8x1, the energy does not change much, but the calculation becomes expensive.

The ENCUT testing was done from an ENCUT value of 350 to 800 eV. The energy difference was for ENCUT of 400 eV and 800 eV is only 0.01% while the time for the calculation is 46.76% higher for ENCUT of 800eV. Therefore, an ENCUT of 400eV is chosen for the calculations. For the initial KPOINT testing, the ENCUT is set at 500eV and for the ENCUT testing, the KPOINTS is selected as 8x8x1.

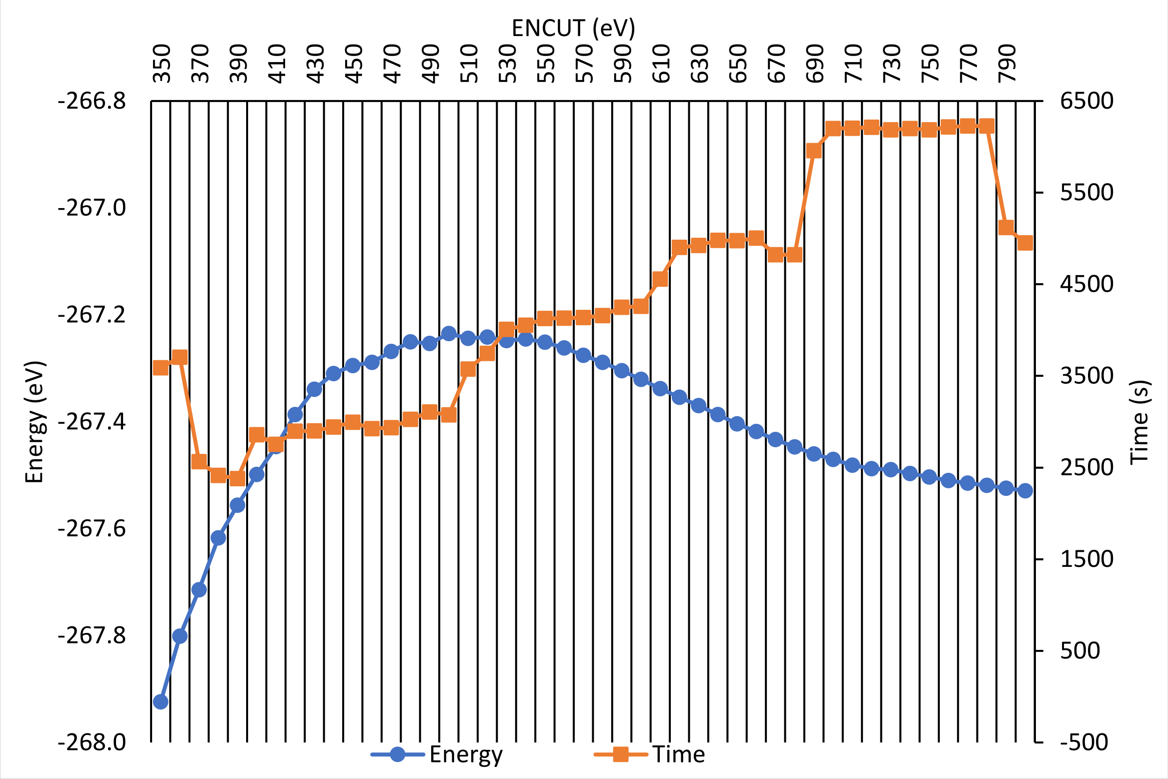

Figure 4-9: Graph of the energy of 3NG substrate with different ENCUT input values v/s the time for the calculation required for the calculation.

4.6 Metal adsorption on 3NG: energetics and stability of the SAC

4.6.1 Energetics of Metal adsorption on 3-N-Graphene

As explained in Chapter 3, the next step in the calculations is the optimization of metal geometries on the 3NG catalyst surface. A multi-step approach is used for optimizing the metal on the surface. The cell volume and the atomic positions are relaxed in the alternating steps as follows:

1. The first step is the optimization of the system with ISIF =2 in INCAR. This means that during the optimization, the cell volume is not changed, but the atoms are relaxed.
2. The second step in the optimization is using ISIF = 7 for optimization. With ISIF =7, the position of the atoms is not changed, but the cell volume is changed but by keeping the cell shape unchanged.

The above steps are alternated until the fifth iteration, after which, if the energy difference between two consecutive steps is negligible, calculations are stopped. The E_B of metal on 3NG is calculated using two different equations as shown:

$$E_B^{3NGM} = E_{Mads} - E_{3NG} - E_{SM}$$

$$E_B^{3NGM} = E_{Mads} - E_{3NG} - E_{cohesisveM}$$

The first equation (Eqn. 55) calculates E_B with respect to the gas phase energy of the SMA, while the second (Eqn. 56) calculates E_B with respect to the cohesive energy of the metal. Calculation of E_B based on the cohesive energy will provide an insight into which metals might form nano agglomerates on the catalyst surface. E_B of the metals is calculated with respect to the cohesive energy and SMA and compared in Figure 4-10.

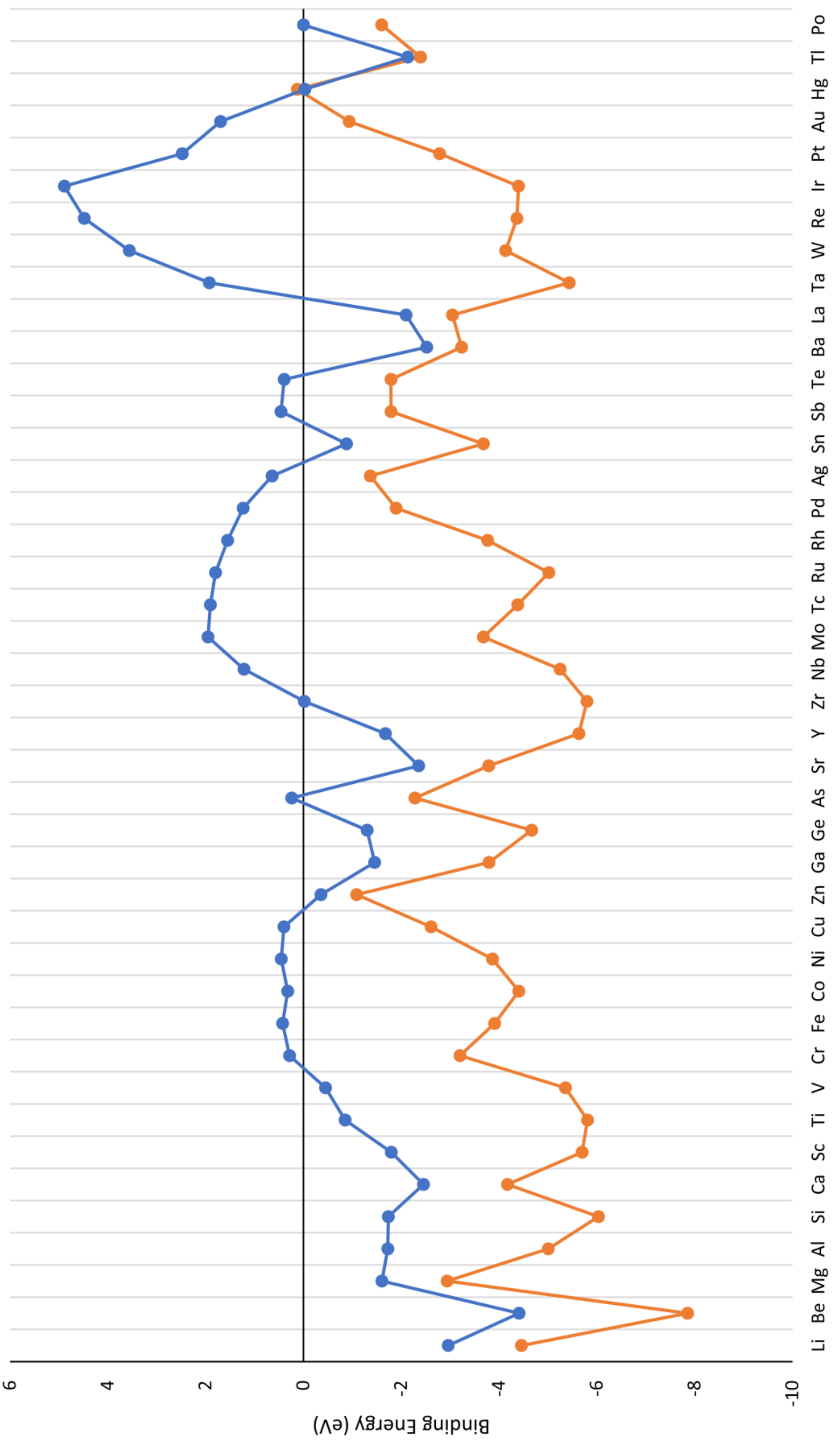

Figure 4-10: E_{B} comparison of metal on 3NG with respect to SM and metal cohesive energy

In Figure 4-11, E_B of metals in 3NG with respect to SMA energy is negative for all metal except Hg. From this it is clear, that the Hg metal will not stay adsorbed on the 3NG substrate. Hence Hg, was not considered for further calculations. For all the cases except Hg, the metals are binding on the to the 3NG sheet. It is noteworthy that for Be and B, the atoms adsorb in between the three nitrogen atoms in a planar manner (shown in 4-11(a)). This characteristic might be attributed to the atomic radius of the atom adsorbed on the surface. Note that the geometry of all the metals except the ones mentioned above are similar to that of Al on 3NG sheet shown in 4-11(b) and are anchored to the 3NG sheet.

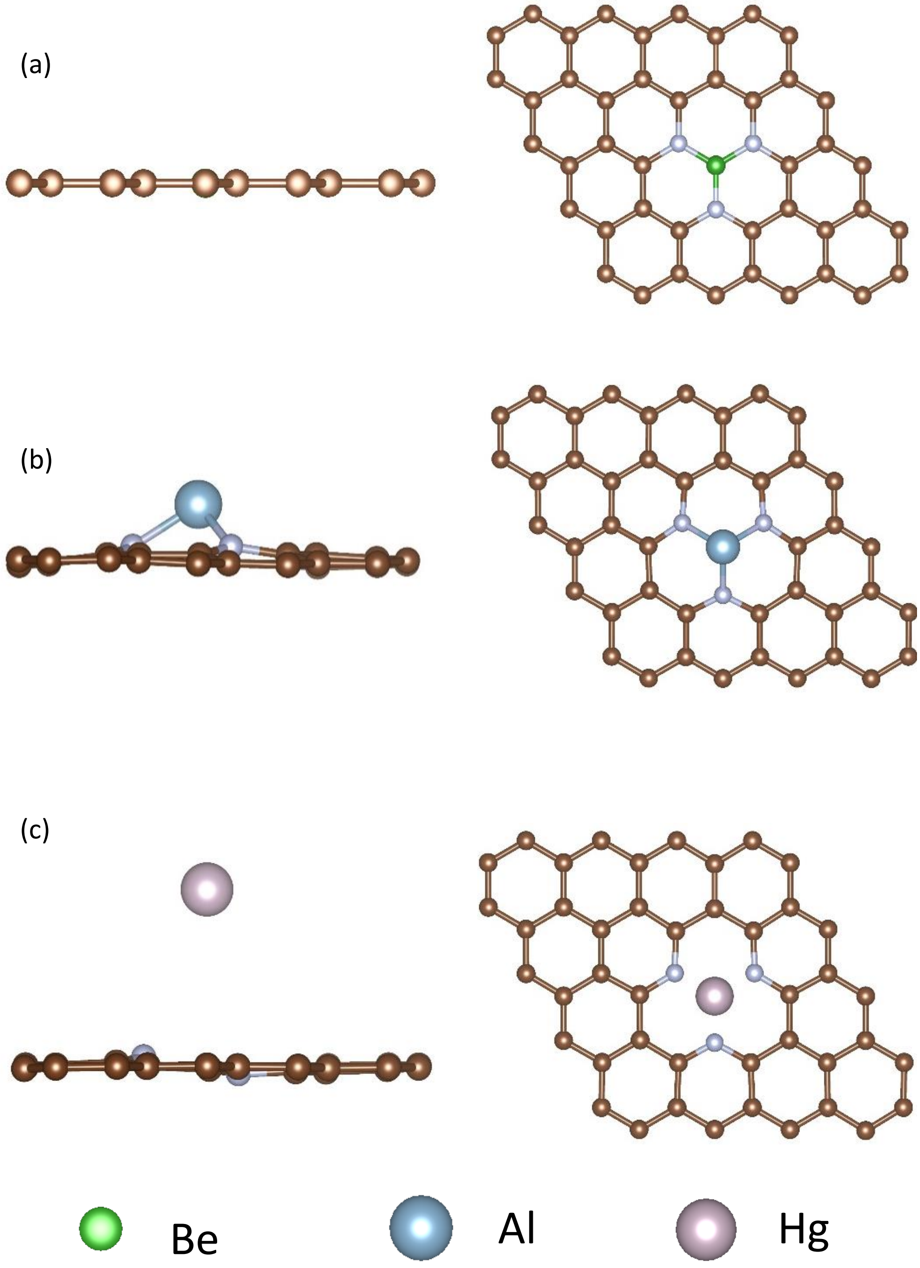

Figure 4-11: Geometries of Be, Al and Hg on 3NG: (a) Final geometry of Be atom on the 3NG graphene sheet. (b) Geometry of Al on 3NG. (c) Final geometry of Hg on 3NG.

4.7 Adsorption of H atom on 3N-Graphene-Metal- Binding Energy and Geometrics

4.7.1 H adsorption on 3N-Graphene-Metal

As explained in the methodology earlier, three different orientations of H atom were tested on 3NGM. In this section, the energies of all these orientations along with the lowest energy orientations are reported. The geometry corresponding to the lowest energy orientation will be the geometry that will be considered here.

Figure 4-12 shows different adsorption positions of H for the same metals. The lowest E_B is recorded as the final E_B. The H atom is on the top of the metal for the following metals: Mg, Y, Ti, Zr, V, Nb, Ta, Cr, Mo, W, Mn, Re, Os, Fe, Co, Ni, Pd, Pt, Zn, Cd, B, Al, Si, Ga and, In. Be, Ca, Sc, Re, Ru, Rh, Ir, Cu, Ag, Au, Tl, Ge, Sn, As, Sb and Po have hydrogen on the hollow part of the 3NG ring (between the carbon atoms). Only for La the hydrogen atom converges to the position above the nitrogen atom of the 3NG. In all these cases, hydrogen is bonded to the metals, while the metals remain anchored to the 3NG surface. For the case of Li, K, Rb, Cs, Ca, Sr and Ba, the H atom is not reacting with these metals doped SACs. The final geometries corresponding to the adsorption position is also recorded.

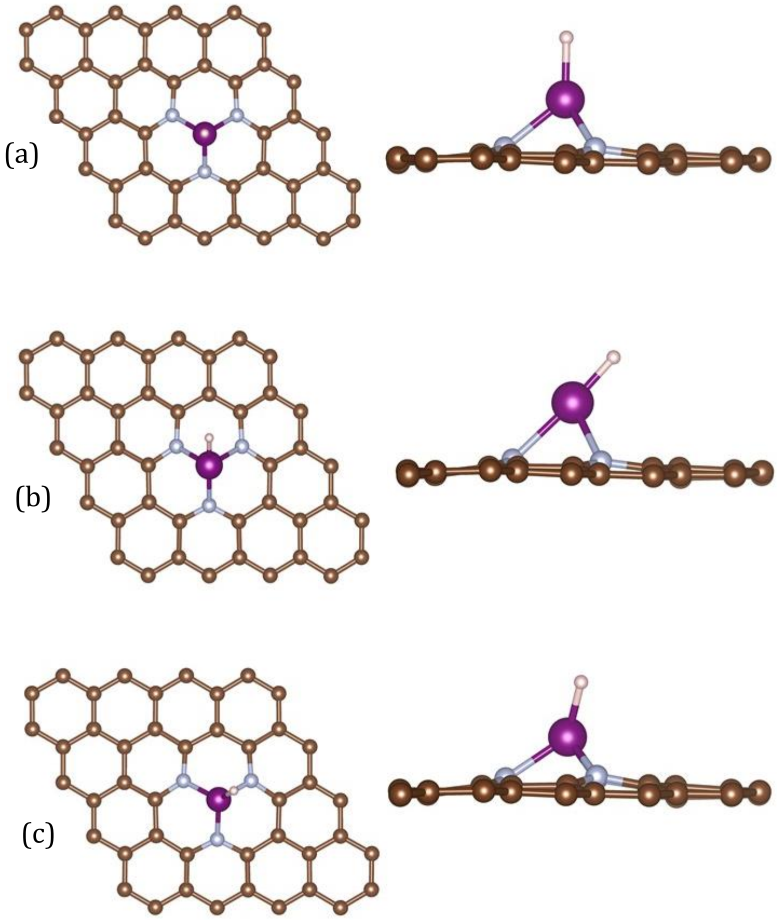

Figure 4-12: Output geometries of E_B of H atom on 3NGM for different SACs considered.

4.7.2 Candidate Single-Atom Catalysts for Hydrogen Evolution Reaction

Once the lowest energies are recorded, the lowest E_B of each orientation is plotted on another graph, Figure 4-13. For the metals with E_B >0 do not interact with the adsorbent H atom and hence not adsorbed on the catalyst surface. This is clear from the geometries. Whereas, for metals with E_B <0, the H atom is adsorbed on the catalyst surface.

The green line in the figure is the E_B of the H atom on the Pt (111) facet [-0.37 eV], which is the conventional best metal catalyst for HER. The orange lines are ±0.25eV of the target value (-0.37eV). This buffer region of 0.5eV around the target value is chosen in such a way that the candidate catalysts are close to the experimental E_B values also. The experimental value for H adsorption on Pt (111) facet is -0.45eV[57].

Here are some important conclusions:

- The single-atom candidate catalysts for HER are **B, Cr, Mn, Fe, Co, Ni, Ga, Ru, In, Sb, La, Sb, and Po**.
- It is important to note that some of these predicted catalysts such as Cr, Mn, Fe Co, Ni, Ru, In, and Sb have the E_B^{3NGM} >0. Hence there is a possibility that these metals might agglomerate on the surface of the 3NG sheet.
- The E_B of H atom on the single Pt atom, less than that of Pt(111) facet. This is because, on single-atom catalysts, the activity of the catalysts becomes stronger than the conventional catalysts. This is because the SACs have higher surface area for catalysis and hence adsorb the adsorbent species stronger. It is noteworthy that since the E_B is higher in this case, the H might poison the catalyst surface hence hindering the further catalytic activity of the catalyst.
- Note that all the *s-group* metals, except Mg, is not interacting with the H atom. These characteristics will be discussed more in-depth in the charge dissipation section. The non-interacting characteristics of the metals can be attributed to the number of valence electrons for these metals.
- For the *d-transition* metals, it is clearly visible that all the metals are interacting with the H atom.
- *p-block* elements have a cross reactivity to the adsorption of H atom on the surface. This is because of the varying number of valance electrons available for bonding and the size of the metal atoms adsorbed on the surface.

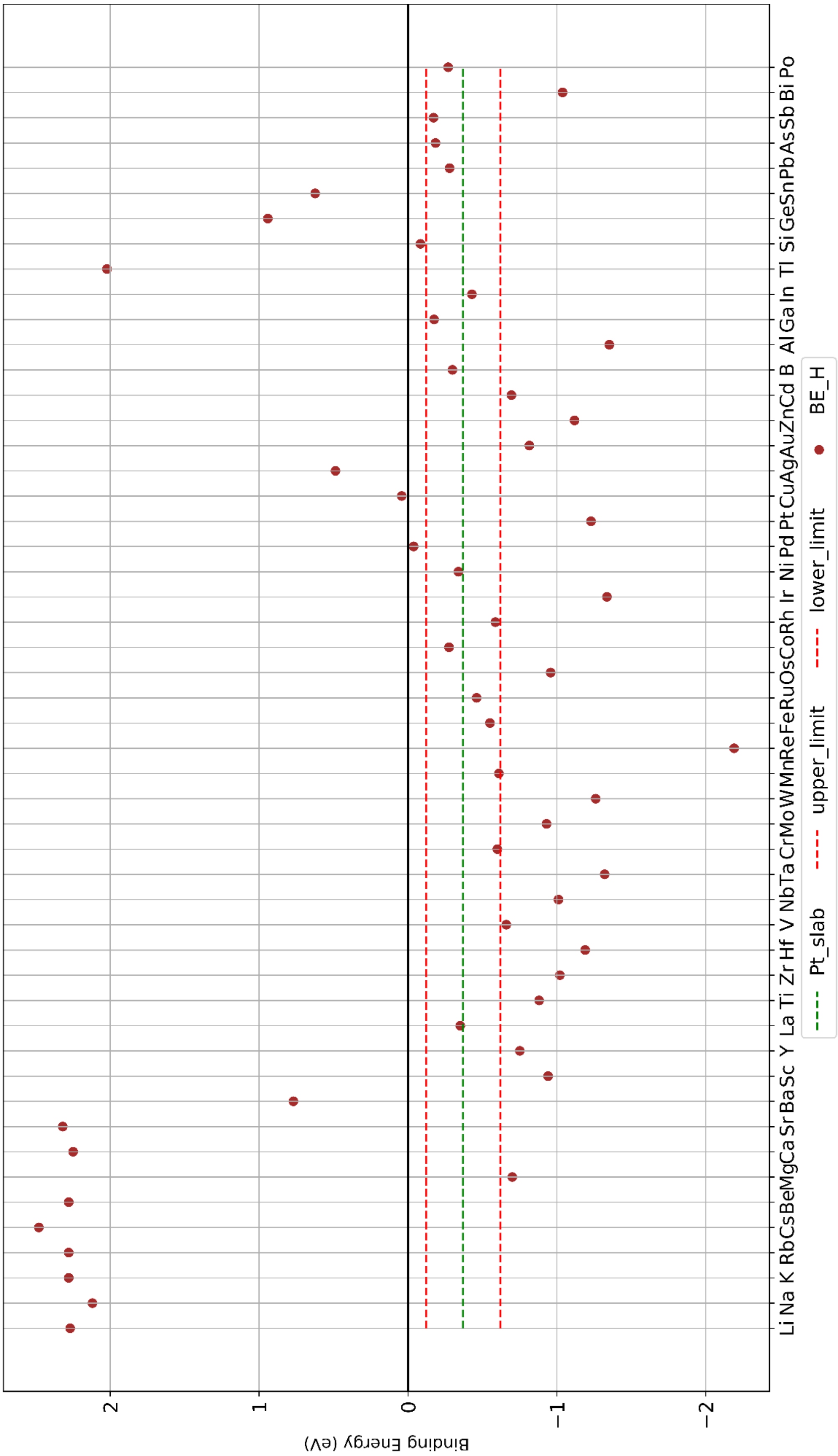

Figure 4-13: E_B of hydrogen atom on 3NGM. The candidate catalysts are the ones in between the target lines (orange lines)

4.8 Adsorption of N atom on 3N-Graphene-Metal -Binding Energy and Geometrics

4.8.1 Binding Energy and Geometrics of N on 3N-Graphene-Metal

The binding energy of the N atom on the catalyst surface is studied to predict the SAC for N_2RR. The nitrogen atom is adsorbed, as discussed in the methodology section. The geometry of different systems of N adsorption considered is shown in Figure 4-14.

With regard to the geometrics and the orientation of N atom on 3NGM, metals such as Li, Na, K, Rb, Cs, Be, Ca, Sr, Ba do not interact with the N atom adsorbing, La, Ti, Zr, Hf, V, Nb, Ti, Cr, W, Mn, Re, Fe, Ru, Co, Rh, Ir, Ni, Pd, Pt, Cu, Ag, Au, Zn, In, Tl, Si, Ge, Sn adsorb the N atom on top of the metal atom. In addition to this, Sc, Y, Sb, Bi, and Po adsorb the N atom in the direction of doped N atom on the graphene sheet. Ta, Mo, B, Al, Ga, Ge, and Sn adsorb the N atom at the hollow site of the graphene ring. Figure 4-14 shows the geometry of the N on top of the 3NGM.

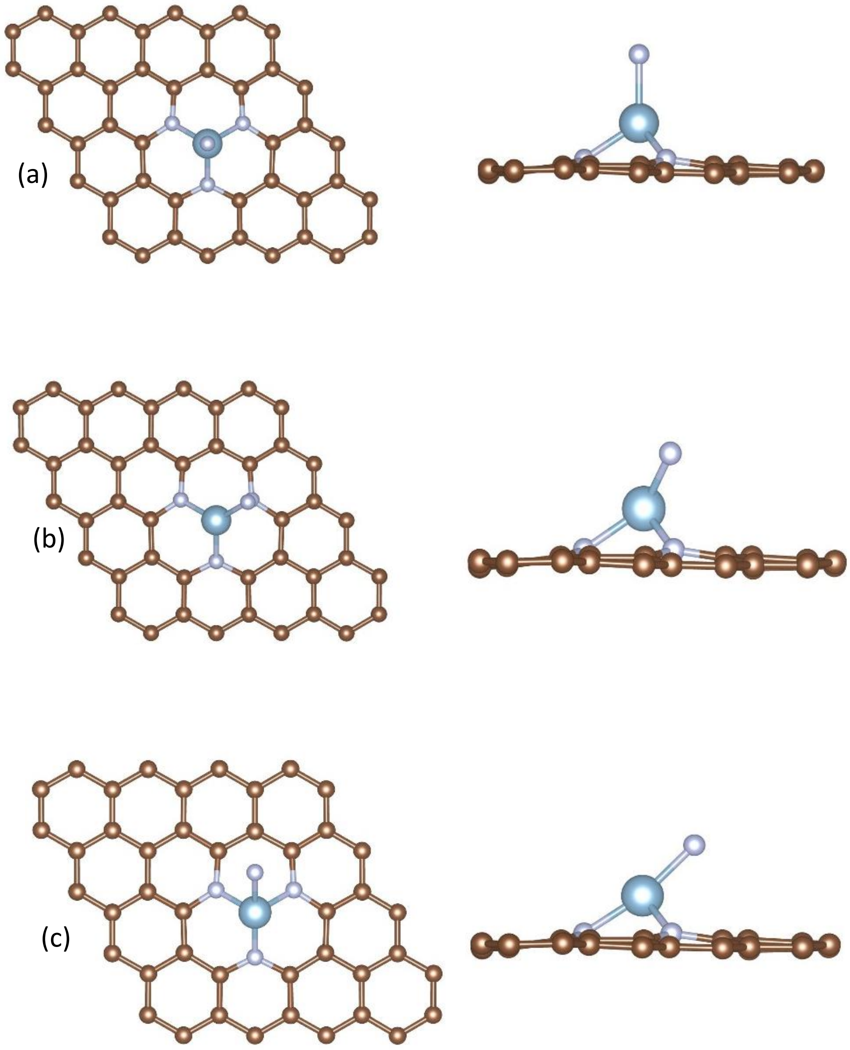

Figure 4-14: Final Geometries of N atom on 3NGM

4.8.2 Candidate SACs for N_2RR

Once the lowest orientation is found out, the data is plotted in a separate graph to find out the candidate catalysts. Similar to the case of HER, the E_B of N atom on the best conventional catalyst was found out, and chosen as the benchmark. This is the E_B of N atom in Ru (0001) surface, and a limit of ±0.25 is chosen on either side of the $E_{B.}$ In Figure 4-15, the candidate catalysts for N_2RR fall in between the red lines of the graph.

It can be seen that Ru, Cr, and Mo are the candidate catalysts for N_2RR. In addition to this, it can also be seen that a lot of SACs have E_B of N>0. This does not imply that all the SACs for which E_B>0, N does not bind to the catalyst surface. To verify this, the geometries of the N binding SACs are explained and shown in figure 4-14. The positive E_B arises from the energy of N atom, which is half of N_2 molecule.

$$E_B^{3NGM-N} = E_{Nads} - E_B^{3NGM} - 0.5 * E_{N2}$$

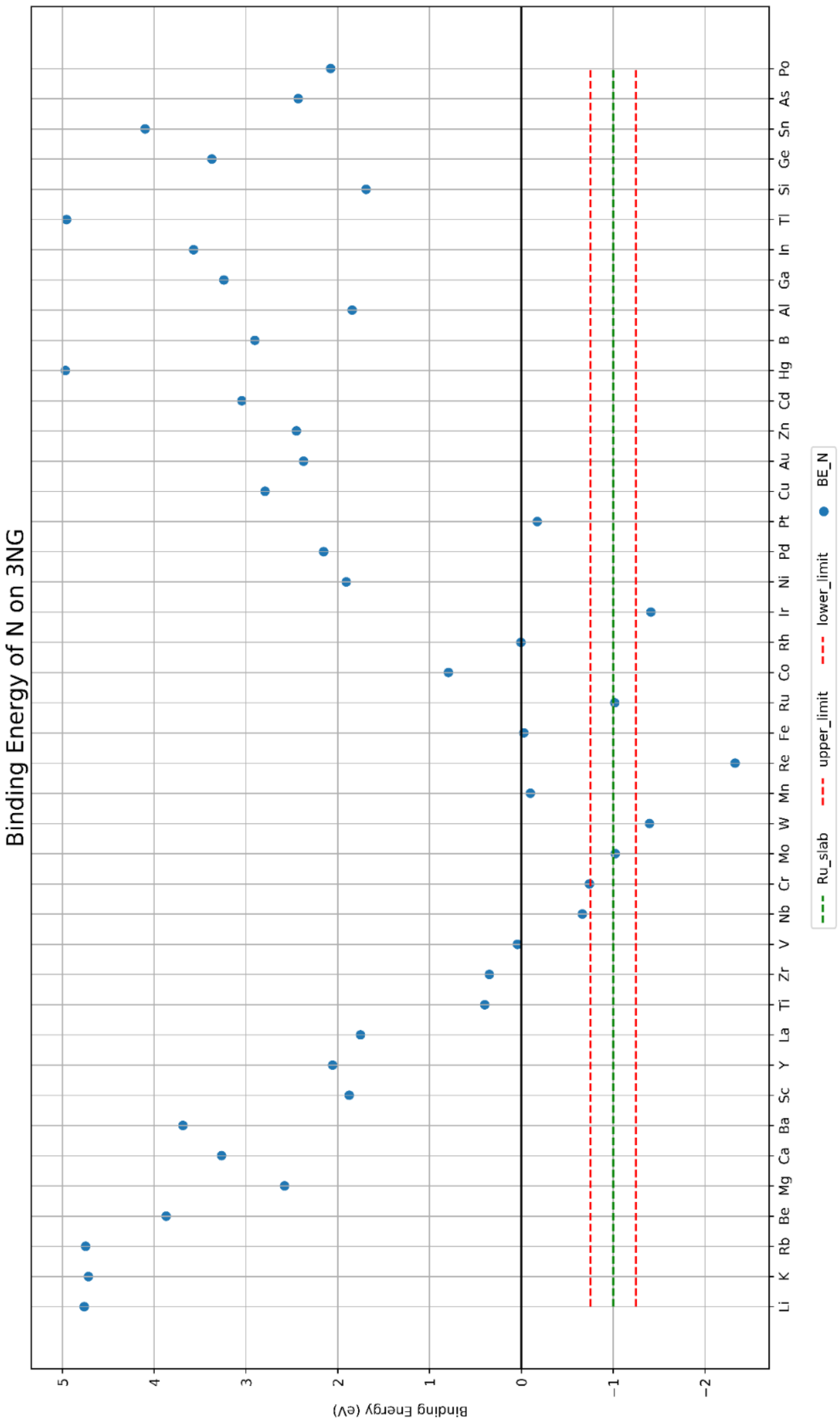

Figure 4-15: E_B of N atom on 3NGM. The candidate catalysts are Ru, Mo, Cr. The candidate catalysts can be seen between the red lines. The green line is the benchmark catalyst Ru (0001)

4.9 Adsorption of CO on 3N-Graphene-Metal - Binding Energy and Geometrics

Literature shows that the descriptor for CO_2RR is the E_B of CO on the catalyst surface [16]. The traditional catalyst used for CO_2RR is Cu(111) facet. The CO is adsorbed on the 3NGM in different orientations, as discussed with the corresponding output BD from SMA calculations. With regard to the geometrics and orientation of CO on 3NGM for metals such as Li, TI, Zr, Cr, Pd, converge with CO directly on top of the 3NGM sheet (Figure 4-16(a)). K, Mo, W, B, Ga, Si and tin converge with CO in the direction of hollow site in graphene(Figure 4-16(b)). Rb, In, Tl and Sb converge when the CO is in the direction of N on the 3NG (Figure 4-16(c)). All the other metals converged with the angular oxygen geometry (Figure 4-16(d)).

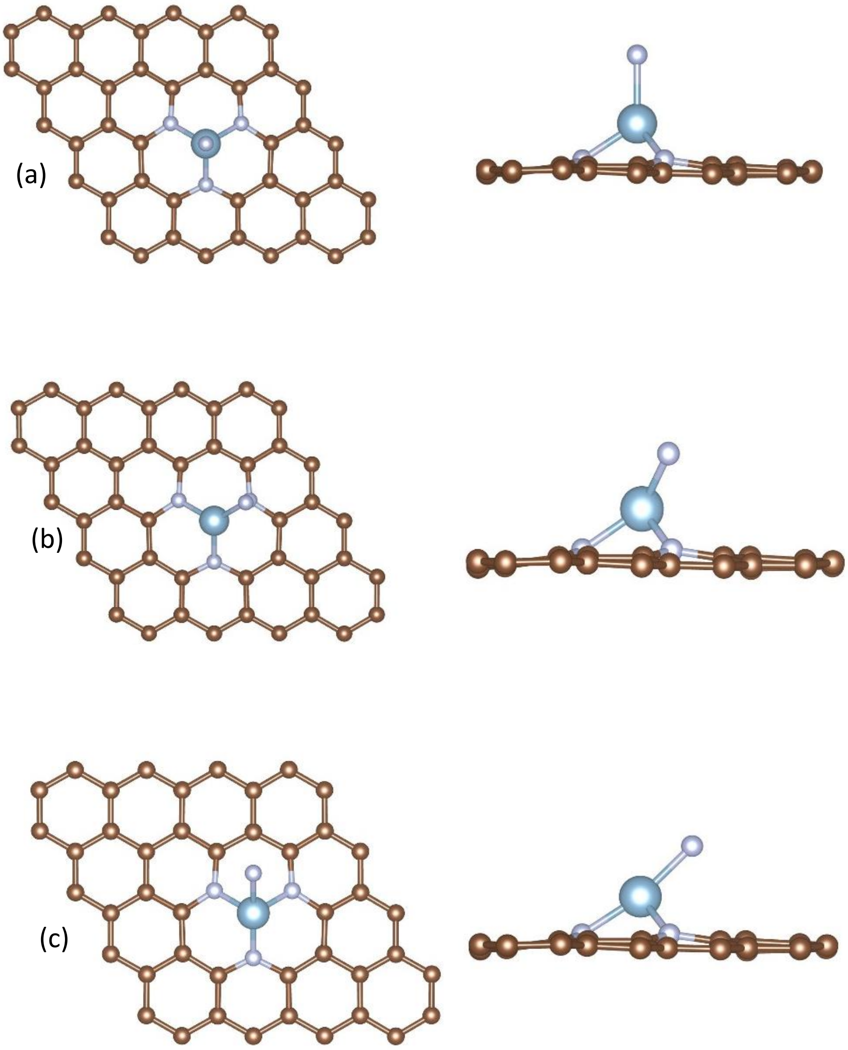

Figure 4-16: Final geometries of all the CO-3NGM systems.

The atoms in the graph are arranged according to the group order, top to bottom of the group. This trend is seen for the above-mentioned groups. The *s-block* and majority of the *p-block* SACs do not exhibit a strong interaction with CO, while the other few do not interact at all. For the *d*-transition elements, it is clear that most of them interact with CO strongly. From alkaline earth metals, until the Mn group, it can be seen that the E_B of CO on the surface increases as we move down the group, and a different trend is observed for the remaining groups of *d*-

transition elements. From the Mn group and so forth, there is an increase in the E_B and then a decrease for the third atom in the group. For e.g. the for Ni group, the $E_{BPt} < E_{BNi} < E_{BPd}$.

The energies are compared and then plotted in Figure 4-17. As explained earlier, the green line is the E_B of CO molecule on the Cu (111) facet (-0.47eV). The orange lines are $\underline{+}0.25$ eV of the green line. This region between the orange lines is the target area. The candidate catalysts for CO_2RR are **Mg, Al, Ca, Zn, Sr, and Ru.** It is seen that as the metal binds more stronger to the graphene sheet, the weaker the interaction with adsorbent. E.g., in case of Cu and Au, when. This can be attributed to the strength of metal binding on the 3NG. It can be summarized that when the metal binding on the substrate is strong, the adsorbate binding on the catalyst is weak and vice-a-versa. From Figure 4-17, Cu atom binds on the catalyst substrate stronger than Au and hence, a weaker interaction with the adsorbent.

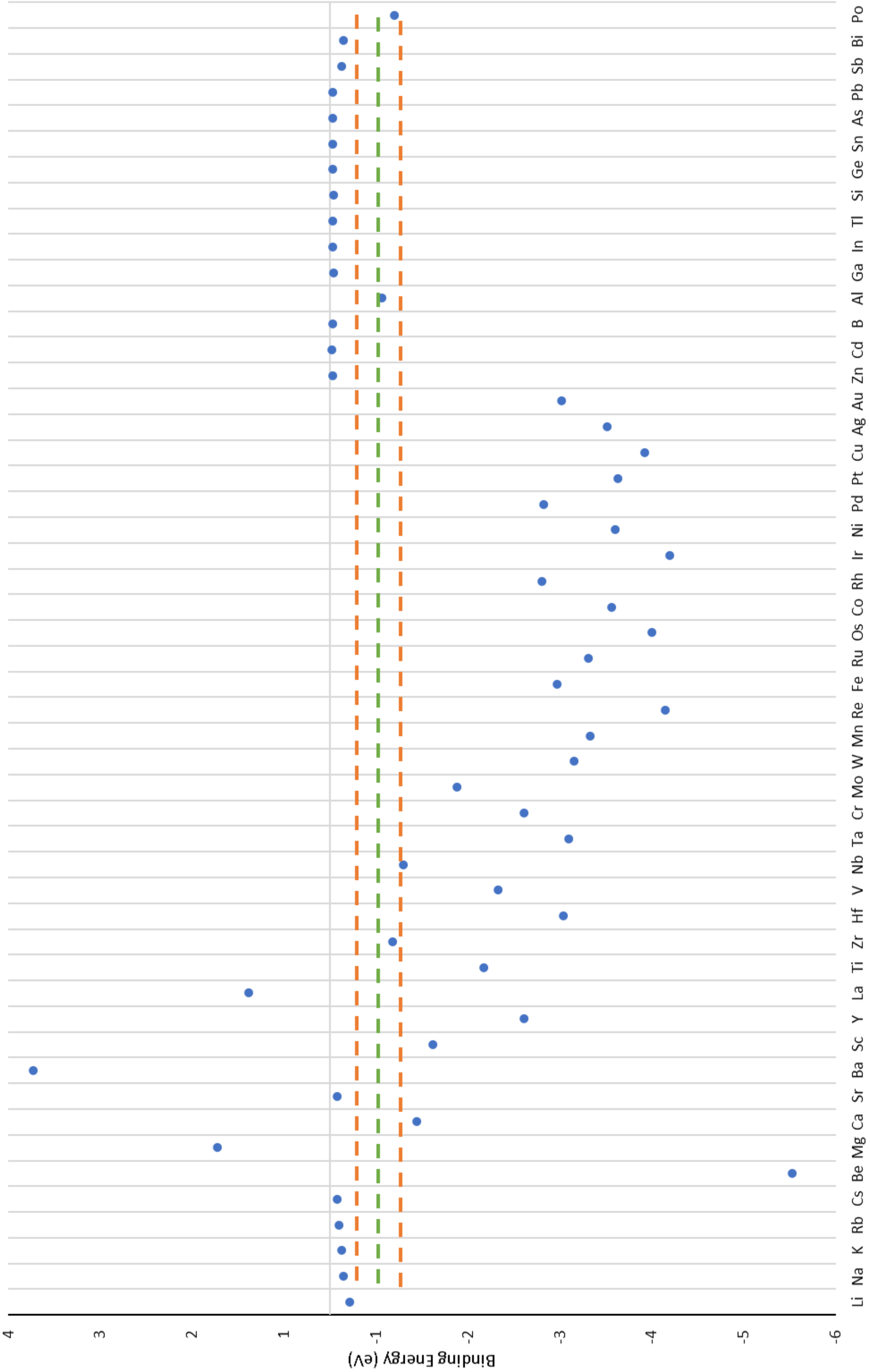

Figure 4-17: E_B of CO on 3NGM . The candidate SACs are shown between the two dashed red lines. The green line is the E_B of CO on the Cu(111) slab surface. This is the benchmark to predict the SACs.

4.10 Bader charge calculations and relation of the Binding Energy and the atomic radii

In this section, the Bader charge calculation results and its variation with the E_B are discussed. The Bader charge represents the charge dissipation from the various species involved in the reaction. Here the results of H on 3NGM are discussed in detail. The results of N and CO are similar to that of Hydrogen.

Figure 4-18 shows the relationship between the Bader charge on the hydrogen atom and the E_B of metal on the 3NG. It can be concluded that, as we move from left to the right of the periodic table, the H atom has a lesser negative charge on it. The trend is evident here, the more the meal interacts with the graphene sheet, the more the interaction with the hydrogen. Even though this is counter-intuitive, this characteristic is expected to be due to the size effects of the atom under the reaction. It is also important to note that this trend is not seen in the case of CO adsorption.

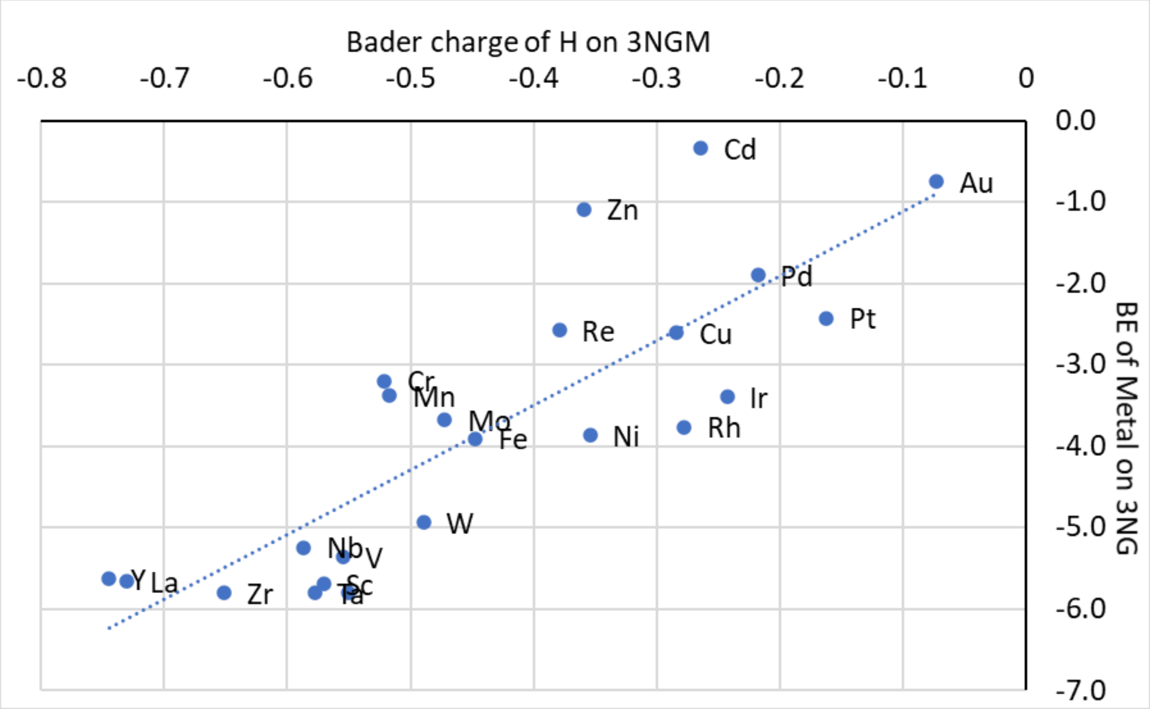

Figure 4-18 Relation of E_B of Metal on 3NGM and Bader dissipation of Hydrogen atom on the 3NG sheet

To check if the adsorption of H atom is dependent on the size of the metal atom anchored on 3NG, the Bader charges of Metal in the 3NGM-H system are plotted (Figure 4-19). Within the same row of the periodic table, as the metal size increases, the Bader charge dissipation of Metal on 3NG sheet and the Hydrogen atom increases. This shows that the catalyst substrate contributes towards the catalytic activity to a greater extent. Hence as expected, the choice of the substrate plays a vital role in the catalytic activity in SACs.

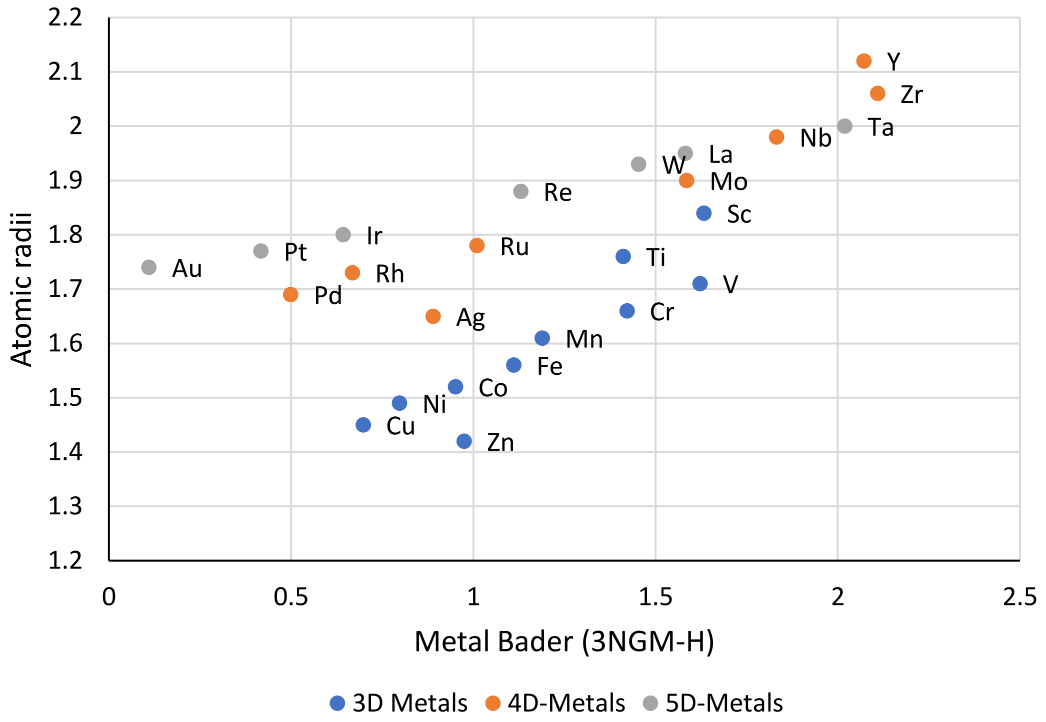

Figure 4-19: Plot of Bader charges on Metal for 3NGM-H system and atomic radii

4.11 Validation of results with available experiments from the literature

4.11.1 Comparing the binding of metals on 3NGM in experiments and this work

In Figure 4-10, there are metals with $E_B > 0$. For these cases, there is a chance that these metals might agglomerate on the 3NGM surface. On the other hand, it should also be noted that for these metals, the $E_{B3NGM\text{-}SM} < 0$. Reading these results together, it can be concluded that for the metals with $E_{B3NG\text{-}SM} < 0$ and $E_{B3NGM\text{-}cohessive} > 0$, e.g., Pt, might form agglomerates on the substrate, at the same time, some of the metals remaining as single atoms. This is shown in Figure 4-20. The HAADF-STEM images of Pt on graphene show the formation of nano-agglomerates for different loading [26]. In Figure 4-20 (*C)*, the formation of Pt dimers on the substrate, while in Figure 4-19 (D), the single Pt atoms are clearly visible. Hence, the experimental results validate the conclusion drawn that the metals can be both be found as agglomerates on the surface, while some Pt atoms still dispersed as single metal atoms. In addition to this work, in a work of Co atoms on 3NG substrate by Fei and co-authors, Co atoms also show a similar kind of behavior [58].

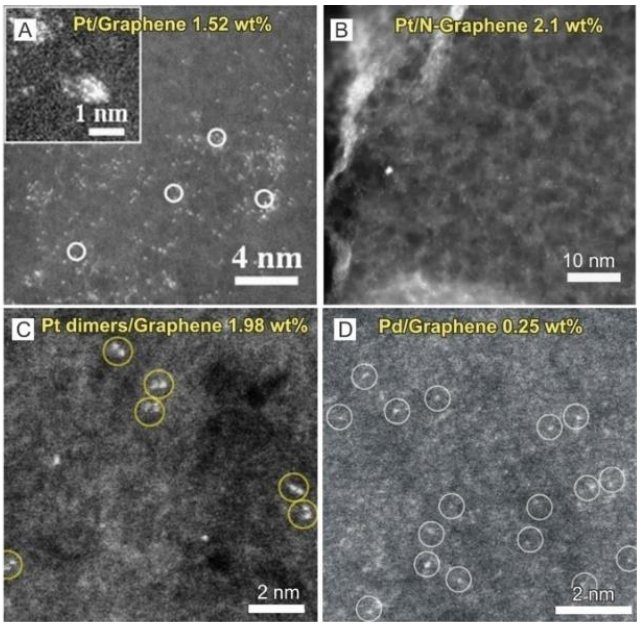

Figure 4-20: SEM image of dispersed Co atoms on 3NG. The SEM image shows the Co atoms dispersed on 3NG. the white dots shoes the Co atoms and the darker area is the substrate. Note the areas where the white dots are clustered together. This indicates the areas where the nano-clusters are formed [26].

Literature suggest various methods are adapted to prevent the formation of nano-agglomerates:

(a) Reducing the metal loading on substrates to less than 1%
(b) Using wet-chemical synthesis to synthesise the SAC
(c) Using spatial confinement method to synthesise the SAC, e.g. MOF

These methods have proven to be effective in controlling the formation of nano-agglomerates on the substrate. In light of the above discussions and the scope of this thesis, we assume that all the atoms remain as dispersed single atoms on the substrate (except Hg) and not as agglomerates.

4.11.2 Comparison of Hydrogen Evolution Reaction results with experiments

Co atoms were immobilized on 3NG by Fei and co-workers[58]. It is seen that the Co metal was dispersed as single atoms on the catalyst surface. In addition to this, the Co-NG (Co immobilized on 3NG) was found to be a suitable catalyst for HER (Figure 4-21). In the Figure 4-21 (a), the over-potential for of SACs on various substrates is shown. It is clear that the Pt is still the best catalyst, but the closest best option in these substrates is Co on 3NG. The TOF of this catalyst is also close to conventional catalysts used for HER (Figure 4-21 (b)).

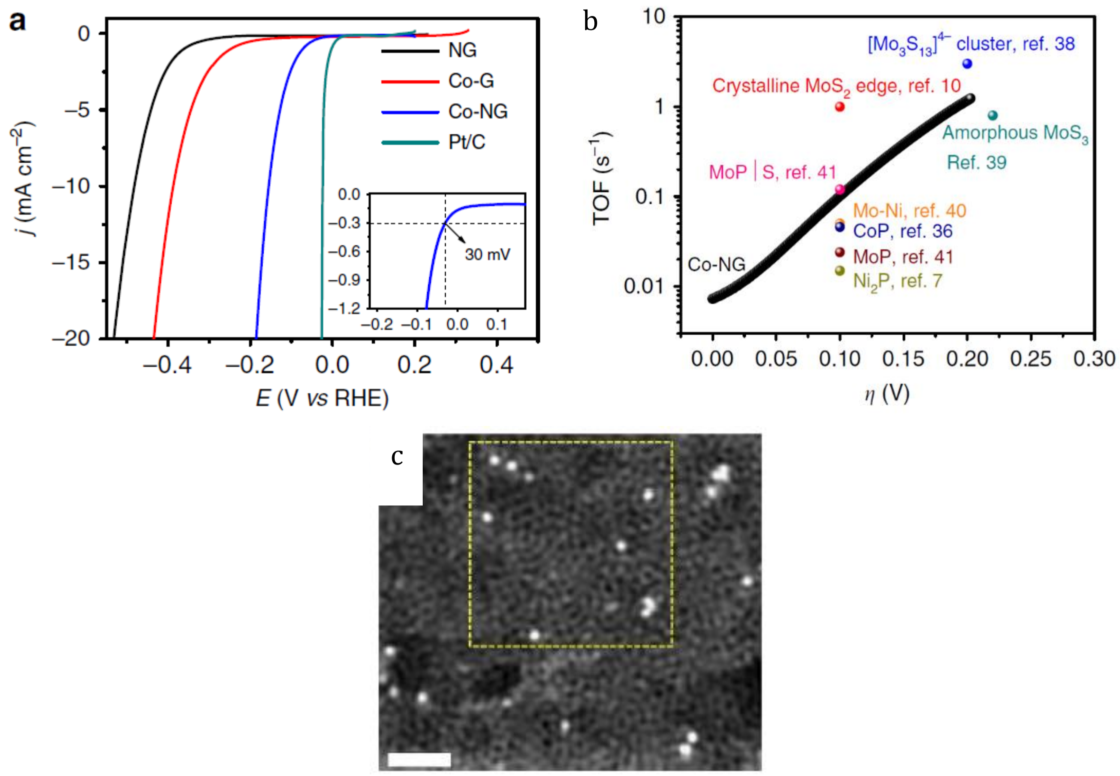

Figure 4-21: Performance comparison of Co-3NG and other catalysts. (a) Compares the current density and the potential between Pt(111), Co on graphene, Co on 3NG, and nitrogen-doped graphene. Co-3NG is still not as good as the conventional Pt catalyst, but still comparable to the other catalysts. (b) Compares the turnover frequency of various catalysts. (c) SEM image of the Co on 3NG. Well dispersed Co atoms (white specks) on 3NG. This also proves that the Co atoms are stable on the 3NG substrate [58].

It is noteworthy that Fei and co-authors validate the prediction of this thesis. With this in mind, the other inexpensive catalysts can be tested to replace the existing Pt catalyst.

4.11.3 Comparison of Carbon dioxide reduction predictions with experiments

Chen and co-workers tested the catalytic activity of Zn on 4NG and the performance of various other substrates, and it is seen that the Zn presence on the graphene has enhanced the catalytic activity. They also prove a low overpotential of 0.39 eV and a Faradaic efficiency of 91% for the novel Zn-N-G catalyst(Zn doped on 4N doped graphene). It should also be noted that the product in this case is CO and not a higher-end chain [59]. This goes is supportive experiment for the prediction of this thesis. Hence, it is suggested that other SACs which are predicted here should also be tested and proven for their catalytic activity.

The following periodic table shows the final best SAC candidate catalysts for HER, CO_2RR and N_2RR.

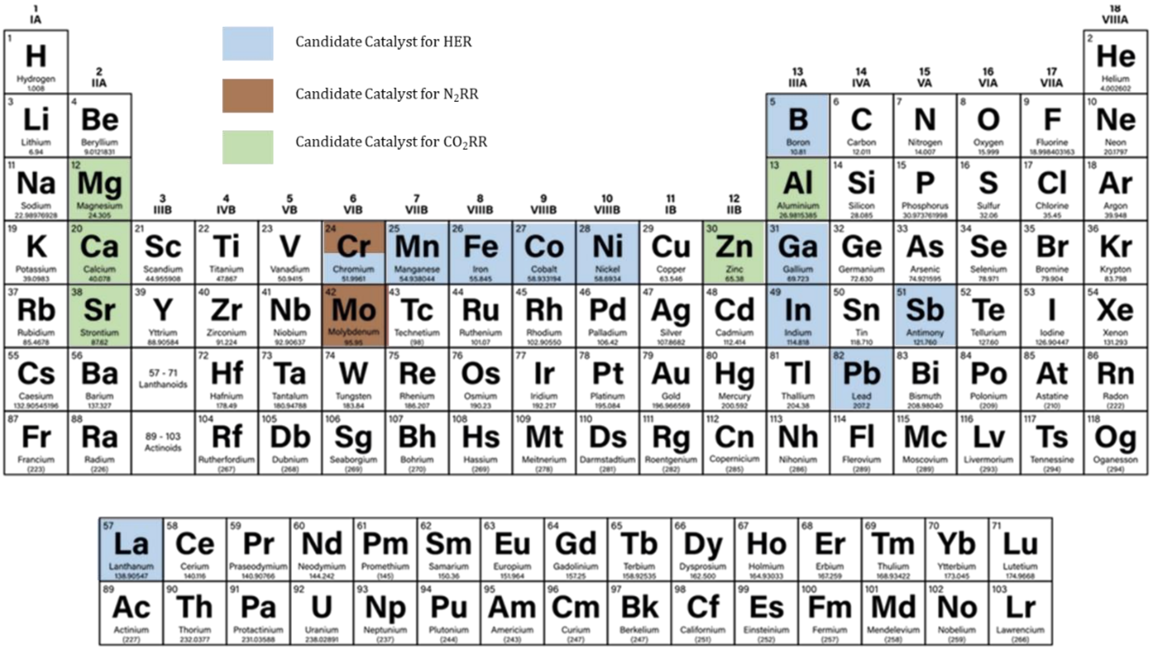
Candidate Catalyst for HER
Candidate Catalyst for N_2RR
Candidate Catalyst for CO_2RR

Figure 4-22: Periodic table with candidate SACs for HER, CO_2RR and N_2RR

5

Conclusion and Outlook

5.1 Conclusion

Several research aims were proposed in Research Aim section. From the calculations reported in the thesis work, the following conclusions can be drawn.

- The aim of the thesis was to predict good SACs for HER, N_2RR and CO_2RR.
    - The catalysts predicted for HER are B, Cr, Mn, Fe, Co. Ni, Ge, Ru, In, Sb, La, and Pb.
    - The candidate catalysts for N_2 RR are Ru, Mo, and Cr.
    - The candidate catalysts for CO_2RR are Mg, Al, Ca, Zn, Se, and La.

- It was also noted that, for *d-transition* metals, the binding strength of adsorbent species on the 3NGM sheet depends strongly on the atomic size and the number of valance electrons available for the binding.

- It was also understood that the substrate effects play an important role in the catalytic activity of the SACs. An electron-rich source is necessary for the catalysis to take place smoothly.

The automation scripts were an integral part of this thesis. With few changes in them, these codes are also useful for any kind of energy optimization, and Bader calculations done for catalysis works.

5.2 Outlook

The study of SACs in view of HER, CO_2RR, and N_2RR has been conducted only recently. This brings into the picture a vast area of novel catalysts that can be used for a variety of applications like catalysts used in the carburetors. The following are some suggestions made in the view of this thesis:

- The studies done here are based on the descriptors of the respective reactions. To gain a better understanding of the reaction mechanism, a full set of surface calculations, including the NEB calculations to detect kinetic barriers, can also be carried out.

- A microkinetic model of these reactions for SACs will provide a strong base for multi-scale modeling and scaling up the process of the reactions on SACs.

- The substrate chosen here is a 3NG sheet. The catalytic activity for the reactions can be tested with various graphene and non-graphene substrates like 4NG sheet, Graphene sheet with multiple vacancies, oxides of *d-transition* metals (e.g., iron oxides, zinc oxides), carbide and sulfide materials like tungsten carbide, and Molybdenum sulfate.

- The catalytic activity of any catalyst is known to be dependent on the morphology of the catalysts. Catalytic activity for various other structures/morphologies of 3NG/other substrates can also be tested.

- A high-throughput study of binding energies and charge dissipation on various nitrogenated graphene can be used to generate data for the machine-learning model, which might be able to predict properties of SACs with other substrates.

Bibliography

[1] I. Arto, I. Capellán-pérez, R. Lago, G. Bueno, and R. Bermejo, “Energy for Sustainable Development The energy requirements of a developed world,” *Energy Sustain. Dev.*, vol. 33, pp. 1–13, 2016.

[2] Z. Salameh, “Factors Promoting Renewable Energy Applications,” *Renew. Energy Syst. Des.*, pp. 1–32, 2014.

[3] P. Brando *et al.*, “Amazon wildfires: Scenes from a foreseeable disaster,” *Flora Morphol. Distrib. Funct. Ecol. Plants*, vol. 268, no. May, p. 151609, 2020.

[4] S. J. Jacobs, A. B. Pezza, V. Barras, J. Bye, and T. Vihma, “An analysis of the meteorological variables leading to apparent temperature in Australia: Present climate, trends, and global warming simulations,” *Glob. Planet. Change*, vol. 107, pp. 145–156, 2013.

[5] U. Haque *et al.*, “The human cost of global warming: Deadly landslides and their triggers (1995–2014),” *Sci. Total Environ.*, vol. 682, pp. 673–684, 2019.

[6] X. Gu *et al.*, “Impacts of anthropogenic warming and uneven regional socio-economic development on global river flood risk,” *J. Hydrol.*, vol. 590, no. June, p. 125262, 2020.

[7] R. Djalante, “Key assessments from the IPCC special report on global warming of 1.5 °C and the implications for the Sendai framework for disaster risk reduction,” *Prog. Disaster Sci.*, vol. 1, no. March, p. 100001, 2019.

[8] “AR6 Synthesis report: Climate change 2022.” [Online]. Available: https://www.ipcc.ch/report/sixth-assessment-report-cycle/.

[9] Organización Mundial de la Meteorología, *WMO statement on the status of the global climate in 2019*, no. 1248. 2020.

[10] Dutch Institute of Fundamental Energy Research, “Plasma Solar Fuels Devices DIFFER.” [Online]. Available: https://www.differ.nl/research/plasma-solar-fuels-devices. [Accessed: 18-Aug-2020].

[11] M. Carmo, D. L. Fritz, J. Mergel, and D. Stolten, “A comprehensive review on PEM water electrolysis,” *Int. J. Hydrogen Energy*, vol. 38, no. 12, pp. 4901–4934, 2013.

[12] A. Valera-Medina, H. Xiao, M. Owen-Jones, W. I. F. David, and P. J. Bowen, “Ammonia for power,” *Prog. Energy Combust. Sci.*, vol. 69, pp. 63–102, 2018.

[13] K. E. Lamb, M. D. Dolan, and D. F. Kennedy, “Ammonia for hydrogen storage; A review of catalytic ammonia decomposition and hydrogen separation and purification,” *Int. J. Hydrogen Energy*, vol. 44, no. 7, pp. 3580–3593, 2019.

[14] F. Chen, X. Jiang, L. Zhang, R. Lang, and B. Qiao, “Single-atom catalysis: Bridging the homo- and heterogeneous catalysis,” *Cuihua Xuebao/Chinese J. Catal.*, vol. 39, no. 5,

pp. 893–898, 2018.

[15] E. Skúlason *et al.*, "Modeling the electrochemical hydrogen oxidation and evolution reactions on the basis of density functional theory calculations," *J. Phys. Chem. C*, vol. 114, no. 42, pp. 18182–18197, 2010.

[16] K. Tran and Z. W. Ulissi, "Active learning across intermetallics to guide discovery of electrocatalysts for CO2 reduction and H2 evolution," *Nat. Catal.*, vol. 1, no. 9, pp. 696–703, 2018.

[17] A. J. Medford *et al.*, "From the Sabatier principle to a predictive theory of transition-metal heterogeneous catalysis," *J. Catal.*, vol. 328, pp. 36–42, 2015.

[18] D. M. Feng, Y. P. Zhu, P. Chen, and T. Y. Ma, "Recent advances in transition-metal-mediated electrocatalytic CO 2 reduction: From homogeneous to heterogeneous systems," *Catalysts*, vol. 7, no. 12, 2017.

[19] "Sigma Aldrich-Metal catalyst Prices." [Online]. Available: https://www.sigmaaldrich.com/nederland.html. [Accessed: 04-Jul-2020].

[20] L. Zhang, Y. Ren, W. Liu, A. Wang, and T. Zhang, "Single-atom catalyst: A rising star for green synthesis of fine chemicals," *Natl. Sci. Rev.*, vol. 5, no. 5, pp. 653–672, 2018.

[21] E. Alonso, F. R. Field, and R. E. Kirchain, "Platinum availability for future automotive technologies," *Environ. Sci. Technol.*, vol. 46, no. 23, pp. 12986–12993, 2012.

[22] X. F. Yang, A. Wang, B. Qiao, J. Li, J. Liu, and T. Zhang, "Single-atom catalysts: A new frontier in heterogeneous catalysis," *Acc. Chem. Res.*, vol. 46, no. 8, pp. 1740–1748, 2013.

[23] A. Beniya and S. Higashi, "Towards dense single-atom catalysts for future automotive applications," *Nat. Catal.*, vol. 2, no. 7, pp. 590–602, 2019.

[24] X. Yang, A. Wang, B. Qiao, and J. U. N. Li, "Single-Atom Catalysts : A New Frontier," vol. 46, no. 8, 2013.

[25] C. Rivera-Cárcamo and P. Serp, "Single Atom Catalysts on Carbon-Based Materials," *ChemCatChem*, vol. 10, no. 22, pp. 5058–5091, Nov. 2018.

[26] N. Cheng, L. Zhang, K. Doyle-Davis, and X. Sun, *Single-Atom Catalysts: From Design to Application*, vol. 2, no. 4. Springer Singapore, 2019.

[27] D. Deng, K. S. Novoselov, Q. Fu, N. Zheng, Z. Tian, and X. Bao, "Catalysis with two-dimensional materials and their heterostructures," *Nat. Publ. Gr.*, vol. 11, no. March, 2016.

[28] B. F. Machado and P. Serp, "Graphene-based materials for catalysis," *Catal. Sci. Technol.*, vol. 2, no. 1, pp. 54–75, 2012.

[29] H. Zhang, G. Liu, L. Shi, and J. Ye, "Single-Atom Catalysts: Emerging Multifunctional Materials in Heterogeneous Catalysis," *Adv. Energy Mater.*, vol. 8, no. 1, pp. 1–24, 2018.

[30] H. Xu, D. Cheng, D. Cao, and X. C. Zeng, "A universal principle for a rational design of single-atom electrocatalysts," *Nat. Catal.*, vol. 1, no. May, 2018.

[31] H. L. Tuller, “Solar to fuels conversion technologies: A perspective,” *Mater. Renew. Sustain. Energy*, vol. 6, no. 1, pp. 1–16, 2017.

[32] B. Gaudernack, “Hydrogen Production from Fossil Fuels,” *Hydrog. Power Theor. Eng. Solut.*, pp. 75–89, 1998.

[33] B. Lu *et al.*, “Ruthenium atomically dispersed in carbon outperforms platinum toward hydrogen evolution in alkaline media,” *Nat. Commun.*, vol. 10, no. 1, 2019.

[34] C. Liu, T. R. Cundari, and A. K. Wilson, “Reaction mechanism of the reverse water-gas shift reaction using first-row middle transition metal catalysts L′M (M = Fe, Mn, Co): A computational study,” *Inorg. Chem.*, vol. 50, no. 18, pp. 8782–8789, 2011.

[35] C. H. Lin, C. L. Chen, and J. H. Wang, “Mechanistic studies of water-gas-shift reaction on transition metals,” *J. Phys. Chem. C*, vol. 115, no. 38, pp. 18582–18588, 2011.

[36] S. Zhao, S. Li, T. Guo, S. Zhang, J. Wang, and Y. Wu, “Advances in Sn - Based Catalysts for Electrochemical - CO 2 Reduction,” *Nano-Micro Lett.*, no. 0123456789, 2019.

[37] J. Gunn Lee, *Computational Material Science: An Introduction*. Taylor & Francis, 2011.

[38] W. Kohn and L. J. Sham, “Self-Consistent Equations Including Exchange and Correlation Effects,” *Phys. Rev.*, vol. 140, no. 4A, pp. A1133--A1138, Nov. 1965.

[39] W. Kohn and P. Hohenberg, “Inhomogenous electron gas,” *Phys. Rev.*, vol. 155, no. 1962, 1964.

[40] J. Gunn Lee, *Computational materials science : an introduction*, 1st ed. CRC press, 2015.

[41] J. P. Perdew and Y. Wang, “Accurate and simple analytic representation of the electron-gas correlation energy,” *Phys. Rev. B*, vol. 45, no. 23, pp. 13244–13249, Jun. 1992.

[42] J. P. Perdew, K. Burke, and M. Ernzerhof, “Generalized Gradient Approximation Made Simple,” *Phys. Rev. Lett.*, vol. 77, no. 18, pp. 3865–3868, Oct. 1996.

[43] J. P. Perdew, K. Burke, and M. Ernzerhof, “Generalized Gradient Approximation Made Simple [Phys. Rev. Lett. 77, 3865 (1996)],” *Phys. Rev. Lett.*, vol. 78, no. 7, p. 1396, Feb. 1997.

[44] J. P. Perdew, K. Burke, and Y. Wang, “Generalized gradient approximation for the exchange-correlation hole of a many-electron system,” *Phys. Rev. B*, vol. 54, no. 23, pp. 16533–16539, Dec. 1996.

[45] J. Wellendorff, T. L. Silbaugh, J. K. Nørskov, T. Bligaard, F. Studt, and C. T. Campbell, “A benchmark database for adsorption bond energies to transition metal surfaces and comparison to selected DFT functionals,” vol. 640, pp. 36–44, 2015.

[46] G. Kresse and J. Furthmüller, “Efficient iterative schemes for ab initio total-energy calculations using a plane-wave basis set,” *Phys. Rev. B*, vol. 54, no. 16, pp. 11169–11186, Oct. 1996.

[47] G. Kresse and J. Furthmüller, “Efficiency of ab-initio total energy calculations for metals and semiconductors using a plane-wave basis set,” *Comput. Mater. Sci.*, vol. 6,

no. 1, pp. 15–50, Jul. 1996.

[48] A. Andri, W. Tang, S. Chill, ChaiWenrui, and G. Henkelman, "Code:Bader Charge analysis." [Online]. Available: http://theory.cm.utexas.edu/henkelman/code/bader/. [Accessed: 04-Jul-2020].

[49] "Richard F.W Bader." [Online]. Available: https://www.chemistry.mcmaster.ca/bader/. [Accessed: 29-Apr-2020].

[50] "C-mp48-graphite cell." [Online]. Available: https://materialsproject.org/materials/mp-48/. [Accessed: 30-Jul-2020].

[51] I. Tezsevin, M. C. M. van de Sanden, and S. Er, "Surface charging activated mechanism change: A computational study of O, CO, and CO2 interactions on Ag electrodes," *J. Energy Chem.*, vol. 50, pp. 307–313, 2020.

[52] K. M. Bal and E. C. Neyts, "Modelling molecular adsorption on charged or polarized surfaces : a critical flaw in common approaches †," pp. 8456–8459, 2018.

[53] "Schrodinger Suite." [Online]. Available: https://www.schrodinger.com/.

[54] J. W. Arblaster, "Crystallographic Properties of Ruthenium," no. 2, pp. 127–136, 2013.

[55] Y. Waseda, K. Hirata, and M. Ohtani, "High-temperature thermal expansion of platinum, tantalum, molybdenum, and tungsten measured by x-ray diffraction," *High Temp. - High Press.*, vol. 7, no. 2, pp. 221–226, 1975.

[56] M. E. Straumanis and L. S. Yu, "Lattice parameters, densities, expansion coefficients and perfection of structure of Cu and of CuIn α phase," *Acta Crystallogr. Sect. A*, vol. 25, no. 6, pp. 676–682, Nov. 1969.

[57] J. Wellendorff *et al.*, "A benchmark database for adsorption bond energies to transition metal surfaces and comparison to selected DFT functionals," *Surf. Sci.*, vol. 640, pp. 36–44, 2015.

[58] H. Fei *et al.*, "Atomic cobalt on nitrogen-doped graphene for hydrogen generation," *Nat. Commun.*, vol. 6, pp. 1–8, 2015.

[59] Z. Chen, K. Mou, S. Yao, and L. Liu, "Zinc-Coordinated Nitrogen-Codoped Graphene as an Efficient Catalyst for Selective Electrochemical Reduction of CO2 to CO," *ChemSusChem*, vol. 11, no. 17, pp. 2944–2952, 2018.

Appendix

A. Molecular energies of H, N and CO

Adsorbent Species	Energy (eV)
CO	-14.424
H_2	-6.978
N_2	-16.270

B. Binding Energy of CO, H and N on different substrates

	CO Eb on different substrates			H Eb on different substrates			N Eb on different substrates		
Metal	SMA	SMC	3NG	SM	SMC	3NG	SM	SMC	3NG
Li	-0.27	-0.75	-0.22	-0.04	2.12	2.27	3.09	4.743	4.763
Na	-0.03	-0.43	-0.15	0.39	2.15	2.12	3.589	3.805	3.765
K	-0.04	-0.30	-0.12	0.46	2.24	2.28	4.008	4.92	4.718
Rb	-0.04	-0.25	-0.10	0.50	2.25	2.28	4.904	4.934	4.748
Cs	3.85	-0.14	-0.08	2.01	2.34	2.48	4.913	4.712	4.705
Be	0.07	-1.44	-5.03	-0.12	0.35	2.28	2.827	2.577	3.871
Mg	-0.03	-0.56	1.22	0.87	0.24	-0.70	3.947	3.655	2.581
Ca	0.15	-0.46	-0.94	0.29	-0.15	2.25	3.161	2.961	3.266
Sr	-0.03	-0.10	-0.08	0.43	0.05	2.32	3.278	3.079	3.994
Ba	-0.22	-0.55	3.22	0.08	-0.23	0.77	2.163	3.026	3.688
Sc	-1.27	-1.61	-1.12	-0.33	-0.65	-0.94	0.044	0.426	1.838
Y	-1.27	-1.62	-2.11	-0.61	-1.04	-0.75	0.156	0.48	2.016
La	-1.31	-2.84	0.88	-0.13	-1.04	-0.35	-1.318	-1.09	1.595
Ti	-1.76	-1.77	-1.67	-0.39	0.28	-0.88	-0.864	-0.589	0.365
Zr	-2.01	-1.76	-0.68	-0.51	-0.34	-1.02	-1.597	-1.308	0.057
Hf	-1.75	-1.45	-2.54	-0.39	-0.36	-1.19	-1.029	-0.96	0.522
V	-1.60	-1.75	-1.83	-0.35	-0.16	-0.66	-0.481	0.481	-0.016
Nb	-1.97	-1.98	-0.80	-0.46	-0.29	-1.01	-1.594	-1.5	-0.693
Ta	-1.99	-2.12	-2.60	-0.19	-0.06	-1.32	-2.014	-1.89	-0.651
Cr	-0.32	-1.43	-2.11	-0.01	0.60	-0.60	0.667	1.822	-0.741
Mo	-0.89	-1.45	-1.38	-0.18	-0.51	-0.93	-0.806	-0.595	-1.022
W	-2.12	-2.50	-2.66	-1.37	-0.33	-1.26	-2.229	-0.802	-1.396
Mn	-0.15	-0.58	-2.83	0.38	0.12	-0.61	1.664	2.973	-0.098
Re	-1.74	-1.18	-3.64	-0.09	-0.36	-2.19	-1.02	1.624	-2.335
Fe	-1.33	-2.11	-2.47	-0.16	0.02	-0.55	1.622	2.513	-0.027
Ru	-3.39	-2.57	-2.81	-1.26	-0.18	-0.46	-1.172	-0.356	-1.017
Os	-2.86	-1.99	-3.50	-0.585	-0.058	-0.958	-1.132	-0.402	-2.615
Co	-2.18	-2.36	-3.06	-0.585	0.504	-0.275	1.501	2.491	0.795
Rh	-2.97	-2.17	-2.31	-1.081	0.374	-0.586	0.582	1.606	0.006
Ir	-3.37	-3.42	-3.70	-1.17	-1.019	-1.336	-0.878	-0.481	-1.411
Ni	-2.55	-2.24	-3.11	-1.164	0.086	-0.338	1.569	2.756	1.861
Pd	-2.19	-2.13	-2.33	-0.651	-0.19	-0.037	2.391	2.61	2.152
Pt	-3.51	-3.48	-3.13	-1.266	-1.182	-1.229	0.705	0.823	-0.172
Cu	-0.62	-2.06	-3.42	-0.519	0.763	0.043	2.595	3.58	2.794

Ag	-0.03	-1.16	-3.05	-0.514	0.65	0.488	3.539	4.084	3.695
Au	-0.57	-2.42	-2.52	-0.788	-0.052	-0.814	2.718	3.384	2.302
Zn	-0.03	-0.82	-0.03	-0.782	-0.187	-1.118	4.551	3.531	2.451
Cd	-0.03	-0.57	-0.02	1.385	0.199	-0.694	4.715	3.957	3.046
B	-1.16	-1.15	-0.03	-1.359	-0.29	-0.298	0.335	2.619	2.905
Al	-0.81	-0.42	-0.57	-1.354	1.339	-1.352	2.159	4.455	1.844
Ga	-0.59	-0.40	-0.04	-0.794	1.933	-0.175	2.522	4.82	3.243
In	-2.09	-0.30	-0.03	-0.601	2.031	-0.429	3.179	4.882	3.214
Tl	-0.42	-0.29	-0.03	-0.385	2.193	2.023	3.002	4.905	4.942
Si	-2.01	-1.60	-0.04	-0.775	-1.088	-0.083	0.059	1.948	1.672
Ge	-1.49	-1.24	-0.03	-0.777	-0.773	0.942	1.198	2.486	3.373
Sn	-1.07	-0.88	-0.03	-0.505	-0.465	0.624	1.925	2.947	4.1
Pb	-0.87	-0.21	-0.03	-0.268	-0.76	-0.279	2.363	-0.602	2.165
As	-1.07	-2.38	-0.03	-0.547	-0.723	-0.184	-0.059	1.358	3.161
Sb	-0.56	-1.68	-0.13	-0.541	-0.368	-0.171	1.164	2.215	2.301
Bi	-0.31	-0.67	-0.15	-0.262	-0.54	-1.038	1.702	-0.802	2.282
Po	-1.49	-0.69	-0.70	-0.404	-0.237	-0.269	2.065	2.016	1.92

C. VASP calculation with developed code

The methodology clearly describes the workflow of the calculations. As mentioned in section 3.5, automation of the codes is necessary to carry out huge number of calculations. In this example, the codes developed and used for the case of HER is explained. It is noteworthy that these calculations are done in both Cartesius and hpc06 at TU Delft. Since the scheduler is different, the submit script for each of these cases will also be different.

C1. Single metal optimization

The first step of calculations is the SM optimization. For this, the SMA is placed in a 15x15x15Å box and optimized as explained in the methodology. The script for this is:

```
#! /bin/bash
#Code to submit the SM optimization to hpc06
#Author- NV

cat ~/Library/metals | while read line
#Reads the list of metals stored in the Library
do #start the while loop
mkdir ${line} #Makes the directory with Metal name
cd ${line}
source POSCAR_SM #Makes the POSCAR for the calculation.
cp ~/DIFFER/thesis/Library/pot_SM .
source pot_SM #Makes the POTCAR to make POTCAR
cp  ~/DIFFER/thesis/Library/INCAR_SM ./INCAR
cp ~/DIFFER/thesis/Library/KPOINTS_SM ./KPOINTS
#Copies the INCAR and KPOINTS, same for all SM optimization calculations
cat >submitvasp<<!
#! /bin/bash
#PBS -l nodes=1:ppn=4:mse
#PBS -m ae
#PBS -m abe
#PBS -M N.Viswanathan@differ.nl
#PBS -N ${line}_SM

module load vasp
cd \$PBS_O_WORKDIR
echo \$PBS_O_WORKDIR
mpirun vasp
!
#Makes the submitvasp file.
qsub submitvasp
# Submits the calculation to the cluster.

cd ..
done #end the while loop
```

!

Script A1: Submit script for SMA optimization

It is important to note that the POSCAR_SM and pot_SM is stored in the bin (All the POSCAR and POTCAR scripts are stored in the bin). Hence they can be executed from there. This avoids the presence of unnecessary files in the working directory, and hence file handling will be easier. The POSCAR_SM script mentioned in the above script is shown below:

```
#! /bin/bash
#Code to make the POSCAR for SMA optimization
#Author- NV

cat >POSCAR <<!
${line}_SM #Name of the calculation
1.00000 #Unit cell dimension
15.000  0.000          0.000
0.000          15.000  0.000
0.000          0.000          15.000 #Cell parameters
${line} #Metal name-POTCAR is made according this name
1
Cartesian #Cartesian/direct co-ordinates
7.5     7.5     7.50
!
```

Script A2: Script to make POSCAR for SMA optimization

Note that the submit script is written in such a way that once the calculation starts or ends, a mail will be sent to the addressed email id. This is how I kept track of whether the calculation was finished or not. After this, the accuracy of the calculations is checked. This was already explained in Chapter 3, but I am explaining it here again.

```
#! /bin/bash
#Code to check if the calculations have reached the required accuracy or not. If
the calculation has reached the required accuracy, then
the name of the directory is printed to a file 'list'; if not, it is printed to the
'tobererun' file.

rm accuracy
rm list
rm tobererun
path=pwd
for d in *
do
        cd $d
        echo "$d" $(grep -r accuracy OUTCAR) >> ../accuracy
        if grep -q accuracy OUTCAR ; then
                echo "$d" >> ../list
        else
                echo "$d" >> ../tobererun
        fi
        cd ../

done
```

Script A3: Accuracy check for SMA optimization

Note that, if necessary, this accuracy check can be included in the ‘submitvasp’ script. But it was not done because it is preferred that the accuracy check of VASP calculations is done manually (this way it is easier to keep track of errors). The energy from the calculation is stored in the ‘Library’ using the following code:

```
#! /bin/bash
# Code to search for the energies from the converged calculations

rm energies_grp.csv
cat ~/Library/metals |while read metal
do

        cat accuracy | while read line #Reads the file ‘accuracy’
        do
                if [ “$metal” == “$line” ] #Checks if the metal in the Library list
is present in list of converged calculations.
                then
                cd ${line}
                        echo "$line", $(grep y= OUTCAR | tail -1 | tail -c 19) >>
../energies_grp.csv #Energy stored as a csv
                        cp energies_grp.csv ~/Library/energies_SM_grp.csv #
                        cd ..
                else
                        echo “$metal has not reached accuracy-redo the calculation”
                fi
        done
done
```

Script A4: Script to extract energy from the OUTCAR file of converged calculations

In this code, the metal list in Library is compared against the list of metals that have reached accuracy. If converged, the energy values are extracted from the OUTCAR file. Else, a message is shown to rerun the calculation. This csv file is also copied to the Library, where all the data is saved.

C2. Single Metal Atom Hydrogen interaction study

Once the SMA optimization is done, the H atom is adsorbed on the SMA. The following script is used for the mentioned calculation:

```
#! /bin/bash
#Code to submit the calculations of H adsorption on SMA
#Author NV
cat ~/Library/metals | while read line
do
mkdir ${line}_2H
cd ${line}_2H
source POSCAR_2H
source pot_H
cp  ~/DIFFER/thesis/Library/INCAR_SM ./INCAR
cp ~/DIFFER/thesis/Library/KPOINTS_SM ./KPOINTS
cat >submitvasp<<!
#! /bin/bash
#PBS -l nodes=1:ppn=4:mse
#PBS -m ae
#PBS -m abe
#PBS -M N.Viswanathan@differ.nl
#PBS -N ${line}_H

module load vasp
cd \$PBS_O_WORKDIR
echo \$PBS_O_WORKDIR
mpirun vasp
!
qsub submitvasp
cd ..
done
```

Script A5: Submit script for SMA-H calculations

The H adsorption on SMAs are done with two different input coniditons-2Å and 1.5Å. The code shown above is for the hydrogen atom which is at 2Å distance from the SMA. The difference is in the POSCAR, which is shown below in POSCAR_2H script:

```
# /bin/bash
#POSCAR for SMA-H interaction study
#Author-NV
cat >POSCAR <<!
${line}_H
1.00000
15.000          0.000           0.000
0.000           15.000          0.000
0.000           0.000           15.000
$line H
1 1
Selective Dynamics
Cartesian
7.5     7.5     7.5     F F F
7.5     7.5     9.5     T T T #If the H atom is 1.5A away, then the z co-#ordinate
will be 9A
!
```

Script A6: POSCAR_2H script to make POSCAR with metal-hydrogen atom input distance 2 Å

In this POSCAR file, 'F F F' represents that during the calculation, the metal atom (the first according to POSCAR) is stationary and only the adsorbent atom (co-ordinates next to 'T T T') moves. More info can be obtained from VASP manual [A1].

Following this, the accuracy check is done with the script shown previously. If accurate, the energy is extracted from the OUTCAR file to a csv file. The E_B of H atom on SMA is calculated in excel. Even though a code has been developed for this, calculation of E_B in excel is preferred because the accuracy of calculation can be double checked.

Another output data that can be extracted from this calculation is the output metal-hydrogen bond-distance and magnetic moments of the system. The following script is used to extract the metal hydrogen bond-distance data:

```
#! /bin/bash

# code to find the bond distance for single atoms and an atomic adsorbent species
#Author: NV

rm bonddistance.csv

cat ~/Library/metals | while read line
do
        cd ${line}_H   #Change the name of the directory according to the submit
script
        mz=$(cat CONTCAR | sed -n '10p' | cut -d' ' -f7)
        mx=$(cat CONTCAR | sed -n '10p' | cut -d' ' -f3)
        my=$(cat CONTCAR | sed -n '10p' | cut -d' ' -f5)
        adx=$(cat CONTCAR | sed -n '11p' | cut -d' ' -f3)
        ady=$(cat CONTCAR | sed -n '11p' | cut -d' ' -f5)
        adz=$(cat CONTCAR | sed -n '11p' | cut -d' ' -f7)
        dist_1=$(echo "scale=10; (($adx-$mx)^2 + ($ady-$my)^2 + ($adz-$mz)^2)" | bc)
        z=$(cat CONTCAR | sed -n '5p' | tail -c 20)
        dist=$(echo "scale=25; $z*sqrt($dist_1)" | bc)
        echo "$line", $dist >> ../bonddistance.csv
        cd ../
cp bonddistance.csv ~/Library/bonddistance_SMA_H.csv
done
```

Script A7: Script to calculate the SMA-H bond-distance.

Note that this script can only be used to calculate the bon-distance data of SMA and a mono-atomic adsorbent species. In the POSCAR/CONTCAR file (the output file describing the co-ordinates of all the atoms in the system), the co-ordinates of atomic species is written from the tenth line. The x, y, z co-ordinates are stored keeping the order and the line number in mind. To extract the magnetic moment from the output file, the script get_mag is used:

```
#! /bin/bash
#Code name: get_mag
# code for reading the magnetic moments from OSZICAR and writing it to magmom.csv

rm magmom.csv
cat ~/Library/metals | while read line
do
        cd ${line}_H
        echo “${line}” , $(grep mag OSZICAR | tail -c 8) >> ../magmom.csv
        cd ..
        cp magmom.csv ~/Library/magmom_SMA_H.csv
done
```

Script A8: get_mag code used to read the magnetic moment from OSZICAR and to write it to a csv file

C3. Single Metal Cation-Hydrogen atom interaction calculations

To calculate the effect of a positive charge on the SMA, the NELECT tag in INCAR is varied as already explained in Chapter 3. The first step of cation optimization is optimizing the SMA in boxes of two different vacuum sizes: 15x15x15Å and 30x30x30Å. The script for this code is similar to Script A2, used to make POSCAR for SMC optimization calculations with a change. From any calculation henceforth, the metal adsorbent input bond-distance will be the bond-distance corresponding to the lowest energy orientation of SMA-H calculation. i.e. if for the case of Li-H interaction, 2Å exhibits lower energy than 1.5Å input, the output bond-distance e of 2Å is the input for any calculation henceforth. This is the case for CO and N interaction studies. The submit script for the calculation is shown using the code submit_SMC_H_15:

```
#! /bin/bash
# Code name: submit_SMC_H_15
# Code for submitting calculations for H single metal positive interactions

while IFS=, read -r Metal bonddist;
do
mkdir SMP_H_${Metal}
cd SMP_H_${Metal}
hz=$(echo "scale=10; 7.5+${bonddist}" | bc) %Calculates the SMA-H BD
source POSCAR_H_SMC
source pot_SMC_H
source positive_smc_H
cp ~/DIFFER/thesis/Library/KPOINTS_SM ./KPOINTS
cat >submitvasp<<!
#! /bin/bash
#PBS -l nodes=1:ppn=4:mse
##PBS -q guest
#PBS -m ae
#PBS -m abe
#PBS -M N.Viswanathan@differ.nl
#PBS -N ${Metal}_SMP

module load vasp
cd \$PBS_O_WORKDIR
echo \$PBS_O_WORKDIR
mpirun vasp
!
qsub submitvasp
cd ..
done < ~/Library/bonddistance_SMA_H.csv #SMA-H BD read from the Library
```

Script A9: SMC_H_15 code to submit the calculation for SMC-H interaction studies

As mentioned earlier, the POSCAR_SMC_H15 is similar to Script A6; only difference is that the *z co-ordinate* of hydrogen atom in POSCAR_SM_H15 is replaced by the bond-distance *hz,* calculated in the above script.

In the script A9, `positive_smc_H` makes the INCAR required for the SMC-H study. The script is shown below:

```
#! /bin/bash
#code to take POTCARS of the metal and make a new INCAR with NELECT is
NELECT(potcatr)-1

nelec=$(sed -n 2p POTCAR)
nelect=$( echo "scale=5; $nelec*1.00" | bc)

cat >INCAR<<!
ENCUT  = 400
EDIFF  = 1e-4
EDIFFG = -0.02

ISIF   = 2

IBRION = 2
POTIM  = 0.5
NSW    = 100
NELM = 100
NELECT = $nelect

ISMEAR = -1
SIGMA  = 0.01
ISPIN  = 2


PREC   = ACCURATE
ALGO   = FAST
LREAL = Auto

LWAVE  = .FALSE.
LCHARG = .FALSE.

GGA = RP

!
```

Script A10: positive_smc_H code to make INCAR for SMC-H calculations

The accuracy check, BD and magnetic moments are read using the same codes shown above.

C4. 3NGM-H calculations

After optimizing the metal atom on the 3NG, the interaction of hydrogen with metal doped graphene is studied. For the adsorption of hydrogen on 3NGM, three different orientations has been identified. Of the three orientations, one of the orientations has already been discussed in the Chapter 3. In this section, the scripts for other two orientations i.e. H atom adsorbed at an angle of 45^0 to the catalyst surface in the direction of hollow site of 3NG and H atom adsorbed at 45^0 to the catalyst surface in the direction of one of the nitrogen atoms. In this section one of these codes along with are and with the code to find BD between hydrogen and metal catalyst is explained. The submit script for adsorbing hydrogen in the direction of 3NG hollow site is shown below:

```
#! /bin/bash
# Code to make inputs of the H/N at an angle of 45deg for 3NG hollow site
# Input- CONTCAR-xyz file
#      - bonddistance of the previous output

# Author- Narasimhan Viswanathan

while IFS=, read -r Metal bonddist;
do

        mkdir 3NG_H_angular_${Metal}
        cd 3NG_H_angular_${Metal}
        cp ~/Library/INCAR .
        cp ~/Library/KPOINTS .
        source pot_3NG_H
        cp ../contcars/CONTCAR_${Metal} ./POSCAR_direct
        source dir2cart .
        #The following lines make calculates the metal co-ordinates according to the
criteria described above.
        mx=$(cat ../contcarxyz/3NG_${Metal}_CONTCAR.xyz | sed -n '34p'| cut -d' ' -
f4)
        my=$(cat ../contcarxyz/3NG_${Metal}_CONTCAR.xyz | sed -n '34p'| cut -d' ' -
f7)
        mz=$(cat ../contcarxyz/3NG_${Metal}_CONTCAR.xyz | sed -n '34p'| cut -d' ' -
f10)
        adsz1=$( echo "scale=10; ${bonddist}*s(0.785)" | bc -l)
        adsy1=$( echo "scale=10; ${bonddist}*s(0.785)" | bc -l)
        adsy=$( echo "scale=5; ${adsy1}+${my}" | bc)
        adsz=$( echo "scale=5; ${adsz1}+${mz}" | bc)
        source dir2cart
        sed -i '7s/.*/28 4 1 /' POSCAR
         sed -i '6s/.*/C N '"${Metal}"'  /' POSCAR
        sed -i '8s/.*/Cartesian/' POSCAR

        sed -i '39 a '"${mx} "' '"${adsy}"' '"${adsz}"' ' POSCAR
        #Writes the calculated metal co-ordinates into the POSCAR

cat >submitvasp<<! #Makes the submit script
#! /bin/bash
#PBS -l nodes=1:ppn=12:mse
##PBS -q guest
#PBS -m ae
#PBS -m abe
#PBS -M N.Viswanathan@differ.nl
#PBS -N ${Metal}_SMP

module load vasp
cd \$PBS_O_WORKDIR
echo \$PBS_O_WORKDIR
mpirun vasp
!
qsub submitvasp
cd ..
done < ~/Library/bonddistance_SMA_H.csv # reads the BD data from the Library
```

Script A11: Submit script to submit calculations for 3NGM-H interaction with hydrogen atom in the direction of 3NG hollow site

In the above code, it is important to note that the CONTCAR of metal optimized on the 3NG sheet is used as the POSCAR for the calculation. This CONTCAR is copied as POSCAR_direct into the working directory. Once the metal co-ordinates are calculated, the co-ordinates are written to the thirty-ninth line of the POSCAR file. The POSCAR in direct co-ordinates is converted to cartesian co-ordinates using the script `dir2cart` shown below:

```
#! /bin/bash
# Code to conevert the direct coordinates to cartesian coordinates
# Input- POSCAR file in direct coordinates
# Output- POSCAR file in cartesian coordinates
rm POSCAR_tmp
head -n 8 POSCAR_direct > POSCAR
ct=9
while [ ${ct} -le 40 ]
do
        line=${ct}p
        jnk=${ct}
        xd=$(cat POSCAR_direct | sed -n $line | awk '{print $1}')
        yd=$(cat POSCAR_direct | sed -n $line | awk '{print $2}')
        zd=$(cat POSCAR_direct | sed -n $line | awk '{print $3}')
        a1uc=$( cat POSCAR_direct | sed -n 3p | cut -d' ' -f6)
        b1uc=$(cat POSCAR_direct | sed -n 4p | cut -d' ' -f5)
        b2uc=$( cat POSCAR_direct | sed -n 4p | cut -d' ' -f9)
        c3uc=$( cat POSCAR_direct | sed -n 5p | cut -d' ' -f13)
        xc=$( echo "scale=10; ${xd}*${a1uc}+${yd}*${b1uc}" | bc -l)
        yc=$( echo "scale=10; ${yd}*${b2uc}" | bc -l)
        zc=$( echo "scale=10; ${zd}*${c3uc}" | bc -l)
        echo $xc $yc $zc >> POSCAR_tmp
        let "ct++"
done
head -n 32 POSCAR_tmp >> POSCAR
rm POSCAR_tmp
```

Script A12: dir2cart script to convert the direct co-ordinates to cartesian co-ordinates

In the above code, the POSCAR_direct copied in the submit script is used as the input. A counter is set at ct=9 to count the number of lines in POSCAR. After this, x, y, and z (direct) co-ordinate of each atom is stored into xd, yd, and zd. Following this, the cell dimensions are stored as a1uc, b1uc, b2uc, and c3uc (where the number stands for the a1, a2, a3 etc.. and uc is unit cell). Once these values are read, the cartesian co-ordinates are calculates as shown in the script above. These values are written to a temporary POSCAR file. The POSCAR_tmp is written to the POSCAR and later deleted. The counter ct is incremented by 1, so that this process is repeated for each line.

Once the calculations are finished and reached required accuracy (checked with the same code shown previously), the BD data is read and written to a file. This is done using the following script.

```
#! /bin/bash

# code to find the bond distance for single atoms and the species

rm bonddistance.csv
cat ~/DIFFER/thesis/SAC_codes/metals_groep | while read line
do
        cd 3NG_H_angularhollow_${line}
        mz=$(cat CONTCAR.xyz | sed -n '35p' | cut -d' ' -f10)
        mx=$(cat CONTCAR.xyz | sed -n '35p' | cut -d' ' -f4)
        my=$(cat CONTCAR.xyz | sed -n '35p' | cut -d' ' -f7)
        adx=$(cat CONTCAR.xyz | sed -n '34p' | cut -d' ' -f4)
        ady=$(cat CONTCAR.xyz | sed -n '34p' | cut -d' ' -f7)
        adz=$(cat CONTCAR.xyz | sed -n '34p' | cut -d' ' -f10)
        #Ox=$(cat CONTCAR.xyz | sed -n '36p' | cut -d' ' -f4)
        #Oy=$(cat CONTCAR.xyz | sed -n '36p' | cut -d' ' -f7)
        #Oz=$(cat CONTCAR.xyz | sed -n '36p' | cut -d' ' -f10)
        dist_1=$(echo "scale=10; (($adx-$mx)^2 + ($ady-$my)^2 + ($adz-$mz)^2)" | bc)
        z=$(cat CONTCAR | sed -n '5p' | tail -c 20)
        #distco_1=$(echo "scale=10; (($adx-$Ox)^2 + ($ady-$Oy)^2 + ($adz-$Oz)^2)" |
bc)
        dist=$(echo "scale=25; sqrt($dist_1)" | bc)
        #distco=$(echo "scale=25; sqrt($distco_1)" | bc)
        echo "$line", $dist >> ../bonddistance.csv
        cd ../
cp bonddistance.csv ~/Library/bonddistance_3NG_H_AH.csv
done
```

Script A 13: 3NG_BD code to find the bond distance between H atom and metal, doped on 3NG

This code is made specifically for single adsorbent atom calculations. For the case of CO, the commented-out parts will be used to calculate the BD. It is important to note that the BD is calculated from the CONTCAR.xyz, and not from the CONTCAR file with direct co-ordinates. The dir2cart script was used to convert the direct co-ordinates to the cartesian co-ordinates.

C5 Bader Calculations

The submission script for Bader calculation is similar to the scripts seen above. The difference in this script is that the CONTCAR should be copied as POSCAR and the calculation starts with a different INCAR file. Since the scripts are similar, the submit script for Bader is not shown here. However, a postrun script is shown. This postrun script reads the Bader output ACF.dat and makes an output csv file will all the charge details.

```
#! /bin/bash
# Code to analyse the bader charge analysis- subtracts the valency from ACF.dat
rm badercharges.csv
h=1
n=5
while IFS=',' read -r Metal valency;
do
        cd 3NG_H_$ngular_${Metal}
        metchg=$(cat ACF.dat | sed -n 34p | awk '{print $5}')
        n1chg=$(cat ACF.dat | sed -n 31p | awk '{print $5}')
        n2chg=$(cat ACF.dat | sed -n 32p | awk '{print $5}')
        n3chg=$(cat ACF.dat | sed -n 33p | awk '{print $5}')
        Hchg=$(cat ACF.dat | sed -n 35p | awk '{print $5}')
        N1chg=$(echo "scale=10; $n-$n1chg" | bc -l)
        N2chg=$(echo "scale=10; $n-$n2chg" | bc -l)
        N3chg=$(echo "scale=10; $n-$n3chg" | bc -l)
        mchg=$(echo "scale=10; $valency-$metchg" | bc -l)
        hydchg=$(echo "scale=10; $h-$Hchg" | bc -l)
        echo ${Metal}, ${N1chg}, ${N2chg}, ${N3chg}, ${mchg}, ${hydchg} >>
../badercharges.csv
        cd ../
done < ~/Library/valency.csv
```

Script A 14: postrun script to make Bader ouput file from Bader output

The script shown above is to read ACF.dat file of a 3NGM-H system. The script only gives the charge of the metal atom, nitrogen atom on 3NG and the adsorbent species. This is taken because, there are no (considerable) changes to charge state of carbon atoms.

C6. Utility Scripts

Some of the calculations might not reach the required accuracy. This might be the case for a good number of SACs. In that case, a script was developed to check the error and resubmit the calculation all together. The script torerun_analysis will give the error messages and lines of output files for all the metals in a single file. This is shown below:

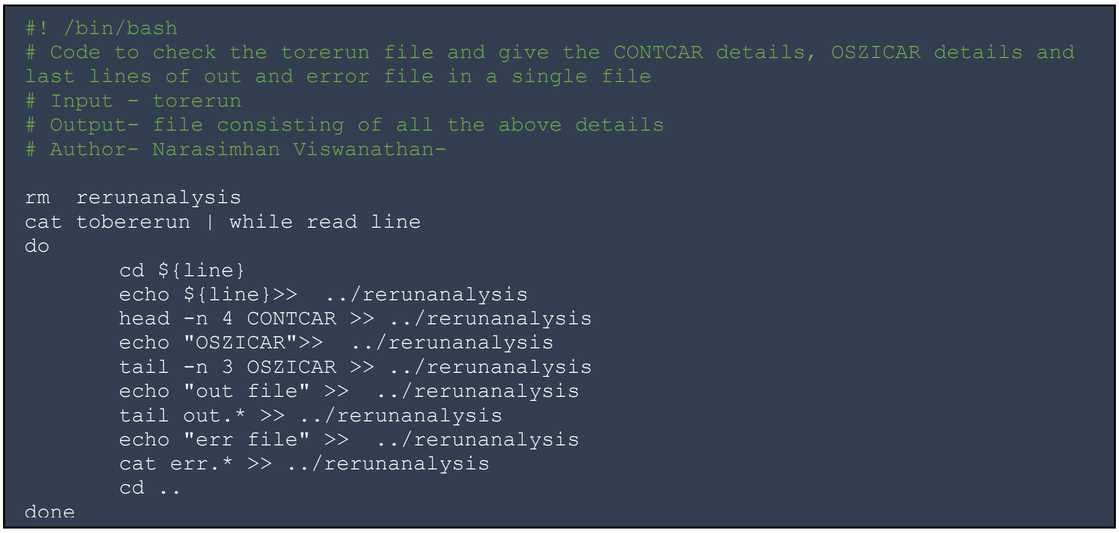

```
#! /bin/bash
# Code to check the torerun file and give the CONTCAR details, OSZICAR details and
last lines of out and error file in a single file
# Input - torerun
# Output- file consisting of all the above details
# Author- Narasimhan Viswanathan-

rm  rerunanalysis
cat tobererun | while read line
do
        cd ${line}
        echo ${line}>>  ../rerunanalysis
        head -n 4 CONTCAR >> ../rerunanalysis
        echo "OSZICAR">>  ../rerunanalysis
        tail -n 3 OSZICAR >> ../rerunanalysis
        echo "out file" >>  ../rerunanalysis
        tail out.* >> ../rerunanalysis
        echo "err file" >>  ../rerunanalysis
        cat err.* >> ../rerunanalysis
        cd ..
done
```

Script A 15: torerun_analysis script generates an output file with the calculation info of the systems which have not reached the required accuracy.

In the utility script torerun_analysis script shown above, the SACs which have not reached the required accuracy are read from the tobererun file. This file is generated during the accuracy check. Once in a specific directory, the code checks for CONTCAR file and prints the first few lines of CONTCAR. This is to see if the CONTCAR is generated with information or not. The script also displays the last line from OSZICAR file, from which the information regarding the energy convergence can be understood. The script also displays last few lines of out and err files generated from the calculation. This process is repeated for all the catalyst systems which have not reached the required accuracy.

The next step in the process is to resubmit these calculations without traversing through the directories. ‘resubmission’ script shown below is used for this purpose.

```
#! /bin/bash
#Script to resubmit the calculations in case that has not reached the required
accuracy

cat tobererun | while read line
do
        cd ${line}
        mv OUTCAR OUTCAR_a
        mv OSZICAR OSZICAR_a
        mv POSCAR POSCAR_a
        cp CONTCAR contcar_a
        mv CONTCAR POSCAR
        qsub submitvasp
        cd ..
done
```

Script A 16: resubmission script to submit the calculations that have not reached the required accuracy to the cluster automatically

These codes can were made specifically for the 3NG calculations, but with few edits, they can be used for calculations in catalysis.

<u>Bibliography:</u>

[A1] G. Kresse and M. Marsman, “Vienna simulation ab-initio package - VASP the GUIDE,” 2012.